Localization, Criticality and Ergodicity – From Single-Particle to Many-Body Quantum Systems with Disorder

Dissertation zur Erlangung des Doktorgrades der Naturwissenschaften (Dr. rer. nat.) der Fakultät für Physik der Universität Regensburg

vorgelegt von

Johannes Dieplinger

aus Traunstein

im Jahr 2024

Promotionsgesuch eingereicht am 5. Juni 2024.

Die Arbeit wurde angeleitet von Prof. Dr. Ferdinand Evers.

Prüfungsausschuss:

Vorsitzender: Prof. Dr. Jascha Repp
Erstgutachter: Prof. Dr. Ferdinand Evers
Zweitgutachter: Prof. Dr. Klaus Richter
Weitere Prüferin: Prof. Dr. Sara Collins

Promotionskolloquium am 25. Juli 2024.

LIST OF PUBLICATIONS

This thesis intends to offer an intuitive approach to the physics of disordered systems. The individual case studies presented in this dissertation are based on a number of projects which have been published in scientific peer-reviewed journals and are now brought together in a comprehensive contextual framework. For a precise formulation of the research questions posed in this thesis, the reader is referred to chapter 1.3, while a summary and contextualization of the results is presented in chapter 9.

PUBLISHED ARTICLES

- **J. Dieplinger**, S. Bera, F. Evers, *An SYK-inspired model with density–density interactions: Spectral & wave function statistics, Green's function and phase diagram*, Annals of Physics **435**, 168503 (2021).
  → covered in chapter 7

- H. Schmid, **J. Dieplinger**, A. Solfanelli, S. Succi, S. Ruffo, *Tricritical point in the quantum Hamiltonian mean-field model*, Physical Review E **106**, 024109 (2022).
  → not covered in the thesis

- M. Moreno-Gonzalez, **J. Dieplinger**, A. Altland, *Topological quantum criticality of the disordered Chern insulator*, Annals of Physics **456**, 169258 (2023).
  → partly covered in chapter 3

- **J. Dieplinger**, S. Bera, *Finite-size pre-thermalization at the chaos-to-integrable crossover*, Physical Review B **107**, 224207 (2023).
  → covered in chapter 8

- A. Altland, P. W. Brouwer, **J. Dieplinger**, M. S. Foster, M. Moreno-Gonzalez, L. Trifunovic, *Fragility of surface states in non-Wigner-Dyson topological insulators*, Physical Review X **14**, 011057 (2024).
  → partly covered in chapter 5

- S. Bera, **J. Dieplinger**, N. P. Nayak, *Quantum Hall criticality in an amorphous Chern insulator*, Physical Review B **109**, 174213 (2024).
  → covered in chapter 4.4

PUBLICATIONS IN PREPARATION

- **J. Dieplinger**, F. Evers, M. Puschmann, *Integer quantum Hall transition in the Chern insulator*, to be submitted in 2024.
  → covered in chapter 4.3

- **J. Dieplinger**, R. Samajdar, R. Bhatt, *Nagaoka ferromagnetism in a long-range repulsive Hubbard model*, to be submitted in 2024.
  → not covered in the thesis

- T. Weber, **J. Dieplinger**, C. Forster, L. Resch, F. Evers, K. Richter, *Classifying localized states as excited states in the localization landscape*, to be submitted in 2024.
  → not covered in the thesis

- **J. Dieplinger**, F. Evers, M. Stosiek, *Spectral gap statistics in dirty superconducting films*, to be submitted in 2024.
  → not covered in the thesis

CONTENTS

1

INTRODUCTION: HOW CAN WE DESCRIBE AND UNDERSTAND COMPLEX SYSTEMS?

Our physical world consists of many degrees of freedom: starting from the number of electrons in a small piece of metal, to all the molecules constituting the atmosphere, interacting due to the interplay of winds, the sun and life (mediated by Coulomb forces), to the number of stars and galaxies in our universe. Consequently, the dynamics of those systems are intractably complex. If a physicist attempted to describe and understand these phenomena by analyzing the interplay of every single degree of freedom with one another – be it the flow of interacting electrons in a computer chip, the emergence of extreme weather, or the dynamics of a supernova – it would most likely be a lost cause from the start[1].

In this context, condensed matter physics is about understanding the interplay of many electrons with each other in the presence of the ionic background of atomic cores constituting a crystalline lattice, for instance in metals, semiconductors or insulators. Condensed matter physics is not about finding the underlying fundamental equations which universally govern the dynamics of our world. On the contrary, these equations underlying any theoretical problem we wish to address have been known for almost 100 years: They are given by the Schrödinger equation of quantum mechanics equipped with some additional corrections originating from special relativity. In the vast majority of problems, the main challenge in condensed matter theory is not to improve the precision of physical constants or to find corrections to underlying fundamental equations (e.g. the standard model). Instead its goal is to establish physical descriptors which reduce the infinite variety of degrees of freedom to few manageable key properties. The challenge consequently boils down to the following question: How can we develop models to separate between these necessary and interesting degrees of freedom and irrelevant details?

It needs to be stressed that what motivates us to develop models that capture the most important microscopic properties of physical system within few effective degrees of freedom is not primarily the desire to simplify the equation so that the mathematical problem – computationally or analytically – becomes tractable. Instead the main motivation is to be able to understand physical systems on

1 Of course there are exceptions where physical phenomena can be – to some degree – understood exactly even if many degrees of freedoms are present, for instance perfect crystals.

the level of (few) observables. Assume for instance we were able to solve the many-electron problem in a metal with $\sim \mathcal{O}(10^{23})$ electrons; the multitude of (irrelevant) details would obscure any insight we wished to gain about the most important and interesting effective degrees of freedom in the first place. Considering this, generating new physical understanding just from the solution to the respective differential equations would remain impossible. Nevertheless, it is exactly that multitude of degrees of freedom which make emergent phenomena possible, such as those so interesting in condensed matter physics, e.g. collective excitations, for instance charge-density waves.

Since the invention of quantum mechanics (and even before), concepts to separate important from unimportant degrees of freedom have been developed, which may be organized in three categories, discussed in the following paragraph and in sections 1.1 and 1.2:

SEPARATION OF SCALES. Maybe historically the first and most extensively used approach is the separation of scales, e.g. in the energy, length or time domain: applied to a specific physical system, one searches e.g. for different energy contributions relevant in the problem and separates low-energy from high-energy sectors. Often, it is possible to obtain a so-called *low-energy effective theory* along these lines. In many applications, this method is closely related to perturbation theory of quantum mechanics. A very common (and possible one of the historically first) application of this approach in (quantum) condensed matter theory is the Born-Oppenheimer approximation (Bruus and Flensberg, 2004)[2].

This simplification assumes that the Schrödinger equation of electrons and nuclei in a molecule or solid can be separated into the motion of fast electrons with fixed nuclei positions on the one hand and the slow movement of the nuclei on the other hand. The energy scales allowing for this separation into the electronic sector and the ionic sector are given by the vastly different masses of electrons and nuclei. The interplay between both subsystems can be reintroduced by perturbation theory (or similarly by a Schrieffer-Wolff transformation) giving rise to phenomena governed by electron-phonon coupling, for instance the Bardeen-Cooper-Schrieffer (BCS) theory of superconductivity (Bardeen *et al.*, 1957; Bruus and Flensberg, 2004).

There are of course many more famous examples of physical phenomena captured by this separation of energy scales, which eventually lead to an effective low-energy theory. Examples are the hydrogenic structure of excitons in semiconductors (Giuliani and Vignale, 2008) and the ferromagnetic or antiferromagnetic properties of strongly correlated electrons in Hubbard-like systems (Sachdev,

2 Also in classical theories of condensed matter the method of separating scales has been used to find low-energy theories, for instance when describing transport as a diffusion process.

2011). Low-energy theories of the form described above lie at the core of almost any phenomenon successfully understood in condensed matter theory[3].

Theoretical physics attempts to generalize this approach further: Instead of developing an effective theory that describes physical phenomena in a system governed by a single Hamiltonian, the goal is to make statements about an entire class of systems. In particular, instead of developing a specific model for a specific physical material subject to a specific physical experiment, we want to understand generic properties of materials and classes of models which may be subject to impurities and imperfections which we are unable to grasp microscopically.

A prime example for this generalization to material classes is the quantum Hall effect. The transverse conductivity of an electronic sample σ_{Hall} subject to a large magnetic field at low temperatures is precisely quantized to a multiple of the fundamental ratio between Planck's constant h and the electronic charge e, i.e.

$$\sigma_{\text{Hall}} = \frac{e^2}{h} \cdot n, \tag{1}$$

where n is an integer or a fractional (Klitzing *et al.*, 1980; Laughlin, 1983). This result is striking because it holds to an extreme precision for a vast variety of materials, a wide range of electronic densities, magnetic field strengths, impurity concentrations and other system specific microscopic details. In other words, the quantization of the Hall conductivity is *universal*.

The striking universality present in many physical systems, most prominently in the quantum Hall effect, calls for a similarly universal methodological approach to describing them. Apparently, when treating each specific physical system separately, the underlying universality is overlooked.

In physics, universality can be found across different system parameters and even across a variety of different platforms. While the quantum Hall effect will play a major role in this thesis, also the long-time dynamics of generic interacting systems tend towards universal behavior in a very different sense compared to the quantum Hall effect: for instance the molecular constituents of the world's oceans and atmosphere and the electrons moving in strongly interacting quantum matter are subject to completely different microscopics. Nevertheless, eventually, both can – in some limits – be successfully described by a variant of hydrodynamics, with very few state variables, for instance temperature and density and some macroscopic material parameters, such as viscosities (Vallis, 2006; Rotunno, 2013; Succi, 2018; Polini and Geim, 2020). Why is this possible despite the strikingly different microscopics?

Two fundamental concepts, which go way beyond condensed matter theory and can be applied to many different scientific fields, play a major role in answering this question. Both are of paramount importance for this thesis: the mathematical concept of topology and symmetries as well as the toolbox of statistical mechanics.

3 Even the Schrödinger equation and quantum mechanics itself is an effective low-energy theory which can be derived from the Dirac equation.

1.1 STATISTICAL MECHANICS, THERMALIZATION AND ITS BREAKDOWN

The basic assumption of statistical mechanics is that systems of many particles – regardless if classical or quantum, or the exact microscopics they underlie – equilibrate while they involve in time. The resulting state is determined purely by macroscopic, averaged quantities, for instance energy and particle density or temperature. In other words, the physical system – while evolving in time – forgets all the details about its initial state from which it started to evolve. The final, in that sense universal, state is called *thermal equilibrium* (Landau and Lifshitz, 1976; Nandkishore and Huse, 2015).

This approach has been incredibly successful at describing, understanding and modeling complex systems. Even many physical systems which do not fulfill the prerequisites of thermodynamics, for instance driven systems like the earth's oceans, can locally be approximated by a thermal state with local thermodynamic quantities, like temperature, density and current fields. This gives rise to a coarse-grained theory of complex systems which still hosts non-trivial dynamics (described by a hydrodynamic theory in this case). It is an *effective theory* in the sense that the microscopic degrees of freedom – e.g. the momentum of individual water molecules – have been integrated out and no longer play a role in the dynamics. Instead, they collectively contribute to emerging properties of matter, e.g. the viscous flow of water.

In particular the second part of this thesis is devoted to discussing systems of many strongly interacting quantum particles evolving towards thermal equilibrium. Searching for generic classes of systems that escape thermalization and retain memory of their initial dynamics forever is of fundamental interest.

1.2 TOPOLOGY AND THE BULK-BOUNDARY CORRESPONDENCE

The second important concept in this thesis, which allows to find universality across very different platforms, is topology.

The mathematical concept of topology as we understand it in theoretical physics allows us to organize a family of systems into equivalence classes which cannot be continuously deformed into each other. This is often illustrated by the famous example of a cup with a handle and a doughnut being topologically equivalent in terms of how many "holes" (mathematically defined as *genus*) they have. On first glance, finding properties which can be distinguished by classifying them into separate equivalence classes should not be difficult. Similar to the cup and the doughnut one could for instance classify physical samples of metals according to their number of "holes". When trying to gain information about the electronic transport of such samples, this of course is not useful. The number of holes in the geometry of the sample will usually not tell us anything about how much current will flow when applying a voltage. Consequently, it is indeed very easy to find some way to categorize physical systems into groups of certain discrete

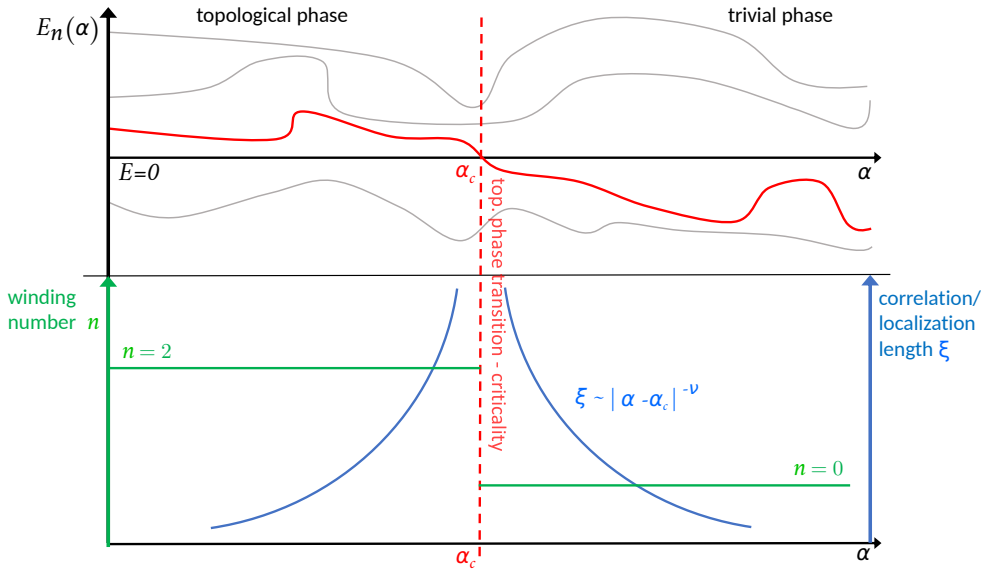

Figure 1: Sketch of a topological phase transition driven by energy bands crossing zero energy. The parameter α deforms a Hamiltonian $\mathcal{H}(\alpha)$ with energy bands $E_n(\alpha)$. When one of the energy bands crosses zero energy at the critical point α_c a topological phase transition occurs. The winding number (here the difference between bands above and below zero energy) jumps and an accompanying correlation or localization length scale diverges, just as in regular second order phase transitions. The divergence is governed by a power law with a critical exponent ν. In the presence of disorder the topological and the trivial phases are typically Anderson insulators (in one or two dimensions), while the critical point hosts a delocalized state. The associated length scale is the localization length and the exponent ν the localization length exponent in the asymptotic limit.

properties; but this is only interesting if we are able to connect these categories to the observables we are interested in and have access to.

The following paragraph is devoted to motivate and explain the basic idea of topology in condensed matter and how it relates to the overall goal of describing very different physical systems efficiently using few topological degrees of freedom, so-called topological invariants. It is partly inspired by the course on topology in condensed matter by Akhmerov *et al.*, 2021, which offers an intuitive but thorough introduction into the broad theme of topology in condensed matter theory.

Consider a very simple physical system where we are mainly interested in electronic transport: a quantum dot, i.e. zero-dimensional quantum system governed by some (unspecified) Hamiltonian connected to a lead or bath whose sole purpose it is initially to fix the chemical potential (henceforth defining the zero energy base line). The quantum dot has several energy levels, some of which lie below and some above zero energy. To classify the system topologically, we now count the energy levels above and below zero energy and calculate their difference n. This number n is clearly a topological invariant, since n can

only change by levels crossing zero energy when deforming the Hamiltonian parameters. When a zero-crossing happens, the topological invariant changes by unity, and a so-called topological phase transition has occurred. The situation is depicted in Fig. 1.

However, whether this is a *useful* topological classification scheme remains questionable. With the current experimental setup this has to be negated as there is no obvious way to connect e.g. the conductance of the quantum dot to this number. The conductance at the Fermi level is zero unless the system is fine-tuned to be just at the critical point of the transition.

We can take this idea a little further. Let us consider an extended system instead of a quantum dot, take for simplicity a one-dimensional quantum wire, and instead of energy levels we consider energy bands. The topological invariant is now understood as the difference of the number of bands above and below zero energy.

To obtain topologically protected transport properties only one additional ingredient is required: a *topologically trivial* reference system, to which we can deform our original system and with respect to which we measure the topological invariant. The atomic limit of a crystal, for instance, can become the trivial reference system, where all wave functions are localized to a single atom. If the original system is now deformed continuously to the reference system, it is dubbed *topologically trivial* if no phase transition, i.e. zero crossing, occurs; and non-trivial if it crossed a finite number of phase transitions.

Usually, in real experiments samples have boundaries in real space. While the sample may be topological, outside of the boundary the vacuum or substrate has to be topologically trivial by definition. It is possible to reinterpret the continuous deformation parameter we encountered in the very beginning of this discussion as the real space coordinate in which the sample is cut, as illustrated in Fig. 2. Then a topological phase transition must occur at the spatial boundary of the sample, if and only if the original sample has a non-trivial topological invariant of its bulk. This means that the boundary of a topological bulk always resides directly at the critical point of the topological phase transition (at the Fermi energy), rendering it a conducting *boundary state*. Because both the topological phase of the sample as well as the trivial phase of the substrate are stable against local perturbations and the microscopic details do not play a role (as long as no further phase transitions are crossed), this is a generic feature.

Illustrated in Fig. 2, the described principle, connecting an insulating, topologically non-trivial bulk with a protected conducting boundary, is called *bulk-boundary correspondence*, and lies at the heart of the popularity of topological insulators and superconductors in condensed matter physics (Hasan and Kane, 2010; Qi and Zhang, 2011; Bernevig and Hughes, 2013; Ando and Fu, 2015). Some famous examples are the zero-dimensional Majorana fermions at both ends of a finite-size Kitaev chain, the edge states in the quantum Hall effect or the surface

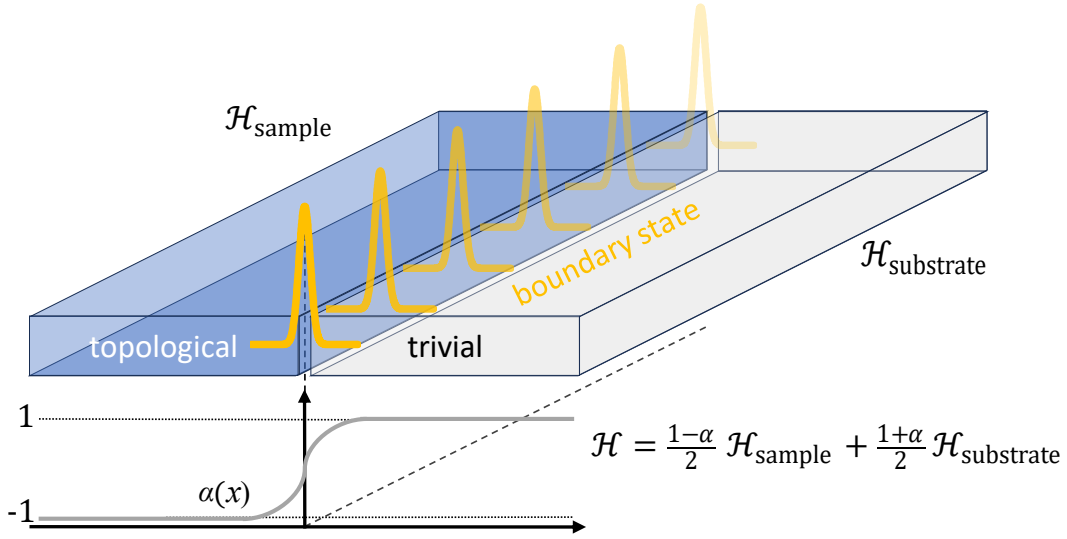

Figure 2: Illustration of the bulk-boundary correspondence in topological matter. A topological sample is connected to a trivial substrate. The interface/boundary is modeled by the function $\alpha(x)$, interpolating between sample and substrate Hamiltonians as a function of the real space coordinate x. At the boundary, a topological phase transition occurs, i.e. an energy level crosses the Fermi level. This zero energy state (orange) is protected, since both substrate topology (trivial) and sample topology (non-trivial) are stable against small (local) perturbations, rendering the boundary conducting, while both bulk and substrate are insulators.

states of three-dimensional topological insulators[4] (Su *et al.*, 1979; Haldane, 1988; Kane and Mele, 2005; Teo and Kane, 2010; Ryu *et al.*, 2010; Akhmerov *et al.*, 2021).

1.3 Outline: Single-particle and many-body systems with disorder

Topology and the bulk-boundary correspondence as well as the toolbox of statistical mechanics and the investigation of the conditions of thermalization provide concepts for understanding generic quantum systems. These concepts allow us to treat single systems with many degrees of freedom as an effective theory with few relevant parameters[5]. Thereby, they additionally enable a more general description across a wide range of physical platforms and microscopic realizations.

4 There are many additional ways of topology entering theoretical physics, beyond the bulk-boundary correspondence. For instance so-called skyrmions are collective excitations of spins in magnetic materials which are topologically protected due to their special defect structure. These instances of topology in materials do not play a role in the remainder of this thesis and are therefore not covered in this introduction.

5 The meaning of *"relevant" vs. "irrelevant"* in this discussion does not necessary imply a context of renormalization group (RG) flow, e.g. at phase transitions.

Such concepts are particularly important if we want to include imperfections and defects in materials in our theory: Related phenomena in individual samples with an individual defect structure are often difficult to understand in theory, moreover, usually we cannot access the microscopic nature of single disorder realizations in experiments. Therefore, in practice, useful theories describe disordered samples usually on the level of statistical ensembles of their disorder realizations.

Imperfections are often viewed as unwanted in technological applications, seeing as they may obscure desired physical properties, for instance in the production of semi-conductor chips for electronic devices. Nevertheless, disorder can also lead to qualitatively new physical phenomena. Most famously, Anderson, 1958 has shown that under some conditions disorder can render electronic wave functions completely localized to small spatial regions, in contrast to Bloch waves extending over the entire sample. The reason is that electrons are scattered coherently and their quantum mechanical paths interfere constructively. Therefore, the electronic probability density may become suppressed in almost the entire physical sample. Consequently – because localized wave functions cannot carry current – disorder may induce metals to become (Anderson) insulators.

This so-called Anderson localization is very generic. Its appearance only depends on a very small number of characteristics of a model system, such as the presence or absence of electron-electron interactions, the spatial dimension of a sample and some key symmetries of the underlying Hamiltonian (Lee and Ramakrishnan, 1985; Evers and Mirlin, 2008; Altland and Simons, 2010). Therefore, it will play a fundamental role in all aspects of this thesis.

OUTLINE OF THE THESIS. The aspects of disordered physics covered in this thesis are diverse – they will span from the integer quantum Hall effect to three-dimensional topological insulators to thermalization and its breakdown in genuine many-body interacting physics. Nevertheless, the phenomenon of wave function localization due to disorder will play a role in each of these topics.

The integer quantum Hall effect is the protagonist of the first part of the thesis. Within those chapters disordered single-particle systems are investigated where Anderson localization is generically present. The quantum Hall effect is the archetype of a system where wave functions are protected against localization and remain conducting by mechanisms of the bulk-boundary principle.

Following the introduction and outline, in chapter 2 the reader is provided with some background regarding Anderson localization on the one hand and the topological description of disordered Hamiltonians on the other hand. A first study of the interplay between the two concepts is introduced in chapter 3, where the phase diagram of a model of the anomalous quantum Hall effect is investigated and some concepts, like the relationship between bulk and edge spectra in topological materials are discussed, providing the basis for the following chapters. The results presented here have been published in Moreno-Gonzalez *et al.*, 2023.

The transition between different quantum Hall plateaus of quantized conductivity is of paramount interest in assessing if the underlying theory is truly universal. In chapter 4 two models of the anomalous quantum Hall effect are studied using large-scale high-precision numerical simulations. Thereby, the critical exponents of the localization length diverging at the plateau transitions are determined and compared to literature results. In contrast to recent beliefs, the observed critical exponents are found to be in full agreement with different models of the integer quantum Hall effect. The study presented is therefore consistent with universality in the quantum Hall symmetry class A. The results of section 4.4 have been published in Bera *et al.*, 2024.

Chapter 5 connects the integer quantum Hall plateau transition with different symmetry classes, here in particular a chirally symmetric topological insulator in three dimensions (class AIII). Interestingly, quantum Hall criticality is found – to some degree generically – on the surfaces of these systems. Here we determine the conditions for this observation and the breakdown of extended surface states, which is again deeply connected to a fundamental principle of the quantum Hall effect: the question if the bulk states of a topological insulator can or cannot be fully localized. Many aspects of this chapter are published in Altland *et al.*, 2024. The results have profound consequences on the applicability of minimal Dirac models for surface states of topological insulators and their breakdown even for such fundamental properties of wave functions as localization vs. delocalization.

The focus of part II lies on introducing interactions to disordered Hamiltonians. In many-body physics, the absence or presence of localization is an open question: Complex correlations in Hamiltonian matrix elements as well as the exponentially large Hilbert or Fock space complicate theoretical investigations. The fate of the localized phase in many-body systems remains unknown. Anderson's argument for localization in single-particle models requires coherent scattering of electronic paths with impurities. However electron-electron interactions induce decoherence. Many-body quantum systems hence generically thermalize while non-thermalizing or integrable systems remain rare or only available when fine-tuning Hamiltonian parameters. The mechanism of thermalization and one possible approach to finding generic many-body localized systems with the help of disorder is discussed in chapter 6.

Available toy models where many-body localization can be approached rigorously often do not have a microscopic justification. Chapter 7 attempts to bring a special class of these model Hamiltonians closer to microscopic realism. The model is based on the famous Sachdev-Ye-Kitaev Hamiltonian and hosts many-body integrable and thermal phases, which are accessible to analytical and numerical approaches. While we still keep the infinite range of interaction and hopping terms present in the model, the interaction structure is reduced to a density-density form reminiscent of real space Coulomb repulsion. This model is shown to have a rich phase diagram hosting some of the regimes also present in

the much better understood extended Sachdev-Ye-Kitaev model. The results of this chapter are published in Dieplinger *et al.*, 2021.

In chapter 8 the dynamical properties of a model hosting an ergodic-integrable transition are investigated. Dynamical observables are potentially accessible in experiments, such as the density-density correlation functions. Here, the underlying question is how the dynamics of key properties change when the localized regime is approached from the ergodic side. Is there a power-law with a decreasing exponent, which slows down the time evolution when approaching localization? Or is there a sudden change in the behavior from a pre-thermal time window to actual thermalization associated with a cross-over time scale, which could be interesting for intermediate time quantum memory even in a thermalizing system? It turns out that in the class of systems investigated the latter is the case. Those results have been published in Dieplinger and Bera, 2023.

Finally, chapter 9 offers a conclusion and a final discussion of the topics covered, and provides an outlook on potential future developments.

Part I

TOPOLOGY, QUANTUM HALL EFFECT AND LOCALIZATION

2

DISORDERED SYSTEMS: ANDERSON LOCALIZATION AND TOPOLOGY

2.1 IMPURITIES IN TRANSLATIONALLY INVARIANT CRYSTALLINE LATTICES

Most condensed matter problems can be described by many electrons moving and interacting in the potential of their ionic cores (Bruus and Flensberg, 2004; Giuliani and Vignale, 2008),

$$\mathcal{H} = \mathcal{H}^{\text{e}}_{\text{kin}} + \mathcal{H}^{\text{e-e}}_{\text{int}} + \mathcal{H}^{\text{ion}}_{\text{kin}} + \mathcal{H}^{\text{ion-ion}}_{\text{int}} + \mathcal{H}^{\text{ion-e}}_{\text{int}}. \tag{2}$$

The summands describe the kinetic energy of electrons, the interaction between electrons, the kinetic energy of the ionic cores, the interaction between the ions, and the interaction between ions and electrons. The microscopic constituents are unquestioned – the underlying interaction is always the Coulomb interaction and the parameters (for instance the electronic mass and charge) are known precisely for the purposes of condensed matter theory. However, this Hamiltonian is usually impossible to deal with in practice. The number of degrees of freedom is just too large for any computer or human to deal with, and the information relevant for experiments – e.g. local observables – becomes hidden in the exponentially large Hilbert space.

Therefore, theorists rely upon a number of tools, such as the Born-Oppenheimer approximation, essentially decoupling the electronic problem from the ionic movements, or even as drastic simplifications as neglecting electron-electron interactions all together. These concepts and many more are often implicitly applied and also used in this thesis.

One of the most prominent approximations specific to condensed matter is that of a translationally invariant ionic crystal. When materials condense to a solid they usually minimize the ground state energy of the ionic positions in real space by forming a crystalline lattice. When considering a single electron in the potential of such a crystal the problem defined in Eq. (2) reduces to

$$\mathcal{H} = \mathcal{H}^{\text{e}}_{\text{kin}} + \mathcal{H}^{\text{ion-e}}_{\text{int}} = -\frac{\hbar^2}{2m}\nabla^2_{\mathbf{r}} + V(\mathbf{r}) \quad \text{with} \quad V(\mathbf{r}) = V(\mathbf{r}+\mathbf{R}), \tag{3}$$

where $\mathbf{R}$ is an arbitrary lattice vector. Famously, the Bloch theorem states that the wave functions $\psi(\mathbf{r})$ of this Hamiltonian are lattice periodic in $\mathbf{r}$ up to a phase,

$$\psi(\mathbf{r}) = e^{i\mathbf{k}\mathbf{r}}u(\mathbf{r}), \tag{4}$$

where $u(\mathbf{r})$ is a lattice periodic function and $\mathbf{k}$ the crystal momentum (Bloch, 1929).

Consequently, the wave functions in a perfect crystal resemble those of a free electron gas: They are extended Bloch waves with a crystal (quasi-) momentum $\mathbf{k}$. The exact symmetries of the lattice, its basis, and particle and energy density then classify their electronic properties into metals, semi-conductors and band insulators (Bruus and Flensberg, 2004). Their conductance properties are therefore prominently determined by the relative position of the energy bands of this periodic single-electron problem with respect to the chemical potential, fixed by leads or thermal baths connected to the sample.

While incredibly many phenomena in condensed matter physics can be explained within this picture or variations of it, qualitatively new things happen when electrons scatter with many impurities while traversing the crystal: The basic assumption being responsible for the very emergence of the band structure picture and consequently the classification of materials according to their energy bands breaks down – translational invariance in real space. The quasi-free motion of electrons in the crystal becomes perturbed. In nature this is of course true in general; no naturally occurring crystalline sample will be of perfect purity.

Theoretically, this fact can often be incorporated in the established theory of translationally invariant crystals. Phenomenologically, when studying the conductivity of a metal, one can for instance introduce a friction term of electrons with some "scattering time" after which the electron collides with impurities, giving rise to a successful description of electrons in samples with few scattering centers within Drude theory (Giuliani and Vignale, 2008). In other instances, single (magnetic) impurities can generate fascinating new physics, which can be described microscopically within "clean" condensed matter theory. A famous example is the Kondo effect, describing fluctuating spins on a magnetic impurity, giving rise to a stable zero energy peak of the conductance of the impurity (Kondo, 1964).

In this thesis the focus will lie on a different regime: the limit of large impurity concentrations. Here translational invariance is broken throughout the sample, and the clean limit may not suffice even on a qualitative level to capture the electronic properties of such systems. Multiple successive scattering events of electrons render their wave function qualitatively different from the Bloch waves introduced in Eq. (4).

Strikingly, a large impurity concentration can fully localize the wave function of a single electron moving in a metallic[1] sample (neglecting electron-electron interaction) to a very small spatial region. This wave function, since it is exponentially suppressed in most of the sample does not resemble the Bloch wave character of a free electron, cannot carry electronic current, rendering the sample insulating. The mechanism underlying this localization phenomenon is the following: A single electron is scattered from many impurities. Classically, the electron would diffuse and eventually extend over the entire real space, analo-

1 when neglecting disorder, in the sense of a band metal

gously to a random walk. Quantum mechanically, however, additional paths of the electron wave function emerge, which constructively interfere at the point of origin of the electron. When these modes dominate the wave function amplitude over the diffusing modes, the electron gets "stuck" and localizes; diffusion is suppressed. This process of constructive interference in the return probability of coherently scattering electrons was predicted by P. W. Anderson in 1958 and has been called Anderson localization (Anderson, 1958; Abrahams *et al.*, 1979; Altland and Simons, 2010).

2.2 ENSEMBLES OF DISORDERED HAMILTONIANS

Introducing disorder to a physical sample comes with a conceptual problem: Theorists do not know (and do not need to know) the microscopic realization of the impurities. However, we still need to be able to make a statement about individual samples (which have individual microscopic realizations of disorder). Experiments teach us that different disordered physical samples can be treated on equal grounds; two pieces of some metal have roughly the same electronic properties even though they certainly have impurities of different strengths and at different microscopic positions. The important fact is that they have the same macroscopic properties, such as homogeneity, temperature, (average) electronic density and (average) impurity concentration.

Consequently, also in theory it often makes sense to not deal with individual Hamiltonians with specific realizations of disorder but with ensembles of disordered Hamiltonians, which all have different microscopics but whose disorder realizations are drawn from the same probability distribution.

To still be able to make meaningful statements about experimental samples, which actually feature a specific microscopic realization of the disorder ensemble the concept of *self-averaging* plays a role: A large macroscopic sample can be partitioned in N small – still macroscopic – parts, with the same physical properties as the full sample, such as the distribution function from which the impurities are sampled. Evoking the law of large numbers then the measured observable of the full sample is given by the average over all parts and the fluctuations vanish with $\sim 1/\sqrt{N}$. Therefore, most experimental samples can be treated on equal grounds as an ensemble of disordered Hamiltonians in theory (Landau and Lifshitz, 1976).

In the following chapters the generalization of statements regarding transport and localization will not only go beyond individual Hamiltonians but even further. Eventually, the goal is to make universal statements about the transport properties and the localization properties of model systems which are characterized by very few, very general properties of their Hilbert space, namely its spatial dimension and some of its key symmetries.

Two forms of localization/delocalization problems can be studied: First, one may examine the localization properties of the bulk of a d-dimensional lattice. This can be most easily illustrated with the Anderson model

$$\mathcal{H} = -t \sum_{\langle i,j \rangle} c_i^\dagger c_j + \sum_i \epsilon_i c_i^\dagger c_i, \tag{5}$$

with t being the hopping energy, $c_i^\dagger (c_i)$ fermionic creation (annihilation) operators, $\langle \cdot, \cdot \rangle$ the sum over nearest neighbor on a d-dimensional hyper-cubic lattice, ϵ_i a random number drawn from a box distribution $\epsilon_i \in [-W/2, W/2]$, and W the disorder strength parameter. The phase diagram in terms of (de)localization is fairly simple. While at dimensions $d \leqslant 2$ all states of its spectrum (Anderson) localize, rendering the Hamiltonian generically insulating, at dimensions $d \geqslant 3$ up to a critical disorder strength W_c delocalized extended states can be found in a finite central region of the energy spectrum (Thouless, 1974; Wegner, 1976; Abrahams *et al.*, 1979). The localization-delocalization (LD) transition at W_c is a metal-insulator transition, with diverging length scales at criticality; similar to regular second order phase transitions.[2] The localization length ξ, characterizing the wave functions on the localized side of the transition, diverges at the critical point with a power law governed by the critical exponent ν.[3] The localization length exponent ν is a characteristic fingerprint of the type of LD transition (Evers and Mirlin, 2008).

The second category of (de)localization appears at the boundaries of topological systems, realizing the bulk-boundary correspondence. Assuming that a bulk topological insulator[4] in d dimensions has an energy/mobility gap[5] around zero energy, at the edges it has extended conducting states in $d-1$ dimensions. Those edge states are a direct consequence of the topological system undergoing a phase transition into a trivial phase. This phase transition can also be investigated

2 Henceforth, LD transitions will be treated with the same terminology as second order phase transitions. It is however a subtle subject, since it is not fully obvious which observable can represent a local order parameter. While conductivity seems to be a good choice for an order parameter, it is not local, since it essentially relies on a two-point correlation function. Formalizing the problem it is widely believed that the objects (Q-matrices) entering σ-models – describing many aspects of disordered Hamiltonians – may serve as an appropriate local order parameter. The details of this description are not important for the thesis; the reader is referred to reviews on Anderson transitions, e.g. by Evers and Mirlin, 2008. For all relevant purposes, e.g. the divergence of a correlation or localization length scale at the critical point, a description based on the theory of second order phase transitions is sufficient.

3 Additional critical exponents appear, which govern the finite-size corrections before the system is in the asymptotic limit of infinite size.

4 In this thesis the term topological insulator refers to all dimensions, not only three-dimensional materials; it includes for instance also the anomalous quantum Hall effect.

5 corresponding to the band gap in a clean translationally invariant system, which may be decreased by disorder

in infinite bulk crystals by varying the system parameters analogously to the conventional LD transitions, for instance the disorder strength W. The extended states at the boundary of a finite system reappear at the critical point of the phase transition, now having support on the entire Hilbert space of the d-dimensional bulk crystal. In contrast to conventional LD Anderson transitions discussed in the previous paragraph, these transitions are so to speak localization-localization or insulator-insulator transitions, since on both sides of the critical point only insulating localized states are found around the Fermi energy. Often, for instance in the quantum Hall effect, isolated energies with a critical extended state can be identified at high or low energies far away from the Fermi level in the topological phase (Laughlin, 1981).

These localization-localization transitions can be characterized very similarly to the conventional Anderson LD transitions: They are reminiscent of second order phase transitions, at which the localization length exponent diverges as a power law with a critical exponent ν. They are different from conventional LD transitions in so far that their phases are not characterized by a *local* quantity, for instance the local density of states. Instead the topological phase is given by a single *global* quantity namely the topological invariant n (Evers and Mirlin, 2008; Ryu *et al.*, 2010).

2.4 TEN-FOLD WAY OF CLASSIFYING DISORDERED HAMILTONIANS

Topological as well as conventional Anderson transitions can be characterized by their behavior at the critical point in some analogy to thermodynamic second order phase transitions. Key fingerprints are for instance the localization length exponent ν, the scaling of the wave function at the critical point or the conductivity at the critical point (Evers and Mirlin, 2008). Before characterizing Anderson transitions in various settings, it is important to know for which kind of systems those transitions can even exist.

Therefore, theorists have tried to find categories how to classify disordered Hamiltonians or topological insulators. In contrast to theories dealing with specific samples or experimental setups, those categories have to be somewhat generic; they should not depend too much on the details of the microscopics. The exact form of the probability distribution of the disorder potential should for instance not influence the possibility of topologically protected boundary states or the exponent governing the localization length at the LD transitions[6].

One key parameter which is of great importance for the existence and the nature of Anderson transitions is the spatial dimension d. We already saw for instance that a LD transition in models similar to Eq. (5) is not possible for $d = 1, 2$ (Abrahams *et al.*, 1979).

6 Here we always assume that the disorder potential is uncorrelated or only short-range correlated.

Cartan label	T	P	C	$d=1$	$d=2$	$d=3$
A (unitary)	0	0	0	0	$\mathbb{Z}$	0
AI (orthogonal)	+1	0	0	0	0	0
AII (symplectic)	−1	0	0	0	$\mathbb{Z}_2$	$\mathbb{Z}_2$
AIII (ch. unitary)	0	0	1	$\mathbb{Z}$	0	$\mathbb{Z}$
BDI (ch. orthogonal)	+1	+1	1	$\mathbb{Z}$	0	0
CII (ch. symplectic)	−1	−1	1	$2\mathbb{Z}$	0	$\mathbb{Z}_2$
D (BdG)	0	+1	0	$\mathbb{Z}_2$	$\mathbb{Z}$	0
C (BdG)	0	−1	0	0	$2\mathbb{Z}$	0
DIII (BdG)	−1	+1	1	$\mathbb{Z}_2$	$\mathbb{Z}_2$	$\mathbb{Z}$
CI (BdG)	+1	−1	1	0	0	$2\mathbb{Z}$

Table 1: Classification of toplogical materials according to the spatial dimension d and fundamental symmetries $\mathcal{T}, \mathcal{P}, \mathcal{C}$ in Wigner-Dyson (top rows), chiral (center rows) and Bogoliubov-de Gennes (bottom rows) classes. The column 'Cartan label' lists the name of the symmetry class according to the symmetry space of the corresponding Hamiltonian given by Élie Cartan in 1926. The symbols $\mathbb{Z}, \mathbb{Z}_2$ indicate the type of invariant provided a topological insulator is possible and here 0 denotes cases where no topological phase can exist. The integer quantum Hall effect is realized in class A. Adapted from Ryu *et al.*, 2010.

The other fundamental concept categorizing ensembles of Hamiltonians are symmetries, because they may also survive perturbations of the microscopic details of Hamiltonians (Ryu *et al.*, 2010).

Unitary symmetries lead to conservation laws, for instance the translational invariance of space is responsible for the conservation of momentum. In quantum mechanics such conservation laws structure the Hilbert space, whose basis can be transformed in such a way that the Hamiltonian of the system is brought to a block diagonal form. The blocks then correspond to the symmetry sectors, characterized by quantum numbers, such as momentum eigenvalues. This type of symmetry can of course also be used in ensembles of disordered Hamiltonians, as long as the disorder respects the underlying symmetry. For instance this is often the case with particle number conservation in many-body systems. Consequently, the properties of these ensembles can be determined separately for each symmetry block or quantum number. Unitary symmetries in that sense allow for a reduction of the complexity of the problem but do not have any further qualitative influence on the properties of the system, in particular on the existence and details of topology and localization.

However, there is an additional class of *non-unitary* symmetries; they do not enable us to block-diagonalize the Hamiltonian, and therefore must have a more subtle influence on its (topological) properties.

These are the three fundamental discrete symmetries, namely time-reversal $\mathcal{T}$, particle-hole $\mathcal{P}$, and chiral $\mathcal{C}$ symmetry (Altland and Zirnbauer, 1997; Ryu *et al.*, 2010). They cannot be expressed as a unitary symmetry and thus do not generate a conservation law; they can rather be understood as "reality conditions" imposed on the Hamiltonian $\mathcal{H}$. Time-reversal symmetry can be expressed by invariance of $\mathcal{H}$ under the operation

$$\mathcal{T} : \mathcal{U}_{\mathcal{T}}{}^{\dagger}\mathcal{H}^{*}\mathcal{U}_{\mathcal{T}} = \mathcal{H}, \tag{6}$$

where $\mathcal{U}_{\mathcal{T}}$ is a unitary matrix, rendering the time-reversal operation $\mathcal{T}$ anti-unitary. The charge-conjugation or particle-hole symmetry can be understood along the same lines, as $\mathcal{H}$ satisfying

$$\mathcal{P} : \mathcal{U}_{\mathcal{P}}{}^{\dagger}\mathcal{H}^{*}\mathcal{U}_{\mathcal{P}} = -\mathcal{H}. \tag{7}$$

Finally, the Hamiltonian can also be classified by its behavior under the transformation

$$\mathcal{C} = \mathcal{T} \cdot \mathcal{P}, \tag{8}$$

which is called chiral symmetry operation.

Now, invariance of $\mathcal{H}$ under $\mathcal{T}, \mathcal{P}$ can either be absent (in this we usually write $\mathsf{T}, \mathsf{P} = 0$), or present where $\mathcal{T}, \mathcal{P}$ either square to plus or minus the identity operator. In these cases we write $\mathsf{T}, \mathsf{P} = -1, +1$.

This consideration renders 9 possibilities for the symmetry properties of $\mathcal{H}$. In 8 of them the behavior under $\mathcal{C}$ is uniquely fixed, while in one case, $\mathsf{T}, \mathsf{P} = 0$, chiral symmetry can either be present or absent, i.e. $\mathsf{S} = 1, 0$. In total this gives rise to ten possible *symmetry classes*, summarized in Table 1 (Altland and Zirnbauer, 1997; Ryu *et al.*, 2010).

2.5 EXAMPLE: INTEGER QUANTUM HALL EFFECT IN CLASS A

The most famous of the above possibilities is class A, realizing none of the three fundamental symmetries. It is the symmetry class which hosts the integer quantum Hall effect (IQHE).

The IQHE arises in a very simple setting: a two-dimensional free electron gas moving in a strong magnetic field. The underlying microscopic Hamiltonian hence is often described as

$$\mathcal{H} = \frac{(\mathbf{p} + e\mathbf{A})^2}{2m}, \tag{9}$$

where $\mathbf{p}$ is the two-dimensional free momentum operator, m the electronic mass, e the electronic charge and $\mathbf{A}$ the vector potential giving rise to a constant out-of-plane magnetic field $\mathbf{B} = \mathrm{curl}\,(\mathbf{A})$, introduced by minimal coupling.

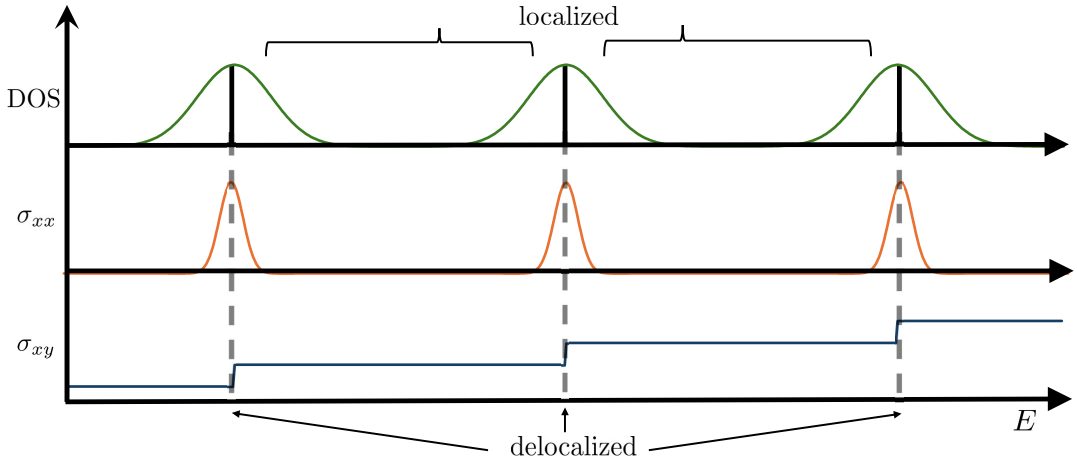

Figure 3: Quantum Hall plateaus and plateau transitions. At the top the density of states resembling disordered Landau bands is shown as a function of energy. In the center of the Landau bands at isolated energies wave functions are protected against Anderson localization. At those energies the longitudinal conductivity of a sample is finite, while in the localized regime in between it is zero. Due to the formation of edge states in the localized phases plateaus of quantized transverse conductivity develop, Altland and Simons, 2010.

Without loss of generality the electrons can move in the $x-y$-plane of a three-dimensional coordinate space, such that the magnetic field is pointed in z-direction, i.e. $\mathbf{B} = (0, 0, B)$. Fixing the gauge of $\mathbf{A}$ to the Landau gauge, one chooses $\mathbf{A} = (0, Bx, 0)$.

Hence, the Hamiltonian reduces to

$$\mathcal{H} = -\frac{1}{2m}\left[\frac{\partial}{\partial x}^2 + \left(\frac{\partial}{\partial y} + eBx\right)^2\right], \tag{10}$$

in real space, allowing for a separation ansatz of the Schrödinger equation $\mathcal{H}\psi_j(x,y) = E_j\psi_j(x,y)$ using a wave function of the form $\psi_j(x,y) = e^{-ik_y y}a_j(x)$.

The remaining x-dependent equation for a_j accordingly reads

$$\left[-\frac{1}{2m}\frac{\partial}{\partial x}^2 + \frac{m\omega_c^2}{2}(x-x_0)^2\right] a_j(x) = E_j a_j(x). \tag{11}$$

This resembles the harmonic oscillator and renders eigenvalues

$$E_j = \omega_c(j+1/2), \tag{12}$$

where $\omega_c = eB/m$ is the classical cyclotron frequency and $x_0 = -k_y/eB$ the orbit center (Giuliani and Vignale, 2008).

These are the highly degenerate (one state per flux quantum) *Landau levels* E_j where the number of flux quanta is $N_\phi = BA/(h/e)$. The system is filled with $N_e = nA$ electrons on a sample of area A, and an electrical field E_x in x-direction.

The current is given by $I \sim en v_D w$, where due to the magnetic field the drift velocity is $v_D = E_x/B$. The Hall voltage is given by $V_H \sim B v_D w$, resulting in the conductivity,

$$\sigma_{\text{Hall}} = \frac{I}{V_H} = \frac{N_e}{N_\phi} \times \frac{e^2}{h}, \tag{13}$$

where N_e/N_ϕ is the filling factor of the Landau levels. This calculation gives rise to the (linear) envelope function $\sigma_{\text{Hall}} \propto n$, with n being the electron density, of the quantum Hall plateaus, but does not explain their quantization.

Disorder in the form of impurities and imperfections of a crystal are always present in an experimental sample. Modeling this by an additional disordered potential in Eq. (9) generates in-gap states in between the Landau levels. Moreover, the degeneracies of Landau levels are lifted and they broaden even in the low-temperature limit. According to the above argument the transverse conductivity increases linearly in the electronic density and is a smooth function of energy. Additionally, the transverse conductance should be finite even in between the Landau levels at all energies, due to the non-zero density of states.

Both however is not the case, the Hall conductivity does not change at all for large variations of electronic density, magnetic field or energy. Instead, it suddenly jumps at special parameter configurations; the Hall conductivity becomes quantized to integer multiples of e^2/h. The resolution of this tension with the theory presented above lies in the combination of topology and Anderson localization.

As we saw in the previous section in symmetry class A in two dimensions generically all wave functions localize. Hence they do not contribute to the transverse and longitudinal conductivity; an Anderson insulator emerges. However, in the center of the broadened Landau bands, wave functions become protected against Anderson localization[7]. Only these contribute to the conductivity in longitudinal direction and are counted to obtain the transverse conductivity; so $\sigma_{xy} = -e^2/h \times n$, where n now is the (integer) number of Landau level centers below Fermi energy[8] (Laughlin, 1981; Halperin, 1982; Altland and Simons, 2010).

This gives rise to the so-called quantum Hall plateaus, characterized by the filling of the protected mid-band Landau level states, n, and the quantum Hall plateau transitions which occur exactly when the Fermi level crosses one of the protected states, cf. Fig. 3.

The integer quantum Hall effect is thus the first and most famous example of topological protection in condensed matter. The plateaus correspond to the

7 This can be rationalized by the intuitive picture of semiclassical percolation of electron orbits in a smooth disorder potential, cf. Huckestein, 1995.. Electrons move around equipotential lines of the disorder potential, which are closed curves – hence localized – for large and small energies, in the tails of the Landau bands. At a special energy, however, namely in the center of the Landau bands the equipotential lines do not close and percolate through the sample, giving rise to extended states, protected from Anderson localization.

8 As the bulk of the system in between two plateau transitions is fully insulating, i.e. exhibits a mobility gap, the transport of the quantized current occurs only at the edges of the sample.

insulating topological phases and the mid-band protected states to the critical states between two topological invariants, giving rise to the quantum Hall edge states at the boundaries of the sample.

We have now seen an example of a microscopic model, namely that of free electrons in a strong magnetic field with generic (weak) disorder, which realizes a topological phase in class A; i.e. without time-reversal, particle-hole or chiral symmetry. However, conceptually there can be different microscopic Hamiltonians with the same symmetry properties exhibiting the same type of plateaus and plateau transitions, and with them the edge states. A magnetic field or even Landau levels are not needed. The resulting, more general, so-called *anomalous quantum Hall effect* will play a major role in this thesis (Haldane, 1988; Chang *et al.*, 2023); a generally valid topological argument – first made by Laughlin, 1981 – is presented in section 3.1.

3

LOCALIZATION-DELOCALIZATION PHASE DIAGRAM OF THE CHERN INSULATOR

Parts of this chapter are based on the publication Moreno-Gonzalez et al., 2023.

A field-free realization of the integer quantum Hall effect has been proposed by Haldane, 1988. Together with the Su-Schrieffer-Heeger chain (Su *et al.*, 1979) this is the first theoretical model of a topological insulator, as we understand it today: a translationally invariant bulk insulator with a non-trivial topological invariant n, which is protected even against disorder, leading to edge states at the real space boundary of finite samples. When disorder is included the band gap becomes a mobility gap and we obtain a topological Anderson insulator[1] with extended, conducting edge states.

Even away from criticality, i.e. in the topological phase where the bulk is insulating, there has to be at least one extended state protected against Anderson localization somewhere in the spectrum (Laughlin, 1981; Halperin, 1982; Moreno-Gonzalez *et al.*, 2023). This state corresponds to the center of the Landau bands in the case of the disordered integer quantum Hall effect. Even though these extended states in the spectrum of the topological phase are guaranteed to exist, it is not clear where in the spectrum, and what properties they have in a general anomalous quantum Hall insulator. This chapter is devoted to their study in a simple two band model of a class A topological insulator, namely the disordered Chern insulator. We will answer the question how much disorder is required to change the energetic position of the delocalized state deep in the bands depending on the parameters of a Hamiltonian model for the anomalous quantum Hall effect, at which disorder concentration the delocalized state breaks down fully and the topological phase is destroyed all together. In particular the phase diagram in terms of the Hamiltonian parameters, the energy and the disorder strength will be determined precisely. Later, this will allow us to study properties of the critical transition point in the anomalous quantum Hall effect in different regions of parameter space and establish if its properties depend on parametric details, for instance the energy of the delocalized state, or if they are universal and exhibit the same fingerprints compared to different topological phase transitions in symmetry class A.

1 in contrast to a topological band insulator in the clean case

QI-WU-ZHANG (QWZ) - MODEL OF THE CHERN INSULATOR. A very simple translationally invariant model of the anomalous quantum Hall effect, or Chern insulator, has been proposed by Qi *et al.*, 2006,

$$\mathcal{H}_{\mathrm{QWZ}}(\mathbf{k}) = \sin k_x \sigma_x + \sin k_y \sigma_y + (R - \cos k_x - \cos k_y)\sigma_z, \tag{14}$$

where $\sigma_{x,y,z}$ are the usual Pauli matrices, and $\mathbf{k} = (k_x, k_y)$ the crystal momentum in two dimensions of the infinite translationally invariant square lattice.

The energy dispersion of this model is given by its two bands in the $k_x - k_y$-plane,

$$E(k_x, k_y) = \pm\sqrt{2[1 + \cos k_x \cos k_y + R(\cos k_x + \cos k_y)] + R^2}. \tag{15}$$

Consequently, the clean QWZ model (14) is a band insulator for $R \neq -2, 0, 2$, while for $R = -2, 0, 2$ it exhibits band closings corresponding to topological phase transitions along the lines described in section 1.2.

Calculating the topological invariant, i.e. the Chern number n[2], of the thus separated insulating regimes we obtain topologically trivial ($n = 0$) phases for $|R| > 2$, while a $n = 1$ ($n = -1$) phase for $0 < R < 2$ ($-2 < R < 0$). The Chern number assumes the role of the filled Landau levels in the integer quantum Hall effect in Sec. 2.5.

To introduce disorder to the Chern insulator, Eq. (14) is Fourier transformed to real space, yielding

$$\begin{aligned}\mathcal{H}_{\mathrm{QWZ}} = \sum_{x,y} \Big[& \psi^\dagger_{x,y}(R\sigma_z + \epsilon_{x,y}\mathbb{1})\psi_{x,y} \\ & + \frac{1}{2}\Big(\psi^\dagger_{x+1,y}\left(\sigma_z + i\sigma_x\right)\psi_{x,y} \\ & + \psi^\dagger_{x,y+1}\left(\sigma_z + i\sigma_y\right)\psi_{x,y} + \mathrm{h.c.}\Big)\Big],\end{aligned} \tag{16}$$

where a disorder potential $\epsilon_{x,y}$ has been added. Here $\psi_{x,y}$ represent the spinors in the degrees of freedom coupled by the Pauli matrices, and x, y label the components of the two-dimensional lattice vectors $\mathbf{r} = (x, y)$ on a square lattice. The boundaries are chosen to be periodic. Disorder is uncorrelated and Gaussian distributed, $\langle \epsilon_{x,y}\epsilon_{x',y'}\rangle_{\mathrm{ens}} = W^2\delta_{xx'}\delta_{yy'}$, where $\langle\cdot\rangle_{\mathrm{ens}}$ denotes the ensemble average, δ the Kronecker symbol and W defines the disorder strength (Moreno-Gonzalez *et al.*, 2023).

3.1 ANDERSON (DE)LOCALIZATION IN SYMMETRY CLASS A

Before studying the critical states present in the spectrum of the anomalous quantum Hall effect, it is instructive to reconsider the topological argument

2 This can for instance be done by integrating the Berry curvature of the band structure in the translationally invariant system. See for instance Thouless *et al.*, 1982; Simon, 1983; Berry, 1984; Bernevig and Hughes, 2013.

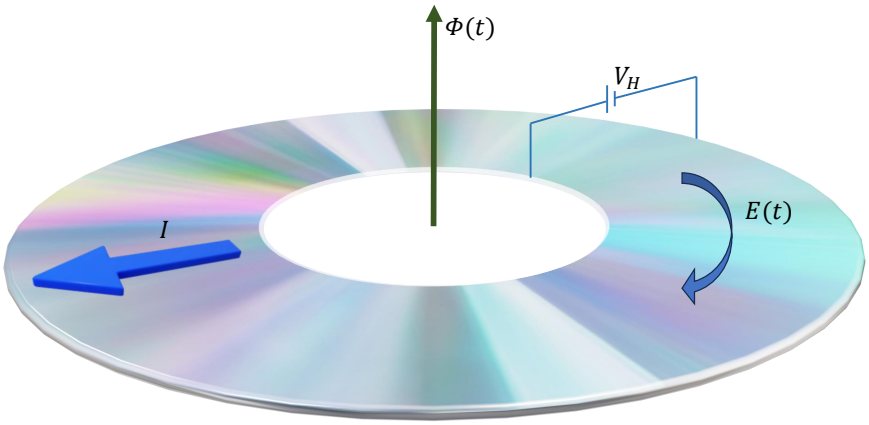

Figure 4: Setup for Laughlin's gauge argument: A time dependent magnetic flux Φ threads an annular geometry with inner and outer edges. An electric field is generated perpendicular to the magnetic field, circling around the hole. A current is supposed to be induced between inner and outer edge, Altland and Simons, 2010.

underlying the existence of extended states in the spectrum of a quantum Hall system even in its insulating phase.

Laughlin, 1981 proposed a thought experiment based on so-called topological pumps, rationalizing the quantization of the Hall conductivity and the emergence of bulk-delocalized states deep in the spectrum.

Consider a quantum Hall insulator in an annular geometry, i.e. a disk with a hole, such that an outer and an inner boundary emerge. Now we apply a time-dependent magnetic flux threading the hole in the center of the annulus, which in turn leads to a tangential electric field around the disk geometry. Together with the magnetic field, this induces a force on the electrons in radial direction. By that a current and a voltage between the inner and outer edges should be generated (Laughlin, 1981; Giuliani and Vignale, 2008). The geometry is sketched in Fig. 4. However, the bulk cannot simply dissipate the energy because it is insulating by assumption.

Additionally, we assume that the change of the magnetic flux is slow, i.e. the system evolves adiabatically and stays in an eigenstate of the instantaneous Hamiltonian. Now the wave functions and the spectrum of the Hamiltonian are periodic with respect to the application of a full flux quantum $\Delta\Phi = h/e$. Adiabaticity therefore implies that the system ends up in an eigenstate of the original Hamiltonian after one flux quantum has been applied during one period ΔT, however, it need not be the ground state. In fact, the only eigenstates available at Fermi level are the edge states, since only there the bands can close. Therefore, exactly one charge must have moved from one edge state to the other,

$$\Delta Q = I\Delta T = \sigma_{\text{Hall}}\Delta T\frac{\partial\Phi}{\partial t} = \sigma_{\text{Hall}}\Delta\Phi = \sigma_{\text{Hall}}\frac{h}{e}. \tag{17}$$

Immediately, it follows that the Hall conductivity must be $\sigma_{\text{Hall}} = e^2/h$ per charge transfer.

Two conceptual facts follow from this simple consideration:

(i) The Hall conductivity is quantized and its quantization can be explained by purely topological arguments. It therefore holds also for different realizations of the anomalous quantum Hall effect (Laughlin, 1981).

(ii) The bulk spectrum of a quantum Hall insulator must contain delocalized states. This follows from the fact that charge must be transferred from one edge to the other, i.e. the edge states at zero energy must be spectrally connected. The existence of at least one conducting bulk state deep in the spectrum connected continuously to the conducting edge state bands must be guaranteed (Halperin, 1982; Altland and Simons, 2010).

The principle presented here – namely the transport of a charge quantum from one to an opposite boundary of a sample via protected bulk states connected spectrally to the edges – is called *spectral flow*. It will play another important role later in this thesis, cf. chapter 5.

The spectral flow principle in class A however does not make any statements about the form, the number or the energy of such delocalized bulk states.

3.2 Results: (de)localization in the Chern insulator & phase diagram

In this section the goal is to characterize the extended bulk states in the topological insulator phase of the Chern insulator (14) numerically and analytically. A focus will be placed on the numerical analysis using multifractal correlations of critical states. The analytical description, developed by M. Moreno-Gonzalez and A. Altland in Moreno-Gonzalez *et al.*, 2023, is shortly summarized and benchmarked against the exact numerics.

For the anomalous quantum Hall effect, as realized in the model Hamiltonian (14), the set of critical states as a function of the three-dimensional parameter space, spanned by R, the disorder strength W, and the energy E can be represented as a critical connected surface, cf. a schematic sketch in Fig. 5.

In the following paragraph the basic idea of multifractal wave functions is introduced. The multifractal dimension will be benchmarked against established values from literature, and used as a fingerprint to identify the set of critical points in the parameter space of the disordered Chern insulator[3].

Multifractal wave functions. Fractal objects are characterized by exhibiting the same or similar shapes on all length scales. They are in that sense self-similar and do not have a finite distinguished length scale, e.g. a correlation or localization length. Examples can be found all over nature; the phenomenon has been described systematically by Mandelbrot, 1982. Fractals can be associated with a fractal dimension.

3 In later sections, in particular in chapters 4, 5, the details of the multifractal dimensions of the quantum Hall transition will play a more important role and are analyzed in greater detail.

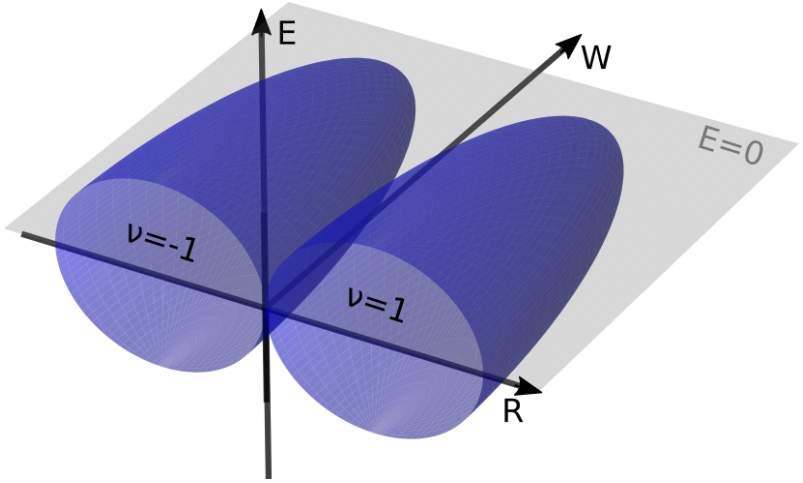

Figure 5: Sketch of the set of critical points in the parameter space (E, W, R) of the QWZ model, Eq. (16). The blue surface represents the critical states, while the topological phases are marked by the intersection between the surface and the plane at zero energy.

When undergoing Anderson transitions (multi)fractality of wave function is induced by strong amplitude fluctuations at the critical point, which occur on all length scales, when the localization length of the disordered sample is diverging. The analysis of the multifractal dimensions of wave functions hence is a quantitative method to characterize the critical fluctuations of localization transitions[4] (Castellanits and Peliti, 1986; Janssen, 1994; Huckestein, 1995).

In practice, we study the qth moments of the probability distribution of an electronic (real space) wave function $\psi^E_{\mathbf{r}}$ at energy E,

$$P_q = \sum_{\mathbf{r}} |\psi^E_{\mathbf{r}}|^{2q} . \tag{18}$$

The sum runs over all real space basis states of the corresponding Hilbert space of the Hamiltonian.

Assuming a scale-free distribution at the critical point, these moments in general scale with the (linear) system size, for instance of a lattice of linear length L, as

$$P_q \sim L^{-\tau_q}, \tag{19}$$

where the exponent τ_q represents the spectrum of multifractal dimensions (Mudry *et al.*, 1996; Evers and Mirlin, 2000; Mirlin and Evers, 2000; Evers *et al.*, 2001; Rodriguez *et al.*, 2008; Evers and Mirlin, 2008).

Comments on the behavior of τ_q in the non-critical cases are in order: Assuming a metallic wave function, such as those observed inside the mobility gap of the

4 *Multi*fractality is a consequence of the peculiar nature of Anderson transitions. The presence of infinitely many relevant operators – in the renormalization group context – implies an infinite set of critical exponents Δ_q describing the strong amplitude fluctuations at the critical point (Evers and Mirlin, 2008).

three-dimensional Anderson model (5), its support extends over all real space basis states. In this trivially extended limit, it resembles a perturbed Bloch wave, with $\tau_q^{\text{metal}} = d(q-1)$. On the other side of the LD transition in the localized phase, the wave function support does not scale at all with the system size L. This results in insensitivity of P_q to L, and hence $\tau_q^{\text{localized}} = 0, -\infty$ for positive or negative q, respectively.

At the critical point τ_q is a generic, non-linear function of q. Its non-metallic part $\Delta_q = \tau_q - d(q-1)$ is therefore often called anomalous multifractal dimension.

Previously, it was discussed that the class of samples to be described are ensembles of Hamiltonians, instead of individual realizations of a given disorder distribution. Therefore, in the following we will average the wave function moments over ensembles,

$$\langle P_q \rangle_{\text{ens}} = L^{-\tau_q^{\text{ens}}}, \tag{20}$$

where $\langle \cdot \rangle_{\text{ens}}$ denotes the ensemble average. Henceforth, we will omit the ensemble notation when discussing wave function moments or critical exponents; it is implied throughout the remainder of this thesis, unless stated otherwise.

Strictly speaking, exclusively critical states have multifractal character. However, we can generalize the defintion of the multifractal exponents τ_q, Δ_q to off-critical wave functions, demoting them to *effective* multifractal exponents, which now are functions of the system size L (and the system parameters, E, W, R) (Rodriguez *et al.*, 2010; Rodriguez *et al.*, 2011). Asymptotically, when $L \to \infty$, these effective exponents will yield either the metallic or the localized limit, as discussed above. Their definition goes along the same lines as for τ_q, Δ_q,

$$P_q^{\text{non-critical}}(E, W, R; L) \sim L^{-\overline{\tau}_q(E,W,R;L)}. \tag{21}$$

Numerically, the effective exponents are approximated by the logarithmic difference

$$\overline{\tau}_q \approx \tilde{\tau}_q \equiv -\frac{\ln P_q(E, W, R; L) - \ln P_q(E, W, R; L/2)}{\ln L - \ln L/2}. \tag{22}$$

In the asymptotic limit of large system sizes L this effective quantity yields the actual multifractal exponents,

$$\lim_{L\to\infty} \tilde{\tau}_q \to \begin{cases} 0, & \text{if } \xi < \infty, (E, W, R) \neq (E_c, W_c, R_c) \\ d(q-1), & \text{if } \xi = \infty, (E, W, R) \neq (E_c, W_c, R_c) \\ \tau_q, & \text{if } (E, W, R) = (E_c, W_c, R_c), \end{cases} \tag{23}$$

where ξ denotes the localization length, and X_c a critical point in parameter space (Moreno-Gonzalez *et al.*, 2023). The benefit of this generalized definition is twofold:

(i) It allows us to define $\tilde{\tau}_q$ throughout the entire parameter space of a given model, and the subset of actual critical points in parameter space can be identified by Eq. (23).

(ii) The behavior of $\tilde{\tau}_q$ as a function of L, X close to the critical points is a hallmark of the divergence of the localization length at the phase transition; by that the determination of the localization length exponent ν is possible. This method will be explained in more detail and used later on in chapter 4.

IDENTIFYING QUANTUM HALL CRITICAL STATES. The multifractal dimension of the quantum Hall critical state is believed to be universal in the asymptotic limit; independent of the microscopic definition of the underlying model. There is however no rigorous proof of this belief (Evers and Mirlin, 2008).

While there is no established microscopic theory of the quantum Hall critical point, analytical models have been proposed which predict $\Delta_q^{(p)} = 1/4q(1-q)$ (Zirnbauer, 1999; Zirnbauer, 2019). Numerically, this result holds approximately, however high-precision studies of the Chalker-Coddington network model of the lowest Landau level suggest deviations, either in the parabolic shape of the dimension in q or in the prefactor of the quadratic function (Evers *et al.*, 2001; Evers *et al.*, 2008; Obuse *et al.*, 2008). Since finite-size corrections to the asymptotic scaling of the wave function moments in the thermodynamic limit decay very slowly, and a microscopic theory is not available there is no great consensus about the exact details of the properties of the quantum Hall critical state; they are still subject to numerical and analytical research. The next chapter is partly devoted to the numerical study of this problem in the anomalous quantum Hall insulator.

For the problem at hand, however, the established approximate form of the anomalous dimension of the critical state, $\Delta_q \approx 1/4q(1-q)$ merely serves as a benchmark to find the subset of critically extended states in the disordered Chern insulator; the exact form of the multifractal dimension does not play a large role at this point.

EXCURSION: ANALYTICAL APPROACH TO DELOCALIZED BULK STATES. As this chapter intends to give insight about the nature of delocalized state deep in the bulk state of a Chern insulator, the reader is provided with a short summary of the analytical approach carried out by M. Moreno-Gonzalez and A. Altland in Moreno-Gonzalez *et al.*, 2023. The following paragraph is not self-contained, as a detailed introduction to the analytical theory of topological actions goes beyond the scope of this thesis. This paragraph is intended as a short overview only, while a more interested reader is referred to the publication Moreno-Gonzalez *et al.*, 2023.

In past works topological insulators in general and in particular also the QWZ-model of the anomalous quantum Hall effect have been approached primarily in the famous Dirac approximation: The band structure of the QWZ model has a band crossing with an approximately linear dispersion at the critical point, such that in its vicinity the dispersion can be approximated by a (massive) Dirac

cone. This approach has been incredibly successful in describing various quasi-relativistic effects in condensed matter, for instance in graphene (Geim, 2009).

However, for the problem at hand it suffers some shortcomings: Even though the low-energy physics may be described well, statements about the properties of the system at large energies or momenta are impossible by construction. As the goal of this section is to describe high-lying bulk states, this fact makes the linearized Dirac theory unsuitable. Additionally, a regularization scheme has to be applied to cure ultra-violet divergences of Dirac cones on a lattice (Pauli and Villars, 1949; Bollini and Giambiagi, 1972; 't Hooft and Veltman, 1972).

A key ingredient to a useful analytical theory of high-lying critical states is to use the full lattice dispersion of (14); it additionally cures ultra-violet divergences by construction. The computation of the critical energy in the insulating phase then proceeds by imposing a half-integer quantization of the Berry flux, which is encoded in the ground state of the clean Chern insulator for weak disorder (Moreno-Gonzalez *et al.*, 2023). For strong disorder the Green's function in the self-consistent Born approximation is constructed, where the impurity scattering is encoded in the quasi-particle self-energy. The critical states then are identified by the quantization of the coupling constants of the topological action for which a representation in terms of the Green's function can be found (Smrcka and Streda, 1977; Khmelnitskii, 1983; Pruisken, 1984; Levine *et al.*, 1984; Moreno-Gonzalez *et al.*, 2023).

In both cases the topological angle Θ, serving as a measure for the coupling constant of the topological part of the action in the Chern insulator, can be calculated for the parameter space (E, W, R), and the subset of critical points is identified by the quantization condition

$$\Theta(E, W, R) \stackrel{!}{=} (2n+1)\pi, \tag{24}$$

where n is an integer (Khmelnitskii, 1983; Pruisken, 1984; Levine *et al.*, 1984).[5]

5 In the presence of disorder an effective field theory can be derived, which is characterized by an action of the from

$$S[Q] = \int d^2r \left(g \operatorname{Tr}(\partial_i Q \partial_i Q) + \frac{\Theta}{16\pi} \epsilon_{ij} \operatorname{Tr}(Q \partial_i Q \partial_j Q) \right). \tag{25}$$

Here $Q = Q(\mathbf{r})$ is a matrix field in two-dimensional real space, whose components are indexed by i, j. The coupling constants (g, Θ) span the space for the renormalization group flow, with fixed points at $(0, 2\pi n)$ on quantum Hall plateaus and $(g^*, (2n+1)\pi)$ for quantum Hall criticality. The coupling constants can be identified with the longitudinal and transverse conductivity, $g = \sigma_{xx}/8, \Theta = 2\pi\sigma_{xy}$. The critical point itself is not described by such a theory, its identity remains unknown. However, as a diagnostic this form of the action is appropriate. Details about field theory of the type described, in particular the derivation for the microscopic model examined in this chapter and the precise form of the coupling constants in terms of the model parameters for small and large disorder are not explained in this thesis. For a comprehensive background the reader is referred to Altland and Simons, 2010, while the problem-specific field theory is detailed in the original publication Moreno-Gonzalez *et al.*, 2023.

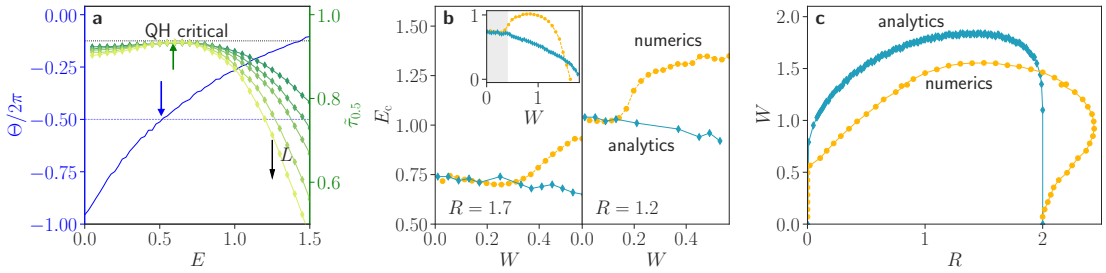

Figure 6: Analytical and numerical prediction for the spectral position E_c of the delocalized state in the topological phase. **a** The blue data shows the topological angle Θ, as a function of energy for $(W, R) = (1.45, 1.2)$. Criticality is present when it equals the blue dashed line at an odd multiple of π, cf. blue arrow. On the right axis the numerical results for the effective dimension $\tilde{\tau}_{0.5}$ for different system sizes from $L = 64 \to 512$ are shown. The dashed horizontal line indicates the multifractal dimension in the parabolic approximation $\tau_{0.5}^{(p)} = 0.9375$ of the quantum Hall critical state. This condition is approximately met at the green arrow. **b** Prediction for the delocalized states taken from multifractal analysis and field theory at $R = 1.7$ and $R = 1.2$ as a function of disorder strength for small W where quantitative agreement between numerics and analytics is observed; and for larger W up to the breakdown of the topological phase (inset). **c** Phase diagram of the disordered Chern insulator in the $R - W$-plane at zero energy, caculated analytically and numerically. The critical states in **b,c** are numerically identified at a linear system size $L = 256$ and finite-size corrections to the critical parameter sets are smaller than the size of the data points when for $L > 128$. Figure adapted from Moreno-Gonzalez *et al.*, 2023, ©2023 Elsevier.

NUMERICAL AND ANALYTICAL RESULTS. To identify the subset of critical points in the parameter space of the Chern insulator the quantities $\tilde{\tau}_q(E, W, R; L)$ and $\Theta(E, W, R)$ are calculated.

In Fig. 6 we compare the results for the identification of the delocalized states obtained from multifractal analysis and the analytical approach sketched above. In panel **a** the effective multifractal exponent for $q = 0.5$ for the parameter set $(W, R) = (1.45, 1.2)$ is shown in green colors as a function of energy. All curves have a maximum in the shown energy range whose value is close to the theoretical prediction of the quantum Hall critical point, assuming an approximate parabolic form according to Zirnbauer, 2019 (black dashed line). As the system size is increased (from dark green to light green colors) the maximum gets more pronounced, while its value stays approximately constant at $\tilde{\tau}_{0.5} \approx \tau_q^{(p)}$, indicating an actual scale free, power-law nature of the wave function, and hence quantum Hall criticality (green arrow). Additional evidence for quantum Hall criticality at the maximum of these curves is given by the (almost) scale invariant distribution functions of the wave function moments, whose analysis is delegated to appendix A.1.

Away from the critical point, the curves bend down towards $\tilde{\tau}_{0.5} \to 0$, indicating localization as expected for the remainder of the spectrum. Additionally, in blue the topological angle $\Theta(E, W, R)/2\pi$ as a function of energy at the same

parameter set (W, R) is shown, as calculated from the field theoretical calculation as sketched above. The theory predicts a critical state when Θ is an odd multiple of π, indicated by the blue dotted line and marked by the blue arrow, which identifies the analytical prediction for the delocalized state in the bulk spectrum. The numerical and analytical predictions are not perfect but agree reasonably, given there is no adjustable fitting parameter.

Panel **b** of Fig. 6 shows the energy of the delocalized state E_c deep in the topological phase of the Chern insulator calculated both with the analytical and the numerical approach for different parameters R as a function of disorder strength W. The spectral position of the delocalized state E_c is calculated by finding the maxima of the multifractal dimension $\tilde{\tau}_{0.5}$, and invoking the conditions (23) and (24), for the numerics and analytics, respectively. For a small disorder strength W both calculations agree even quantitatively, while at larger W the analytical theory breaks down on a quantitative level. This can be attributed to the proximity to a quantum critical point, where the longitudinal conductance assumes values of order one, $\sigma_{xx} \sim \mathcal{O}(1)$. Here the field theory is no longer applicable (Moreno-Gonzalez *et al.*, 2023).[6]

The numerical prediction for E_c, which is exact up to irrelevant finite-size corrections, shows a transient increase for intermediate W, which is not captured by field theory. At large disorder strengths W, numerics and analytics both suggest a decrease of E_c until it eventually reaches zero energy, thus signaling the breakdown of the topological phase and a transition to the topologically trivial phase at very large disorder strength W.

By monitoring the critical energy, and its decrease to zero, it is also possible to capture the phase diagram of the Chern insulator at large disorder, by tracking $\tilde{\tau}_q(E = 0, W, R; L)$ and $\Theta(E = 0, W, R)$. The resulting numerical and analytical predictions for the topological phase boundaries are shown in panel **c** of Fig. 6.

Again, we observe a rough qualitative agreement between the two approaches, however, some aspects are not captured by the analytical theory; for instance the extension of the topological phase above the clean value for $R > 2$ is only visible in the exact numerics.

CONCLUSION: CRITICAL SURFACE OF THE CHERN INSULATOR. Generic states in the disordered Chern insulator are Anderson localized. However, symmetry arguments guarantee the existence of at least one energy in the spectrum where wave functions are extended, as long as topology survives. The present chapter has now investigated the spectral position and properties of these delocalized states.

We found that these energies can appear deep in the bulk, while they approach zero when the system is close to a topological phase transition. By that it is possible to identify the entire subset of critical wave functions in the parameter space

6 The prerequisites for the applicability of the theory developed in this context are not explained in this thesis, the interested reader is referred to the detailed derivation of the field theory for the present model in Moreno-Gonzalez *et al.*, 2023.

of the disordered Chern insulator (E, W, R) as a "critical surface" of delocalized states. It is schematically visualized in Fig. 5.

3.3 Outlook: delocalized bulk states in other symmetry classes?

The Chern insulator is a fundamental and maybe the simplest example of topological insulators. Given that even basic properties of more complex topological insulators remain poorly understood it can be hoped that the understanding of the delocalized states of this simple example may help in grasping the surface criticality of disordered three-dimensional systems (Sbierski *et al.*, 2020; Lapierre *et al.*, 2022).

In recent years remarkable properties of topological insulators in more complex classes of the ten-fold way have surfaced: It seems that generic surface states of three-dimensional topological realizations of for instance class AIII are protected against localization much more generically than expected (Sbierski *et al.*, 2020). In this context the concept of spectral flow, which was introduced in section 3.1 and featured prominently in the determination of the critical properties of the Chern insulator in the present chapter, plays another important role: Its absence or presence will be decisive for the localization properties of surface bands of topological insulators (Altland *et al.*, 2024).

Before turning to more complex topological insulators and generalizing to different symmetry classes in chapter 5, the quantum Hall effect, realized in class A, will be studied from a different perspective in the next sections.

4

CRITICAL EXPONENTS AT THE QUANTUM HALL TRANSITION

4.1 MOTIVATION: UNIVERSALITY OF QUANTUM HALL CRITICALITY

Although systems belonging to the same symmetry class in the ten-fold way may differ drastically in their microscopic definitions, it is believed that they share some fundamental properties. This hypothesis is called *universality*. It can be rationalized by the general structure of the field theories describing disordered systems: The microscopic theory is coarse-grained from the microscopic length scales to much larger, eventually mesoscopic or macroscopic sizes, at which the details of the underlying theory are hidden, and only properties such as dimension and symmetries remain visible. The procedure of obtaining this simplified coarse-grained theory is called renormalization group flow, which is believed to be described only by very few renormalized coupling constants such as the transverse and longitudinal conductivity of the system (Evers and Mirlin, 2008).

In many cases it is reasonable to believe that systems belonging to the same symmetry classes hence "flow" (in the space spanned by these renormalized quantities) to very few or in the simplest case even to a single *universal* fixed point at the level of the coarse-grained theory. If this is the case such systems should share fundamental properties, such as the functional behavior of the correlation or localization length in the vicinity of the critical point; i.e. the critical exponent of the localization length ν.

To date a microscopic critical theory of the quantum Hall transition is missing (even though the plateaus and their quantization are fairly well understood). Even basic properties such as the existence of a single or multiple fixed points remain mysterious.

Without the availability of an analytical theory a natural access point to the solution of this problem is the numerical study of the critical exponents of different realizations of quantum Hall criticality (Evers and Mirlin, 2008).

CRITICAL EXPONENTS IN LITERATURE. The most studied realization of a quantum Hall plateau transition is the network model introduced by Chalker and Coddington, 1988 (CC). Analyzing its critical scaling, Slevin and Ohtsuki, 2009 reported a localization length exponent of around $\nu \sim 2.6$, which significantly

exceeded the estimates based on previous studies, $\nu \sim 2.3 - 2.4$ (Huckestein, 1995). Subsequently, it turned out that further irrelevant finite-size correction to the asymptotic scaling needed to be taken into account. However, the estimate on $\nu \sim 2.6$ was corroborated (Obuse *et al.*, 2012), and received further support (Amado *et al.*, 2011; Fulga *et al.*, 2011; Slevin and Ohtsuki, 2012; Nuding *et al.*, 2015; Dresselhaus *et al.*, 2022). Even though the Chalker-Coddington network was constructed to keep scaling corrections small these hopes did not materialize in unambiguous estimates for ν; the numerical uncertainty, mainly mediated by irrelevant corrections, is still significantly larger than those for the critical exponents of other types of Anderson transitions, such as the three-dimensional metal-insulator transition in class AI (Rodriguez *et al.*, 2011).

To investigate universality also different models of the integer quantum Hall transition have been examined. Studies of a tight binding model with a magnetic field have corroborated both the estimates for the localization length exponent $\nu \sim 2.6$, but also for the exponents of the leading and subleading irrelevant finite-size correction to scaling (Puschmann *et al.*, 2019; Puschmann and Vojta, 2021) or predicted a slightly smaller ν (Zhu *et al.*, 2019). Even though it was believed that these models – featuring several Landau levels – obscure the asymptotic scaling of the critical states, and the spectral position of the critical point is a priori not known, the scaling corrections turned out to be comparable to the CC network.

Despite of the unavailability of a rigorous analytical prediction for the critical exponents of the quantum Hall transition and the numerical uncertainty of their values proves to be considerably larger than for other transitions, $\nu \sim 2.5 - 2.6$ seemed to emerge to be the consensus. However, this result is in tension with the experimental value for the quantum Hall plateau transition, $\nu \sim 2.38$ (Koch *et al.*, 1991; Li *et al.*, 2009); the discrepancy may be caused by electron-electron interaction effects present in the experimental samples.

In recent years the controversy regarding the critical properties of the quantum Hall effect gathered momentum once again. This is partly because of the following reason:

Zirnbauer, 2019 suggested a field theoretical description of the integer quantum Hall transition; in particular a conformal field theory with a renormalization group flow implying $\nu = \infty$. This is of course in tension to the numerical observation of finite ν; the discrepancy is suggested to be solved by the almost logarithmically slow irrelevant corrections accompanying the asymptotic scaling, since the leading irrelevant finite-size correction exponent is predicted to be $y = 0$ within this theory. When not taking into account this *marginal* flow in the numerical analysis, only *effective* exponents ν will be observed for a window of finite system sizes which are not universal and obscure the true asymptotic limit $\nu = \infty$. Accordingly, the spread of numerical results for ν in different computational finite-size studies is understood as a consequence of ignoring the logarithmic corrections due to the marginal renormalization group flow.

Several numerical developments in recent years can be interpreted in the light of Zirnbauer's suggestion.

(i) Dresselhaus *et al.*, 2021 reported evidence for marginal scaling by observing a localization length exponent far from the previously established result, $\nu \sim 3.9$, in a two-channel CC network. However in a different work the same authors investigate the sheet conductance scaling of a CC network and observe $\nu \sim 2.6$ with a remarkably small uncertainty, which is in full agreement with previous studies of the scaling properties of the CC network (Dresselhaus *et al.*, 2022).

(ii) Gruzberg *et al.*, 2017 studied a geometrically disordered CC network and found $\nu = 2.38$, suggesting non-universality, triggered by a modification of the quantum Hall critical RG fixed point by geometric disorder. Subsequently, this results was interpreted as evidence for the existence of a critical line of quantum Hall criticality (Gruzberg *et al.*, 2017; Klümper *et al.*, 2019).

(iii) Recently, Sbierski *et al.*, 2021 investigated the critical properties of Dirac fermions, realizing a model of the anomalous quantum Hall effect. The authors concluded that ν is depending on the energy of the critical state, i.e. its spectral distance from the Dirac point. The critical exponent varied in the range between $\nu \sim 2.3 - 2.6$. This is inconsistent with a universal critical fixed point and may support the notion of a critical line or marginal flow as suggested by Zirnbauer. The model studied by Sbierski *et al.*, 2021 is a variant of the QWZ model of the anomalous quantum Hall effect studied in chapter 3; the paper mainly focused on the linearized model around the Dirac point.

Motivated by the friction of the result by Sbierski *et al.*, 2021 with universality, the following section is devoted to the study of the critical exponents in the full lattice model of the disordered Chern insulator, Eq. (16). The critical properties of the anomalous quantum Hall transition in this model will be investigated by multifractal analysis and a recursive Green's function method and compared to results obtained in a tight binding model with a magnetic field, as studied in Puschmann *et al.*, 2019; Puschmann and Vojta, 2021, in section 4.3.

Subsequently, in section 4.4 an amorphous variant of the anomalous quantum Hall effect will be investigated, realizing a geometric type of disorder. The resulting critical exponents will be compared in the light of universality with previous studies on the Chalker-Coddington network on the one hand, and on the other hand with the geometrically disordered model of the quantum Hall transition studied by Gruzberg *et al.*, 2017.

4.2 Scaling theory at localization transitions

To study the asymptotic and irrelevant scaling properties of the localization length close to the quantum Hall transition, a short introduction is needed on how to gain access to the thermodynamic limit, which is necessary to observe a proper transition, in a (usually finite-size) numerical simulation.

First, a dimensionless quantity X has to be defined, which depends decisively on the localization properties. From the way Anderson localization has been defined as the absence of diffusion in the correlations of local electronic densities, a very direct observable to measure or simulate is the conductance of a disordered

sample placed between some leads (cf. Dresselhaus *et al.*, 2022 for a recent study). Additionally, the localization length can be measured indirectly via the calculation of the Lyapunov exponent, quantifying the envelope of a wave function, as done recently by Puschmann *et al.*, 2019. By the construction of the multifractal analysis, also the (multifractal) dimension of the wave function at finite sample sizes can be taken to characterize the localization properties (Rodriguez *et al.*, 2011). Since a numerical calculation is carried out on a real space lattice, the linear lattice size L is always finite. Therefore, a method to extrapolate finite-size results to the asymptotic scaling in the thermodynamic limit is needed.

Based on the scaling theory of localization introduced by Abrahams *et al.*, 1979, it is assumed that the quantity X is a function of the single parameter L/ξ, i.e. the ratio of the (linear) system size to the localization or correlation length; $X \equiv X(L/\xi)$. At the critical point no length scale can exist, and ξ diverges as

$$\xi \sim \mid x_r \mid^{-\nu}, \tag{26}$$

where x_r is the parametric distance to the critical point (Puschmann, 2017).

X therefore assumes the critical value $X_c = X(0)$ and the scaling relation reads

$$X \sim X(x_r L^{1/\nu}). \tag{27}$$

At finite L however additional corrections affect this scaling. Assuming only one (RG) relevant exponent $\nu > 0$, while all other exponents $y_i < 0$ are irrelevant, the above relation holds in the thermodynamic limit. For numerically accessible system sizes, however, y_i may play a significant role. Assuming only a single irrelevant exponent $y \equiv -y_1$, the scaling relation reads

$$X = X(x_r L^{1/\nu}, x_i L^{-y}), \tag{28}$$

where x_r, x_i are relevant and irrelevant scaling variables, and $1/\nu, -y$ are relevant and irrelevant scaling exponents.

The scaling variables can be represented in finite Taylor series of the system parameters a, such as energy E or disorder strength W: $x_r(a) = a + \sum_{j=2}^{m_r} b_j a^j/j!$ and $x_i(a) = 1 + \sum_{j=1}^{m_i} c_j e^j/j!$, up to orders $m_{r,i}$ (Slevin and Ohtsuki, 1999; Ohtsuki *et al.*, 1999). Analogously, the scaling relation can be represented as a Taylor series in its first and second argument up to orders $n_{r,i}$ (Puschmann, 2017).

As both phases accompanying the quantum Hall plateau transition are equivalent, only powers > 1 of the relevant scaling argument contribute. The leading relevant behavior close to the critical point of the quantum Hall transition will therefore be scaling with $\sim L^{2/\nu}$ (Slevin and Ohtsuki, 2009).

In principle, we could determine the exponents ν, y_1, y_2, etc. by fitting the data we obtain for instance for the conductance using the above general scaling relation. This has been done successfully in the past e.g. by Slevin and Ohtsuki, 2009; Dresselhaus *et al.*, 2022. However, in models which do not scale as favorable as the Chaker-Coddington network where the critical point is known exactly, the

large number of fitting parameters can cause numerical instabilities. We therefore complement the above scaling ansatz with a more pedestrian, step-by-step way, which additionally allows for a visual inspection of the intermediate fitting steps: We calculate the quantity X as a function of the system parameters a across the transition and the linear system size L, and expand it in a finite Taylor series around its extrema at $a_m(L)$ close to the critical point,

$$X(a, L) = X^{(0)}(L) + \sum_{i=2}^{r} X^{(i)}(L)(a - a_m(L))^i, \tag{29}$$

where we usually choose the expansion order to be $r = 3, 4$, with fitting parameters $X^{(i)}, a_m$. For the critical point and the critical value of X, we then have $X_c = \lim_{L\to\infty} X^{(0)}(L)$ and $a_c = \lim_{L\to\infty} a_m(L)$. The corresponding scaling asymptotics can then be written by including the irrelevant exponents $y_{1,2}$, by

$$\begin{aligned} a_m(L) &= a_c\,(1 + d_1 L^{-y_1} + d_2 L^{-y_2}) \\ X^{(0)}(L) &= X_c\,(1 + e_1 L^{-y_1} + e_2 L^{-y_2}) \\ X^{(2)}(L) &= L^{2/\nu}\,(f_0 + f_1 L^{-y_1} + f_2 L^{-y_2}), \end{aligned} \tag{30}$$

where d_i, e_i, f_i and a_c, X_c and the exponents ν, y_1, y_2 are fitting parameters. The quality of the fit can be evaluated by a χ^2-test.

4.3 CRITICAL EXPONENTS IN THE SPECTRUM OF THE DISORDERED CHERN INSULATOR

This section is based largely upon a collaboration together with M. Puschmann and F. Evers. The multifractal analysis was carried out by the author of this thesis while M. Puschmann contributed the computation of the Lyapunov exponents complementing the finite-size scaling analysis.

Recently, Sbierski *et al.*, 2021 have concluded that in a linearized version of the Chern insulator (14), i.e. with free Dirac electrons, the properties of the quantum Hall critical point are non-universal. In particular, at the Dirac point, which henceforth will be referred to as the zero energy point in the spectrum, the localization length exponent is considerably smaller than the established CC result, $\nu_{E=0} = 2.33(3)$; at large energies deep in the spectrum, the authors observe $\nu_{E=0.7} = 2.53(2)$, largely consistent with CC values, by e.g. Slevin and Ohtsuki, 2009. These calculations in the linearized Dirac model of the Chern insulator have been complemented by a transport simulation of the full lattice model, where it was argued that the irrelevant scaling corrections in the case for $E = 0$ could be omitted.

By a careful large scale analysis of the critical properties of the quantum Hall critical point in the QWZ model of the disordered Chern insulator, we revisit the results presented by Sbierski *et al.*, 2021 for the linearized Dirac model, by taking into account the full lattice dispersion and irrelevant scaling corrections.

Numerically, we take a two-fold approach. First, the effective multifractal dimension $\tilde{\tau}_q$, Eq. (22), is analyzed in the disordered Chern insulator on square lattice with periodic boundaries. Second, the Lyapunov exponent is calculated in a quasi-1d setup, quantifying the envelope and hence the localization length of typical wave functions (Puschmann and Vojta, 2021), cf. appendix C. Analogously to the study by Sbierski *et al.*, 2021, we calculate the critical exponent ν for delocalized states at different energies in the spectrum of the Chern insulator, i.e. somewhere on the critical surface identified in chapter 3. This allows us to choose different energies E, as in the Dirac model, and adjust the remaining system parameters (W, R) such that the critical surface is crossed, and a phase transition occurs, accompanied by a diverging localization length characterized by an exponent ν.

4.3.1 *Localization length exponent ν and irrelevant finite-size corrections*

EFFECTIVE MULTIFRACTAL DIMENSION. Fig. 7 (left panels) shows the anomalous part of the effective multifractal dimension $\tilde{\Delta}_q$ at $q = 0.5$ as defined in Eq. (22), rescaled by the parabolic part $\sim q(1-q)$. The system parameters W, R are varied across the critical surface of the Chern insulator at two different energies $E = 0.6$ (**a**) and $E = 0$ (**b**) for different linear system sizes L. Both panels show approximately parabolic behavior across the transition, whose minima are close but

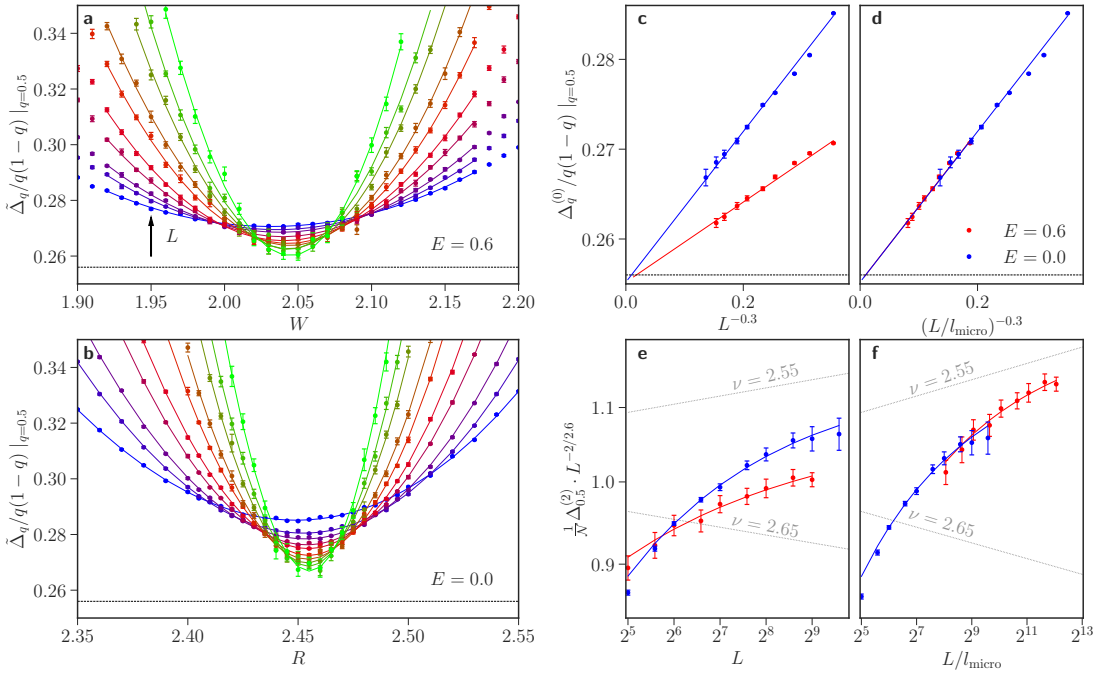

Figure 7: **a**,**b** Effective multifractal exponents $\tilde{\Delta}_q\ |_{q=0.5}$ as a function of the tuning parameter for system sizes $L = 16 - 768$, evaluated at the transition at $E = 0.6$, $R = 1.2$ (**a**) and $E = 0$, $W = 1.4$ (**b**). Data points represent the ensemble average and the 1σ confidence interval. Lines follow the fit using Eq. (29) to order $r = 3$. **c-f** Scaling analysis using Eq. (29) and (30) of the multifractal data at the transitions $E = 0$ and $E = 0.6$. **c** $\Delta_{0.5}^{(0)}(L)$, extracted from the fit with Eq. (29) to order $r = 3$, as a function of system size. Lines are guide to the eye, illustrating the asymptotic scaling according to an assumed irrelevant behavior with $y = 0.3$. **d** Finite-size scaling of $\Delta_{0.5}^{(0)}(L)$, with the L-axis rescaled by an effective microscopic correlation length l_{micro}. **e** Scaling of the curvature $\Delta_{0.5}^{(2)}(L)$ as function of L, reduced by the power law $L^{2/2.6}$. **f** Curvature as a function of L rescaled by l_{micro}. All lines are guides to the eyes only and follow an extrapolation with a single irrelevant scaling exponent $y = 0.3$.

not exactly at the theoretical prediction by Zirnbauer, 2019, $\Delta_q^{(p)}/q(1-q) = 0.25$. The discrepancy can be attributed to both additional irrelevant finite-size corrections and possibly actual deviations from Zirnbauer's theory (Obuse *et al.*, 2008; Evers *et al.*, 2008), which will be discussed later in more detail. Additionally, it can be observed that the curvature of the data around the minima becomes larger with increasing L. This can be explained by the divergence of the localization length at the critical point and allows for a determination of the critical exponent ν. The data is modeled by a series expansion around the apex value according to Eq. (29) to order $r = 3$ in a window around the extrema (solid lines). The apex value $\Delta_{0.5}^{(0)}(L)$ and the curvature $\Delta_{0.5}^{(2)}(L)$ are analyzed further; the former allows for an extrapolation of the asymptotic multifractal dimension, while the latter for an analysis of the localization length exponent ν.

Fig. 7 (right panels) shows the system size dependence of these two parameters. The apex value $\Delta_{0.5}^{(0)}(L)$ converges to the the asymptotic anomalous dimension; its value can be extrapolated using the model in Eq. (30). The data sets for the two energies $E = 0, 0.6$ differ largely only in a factor in the horizontal axis, suggesting the existence of a microscopic length scale l_{micro}, discriminating between the two energies. When adopting l_{micro} as a unit of distance[1], the values of $\Delta_{0.5}^{(0)}$ collapse to a single curve. Additionally, the curvature $\Delta_{0.5}^{(2)}$ – encoding the localization length exponent ν – can be reduced to a master curve by measuring the system size L in units of l_{micro} upon a proper normalization[2]. The existence of a master curve capturing the finite-size scaling of critical points at both energies suggests universality by itself even without the precise knowledge of the exponents ν, y: The only difference between the two parameter sets is the microscopic length scale, which by definition is irrelevant for the asymptotic scaling and the localization properties in the thermodynamic limit.

Additionally, the lower right panels of Fig. 7 suggest that the system sizes studied are still in the transient regime: irrelevant scaling corrections play a large role, particularly at $E = 0$. However, by visual inspection it is highly plausible that the master curve, i.e. both energies $E = 0, 0.6$ will exhibit an asymptotic scaling with an exponent $2.65 \geqslant \nu \geqslant 2.55$ (grey lines). The visualization of the microscopic length scale present in the system size scaling of the effective multifractal exponent highlights the importance of a detailed study of irrelevant finite-size corrections: Underestimating their size and the curvature present in the data of the lower right panels easily results in an underestimation of the exponent ν for the $E = 0.0$ transition (blue) compared to the $E = 0.6$ transition (red).

To make a concise numerical estimate of ν, y one has to analyze the data with great caution when neglecting higher order irrelevant scaling corrections, which have caused under- or overestimated critical exponents in various settings of the notoriously difficult quantum Hall plateau transition in the past. Therefore, ideally we take into account a second irrelevant scaling correction as outlined in Eq. (30), and check the stability of the relevant and leading irrelevant exponent with respect to its inclusion. The statistical quality of the data presented in Fig. 7 is not sufficient to secure a stable fit using a complex data model as in Eq. (30) taking into account higher order irrelevant scaling corrections.

Therefore, a computationally more favorably scaling technique is employed to support the multifractal analysis with the caveat of a slightly more indirect measure of the localization properties of single wave functions: A recursive Greens function approach (RGFA) allows for a determination of the so-called Lyapunov exponent Γ, effectively quantifying the envelope of wave functions in a quasi-1d realization of the disordered Chern insulator, and hence their localization length. As the main focus of this chapter is on (effective) multifractality close

1 normalized to the lattice spacing for $E = 0$

2 which is insignificant for the asymptotic scaling, since it only encodes a prefactor of Hamiltonian parameters W, R

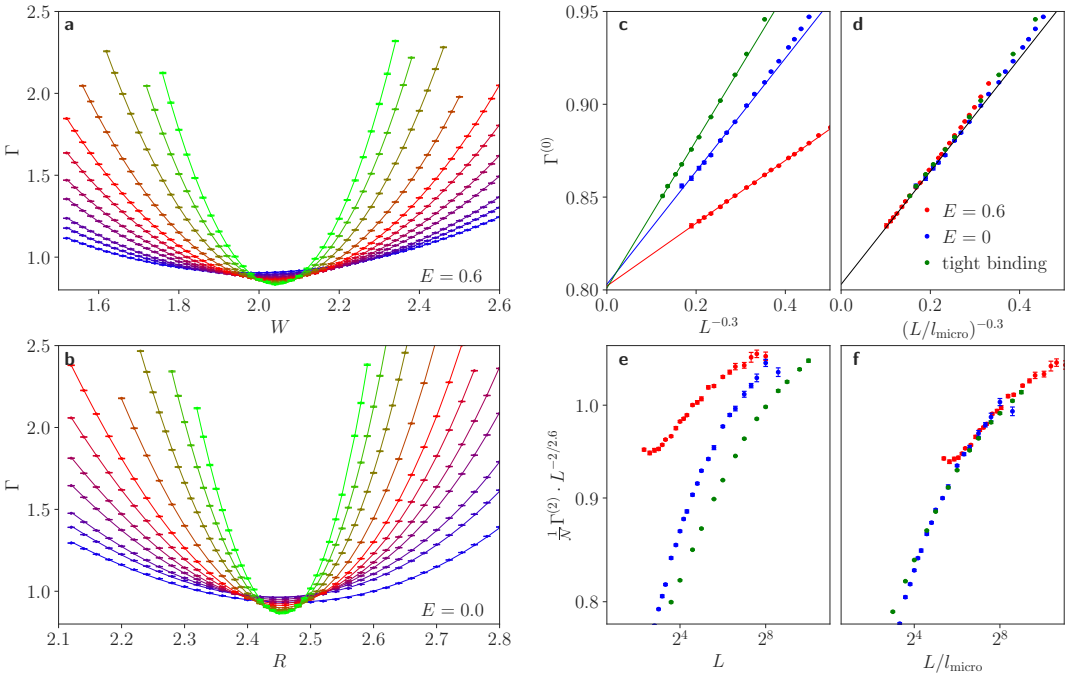

Figure 8: Lyapunov exponent calculated with RGFA across the transitions shown in Fig. 7. Statistical analysis proceeds analogously to Fig. 7. Systems of width $L = 8 \to 256$ (blue to green) have been taken into account. Additionally, Lyapunov exponents and the corresponding extrapolation are shown in panels **c-f** for a tight binding model including a magnetic field, leading to Landau levels (green data), published by Puschmann and Vojta, 2021; data shown with permission by M. Puschmann.

to the quantum Hall transition, the algorithm of the RGFA method is not of primary interest in this context. A rough overview is provided in appendix C. The numerical implementation has been developed by Puschmann and Vojta, 2021, its adaption to the disordered Chern insulator and the data generation has been carried out by M. Puschmann. A more detailed introduction to the characterization of the quantum Hall plateau transition in a tight binding model with magnetic field using RGFA is explained in Puschmann and Vojta, 2021.

4.3.2 *Critical exponents in different class A models: consistency with universality*

Fig. 8 shows the Lyapunov exponent Γ across the transitions at $E = 0, 0.6$ (**a** and **b**) which is analyzed according to the series expansion Eq. (29), analogously to Fig. 7. Qualitatively, the data is very similar to the analysis of the effective multifractal exponents. Due to the increased statistical quality of the RGFA calculation compared to the MFA study, subleading irrelevant scaling corrections are visible, for instance in the curvature of the Lyapunov exponent at the $E = 0.6$ transition (red data in **f**). However, the data for both transitions collapses clearly to a master curve, strengthening the universality hypothesis, in a large regime of effective system sizes L/l_{micro}. As the Lypaunov exponent Γ was analyzed using

the same method by Puschmann and Vojta, 2021 for a tight binding model on a simple square lattice under the influence of a magnetic field, a direct comparison of the quantum Hall transition in the Chern insulator to the normal integer quantum plateau transition becomes possible: The corresponding data, published in Puschmann and Vojta, 2021, is superimposed in panels **c**-**f** (green data).

Strikingly, by defining a microscopic length scale of this fully independent microscopic realization of a quantum Hall transition, both the apex value $\Gamma^{(0)}$ – converging towards the critical Lyapunov exponent (Puschmann *et al.*, 2019; Puschmann and Vojta, 2021) – as well as the curvature $\Gamma^{(2)}$ – asymptotically scaling with ν – can be collapsed on top of the previously found master curve of the Chern insulator, upon normalization by $\mathcal{N}$. This is a smoking gun for the critical exponents ν, y being identical not only for different energies within the model of the disordered Chern insulator, but also with the well studied integer quantum Hall transition in its conventional Landau level realization on a square lattice.

So far we have shown visually and by comparison across a different realization of the quantum Hall transition that universality is consistent with the quantum Hall transitions of the Chern insulator studied in this thesis. Finally, we quantify the critical exponents, to provide a comparison with the remaining literature, for instance the much studied Chalker-Coddington network models. In table 2 several independent data fits based on the model Eq. (30) are summarized using both RGFA and MFA calculations for $E = 0, 0.6$ in the disordered Chern insulator.

In the regime studied in this chapter up to the system sizes numerically accessible a critical exponent $\nu = 2.6$ (as well as irrelevant corrections of $y \sim 0.3 - 0.4$ and $y' \sim 1.0 - 1.5$) consistent with previous high-precision studies on the Chalker-Coddington network or tight binding models of the integer quantum Hall effect can be found. The statistical errors are still sizable, in particular for the irrelevant scaling exponents and when performing a full fit using only the MFA data, which is of slightly reduced statistical quality, compared to the RGFA data.

It has to be noted, as irrelevant finite-size corrections are obviously present and sizable in the system size regime studied here, it cannot be fully excluded that there is a change of the trend away from the established values for the exponents $\nu = 2.6$ and $y \sim 0.3 - 0.4$ starting at much larger system sizes.

4.3.3 *Excursion: Generalized multifractality at criticality in the disordered Chern insulator*

Multifractal exponents quantify the large amplitude fluctuations of wave functions at the critical point of an Anderson transition. They therefore govern the scaling of (auto)correlation functions of a wave function at different spatial positions (Evers and Mirlin, 2008).

The notion of multifractality in the context of Anderson transitions can be generalized to correlation functions across different wave functions close in energy.

Energy	Quantity	$\nu(\Delta\nu)$	$y(\Delta y)$	$y'(\Delta y')$	$Y_c(\Delta Y_c)$	$X_c(\Delta X_c)$	L_{min}	χ^2
$E = 0.6$	RGFA, Γ	2.62(7)	0.31(11)	1.39(19)	0.803(14)	2.045(2)	48	0.77
$E = 0.6$	RGFA, Γ	2.61(2)	0.34(2)	1.29(9)	0.808(3)	2.045(1)	12	0.93
$E = 0.6$	MFA, $\tau_{0.5}$	2.62(13)	0.39(30)	1.4(1.4)	0.936(1)	2.048(6)	32	0.75
$E = 0.6$	MFA, $\tau_{0.5}$	2.64(8)	0.35*	1.5(8)	0.9365(4)	2.049(2)	32	0.76
$E = 0.0$	RGFA, Γ	2.66(4)	0.40(7)	1.05(21)	0.818(9)	2.454(1)	20	1.60
$E = 0.0$	RGFA, Γ	2.59(3)	0.36(6)	1.09(21)	0.815(10)	2.454(1)	16	1.76
$E = 0.0$	MFA, $\tau_{0.5}$	2.59(17)	0.4(0.4)	1.5(1.5)	0.936(3)	2.454(2)	64	1.30
$E = 0.0$	MFA, $\tau_{0.5}$	2.61(7)	0.35*	1.6(1.2)	0.9359(5)	2.454(2)	64	1.40

Table 2: Estimates for the critical parameters at the quantum Hall transitions at $E = 0.0$ and $E = 0.6$, using the ansatz in Eq. (30) with data extracted from Eq. (29) for system sizes $L \geqslant L_{min}$. Y represents the dimensionless observable studied. To evaluate the quality of the fit a χ^2-test is performed. To stabilize the fit for larger L_{min} the subleading irrelevant correction for the curvature has been set to zero. Errorbars denote the 1σ-confidence intervals. *fitting ansatz has been performed using a fixed value for y, to obtain a stable fit. $y = 0.35$ is motivated by previous works on the quantum Hall transition and the fits using RGFA. Raw data for RGFA analysis is used with permission by M. Puschmann.

The generalized moments can be defined as two-point correlation functions featuring two different wave functions ψ^{E_1}, ψ^{E_2} with $E_1 \approx E_2$ as

$$P_{qq}(\mathbf{r}) = \sum_{\mathbf{r}'} \begin{vmatrix} \psi^{E_1}_{\mathbf{r}'} & \psi^{E_2}_{\mathbf{r}'} \\ \psi^{E_1}_{\mathbf{r}'+\mathbf{r}} & \psi^{E_2}_{\mathbf{r}'+\mathbf{r}} \end{vmatrix}^{2q}, \tag{31}$$

where $\mathbf{r}' = (x', y')$ runs over all lattice sites and $|\cdot|$ here denotes the determinant of the 2×2-matrix. This expression can naturally be extended to n-point correlation functions, and reduces to P_q, Eq. (18), in the case of a single wave function.

The dependence on the linear system size L can be similarly described by power laws governed by an extended set of critical exponents, $P_{qq} \sim L^{-\tau_{qq}}$ in the asymptotic limit $r = |\mathbf{r}| \to 0, L \to \infty$ (ensemble averaging is implied). The topic has gained attention in recent years since the study of generalized multifractality is believed to enable a better understanding of criticality at Anderson transitions such as the conditions for local conformal invariance at the critical point (Karcher *et al.*, 2021; Karcher *et al.*, 2022; Babkin *et al.*, 2023; Karcher *et al.*, 2023).

Due to the periodic boundaries of the disorder configurations drawn from Eq. (16), it is natural to measure distances using a toroidal metric instead of r directly,

$$\rho(\mathbf{r}) = \frac{L}{\pi}\sqrt{\sin^2(\pi/L \cdot x) + \sin^2(\pi/L \cdot y)}. \tag{32}$$

Without loss of generality only the x-direction of the correlation function is investigated; additionally we focus on $q = 1$. The correlation function in dependence on r is solved via the fast Fourier transform (FFT) algorithm (implemented

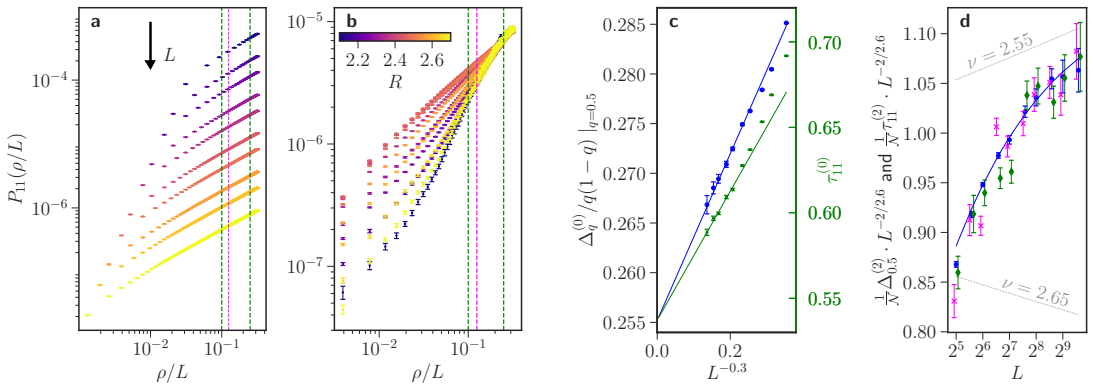

Figure 9: **a** Spatial dependence of the correlation function $P_{11}(x, y = 0)$. System size dependence for $L = 16 \to 768$ at criticality $(E, W, R) = (0, 1.4, 2.44)$. **b** P_{11} for different R across the quantum Hall plateau transition, $L = 256$. The green vertical lines define the window where the effective subleading multifractal exponent $\tilde{\tau}_{11}$ is extracted. Complementarily, we track the value of P_{11} at the magenta vertical line. **c** $\tau_{qq}^{(0)}$ extracted from the fit with Eq. (29) as a function of system size; approximate slope of the curves in **b** calculated by a finite difference between the values at the green vertical lines in **b**. Blue data is taken from Fig. 7. **d** Curvature $\tau_{11}^{(2)}$ normalized and reduced by the expected scaling $L^{2/2.6}$ from Fig. 7, together with the MFA data from Fig. 7. Green data corresponds to the approximated slope of panel **b** while magenta data corresponds to the values intersected by the magenta vertical line in panel **b**. The assumed irrelevant scaling exponent is $y = 0.3$.

in `SCIPY`) and the convolution theorem. An effective exponent – analogous to Eq. (22) – is extracted by

$$\tilde{\tau}_{11}(L) = \ln(P_{11}(\rho_1, L)/P_{11}(\rho_2, L))/\ln(\rho_1/\rho_2)\,, \tag{33}$$

where $\rho_{1,2}$ are distances between which we approximate the slope of the correlation function as its finite difference.

The spatial dependence of P_{11} is shown in Fig. 9 **a**. At the critical point $(E_c, W_c, R_c) = (0, 1.4, 2.44)$ – for which results on regular MFA and RGFA have been presented earlier in this chapter – the correlation functions resemble power laws over a wide range of ρ with approximately the same exponents for all L[3]. The mapping to the toroidal distance guarantees validity of the power law behavior up to distance of order $\sim L/2$. We extract the power law exponents at intermediate ρ as a finite distance between two values ρ_1, ρ_2 (vertical green lines). Complementarily, we track the value of the correlation functions at a fixed value of ρ (magenta vertical line). In panel **b** the Hamiltonian parameters are varied across the transition, demoting the exponents to effective exponents, analogously to Eq. (22), because the correlation function does not resemble a (simple) power law in this regime.

3 up to additional irrelevant scaling corrections for finite r, ρ, L

In panels **c, d** the effective subleading exponent $\tilde{\tau}_{11}$ is analyzed analogously to the leading MFA in Fig. 7. Assuming irrelevant scaling similar to Fig. 7 the asymptotic subleading exponent τ_{11} can be extrapolated. For the generalized multifractal exponents the parabolic paradigm for τ_q – as cited above – can be extended, namely,

$$\tau^{(p)}_{qq'} = \frac{1}{4}\left[q(1-q) + q'(3-q')\right], \tag{34}$$

and compared to the numerical data. A simple power law extrapolation in panel **c** yields $\tau_{11} \sim 0.55(2)$, which differs significantly from the parabolic prediction, $\tau^{(p)}_{11} = 0.5$. However, for a thorough finite-size scaling analysis a simulation with high statistical accuracy and at different moments q would be in order. This calculation serves only as an outlook on a more focused investigation of possible deviations of the parabolic prediction for the generalized multifractal dimensions in future research.

Tracking the curvature – again analogously to Fig. 7 – of the effective exponent close to the critical point, $\tau^{(2)}_{11}$, extracted from Eq. (29), we can compare its scaling with the leading multifractal exponents $\tau^{(2)}_{0.5}$ (blue data, taken from Fig. 7) in panel **d**. The green data corresponds to the approximated slope of the curves in panel **b**, the magenta data simply tracks the values of P_{11} at the magenta vertical line in **b**. Both data sets lie on top of the data for the leading exponents and the guide to the eye assuming $\nu = 2.6, y = 0.3$. Hence, in principle also the localization length exponent can be studied using the generalized multifractal dimensions. However, the statistical errorbars are significantly larger than for the leading exponents, even though the same set of ensemble configurations has been used. This hints at the observation that the subleading MFA has a reduced signal-to-noise ratio and is hence less effective to analyze the transition.

In the future it would be particularly interesting to perform a more thorough study of the multifractal dimensions $\tau_{qq'}$ to study possible deviations from the generalized parabolicity, Eq. (34). This first study in the Chern insulator as well as first recent numerical effort in different models suggest that the deviations might be larger and therefore more easily accessible in the subleading compared to the leading multifractal analysis (Babkin *et al.*, 2023). An understanding of possible deviations from parabolicity could have interesting implications for the presence or absence of local conformal invariance and other properties of critical points of Anderson transitions in two spatial dimensions (Karcher *et al.*, 2022).

4.4 AMORPHOUS REALIZATION OF THE CHERN INSULATOR

This section is based on the publication Bera et al., 2024. The multifractal analysis was carried out by the author of the thesis, while S. Bera and N. P. Nayak contributed the transport calculation.

In the previous section we have not been able to corroborate a critical line scenario for quantum Hall criticality with an energy dependent localization length exponent ν in the QWZ model of the disordered Chern insulator. However, as discussed, additional evidence for deviations from a universal set of critical exponents of class A transitions has been presented in recent years.

A study of a geometrically disordered CC network model by Gruzberg *et al.*, 2017 observed a localization length exponent $\nu \sim 2.37$ suggesting strong deviations from the established result for (regular) CC models and tight binding models in a magnetic field ($\nu \sim 2.6$). This was interpreted as evidence either for a second fixed point in the renormalization group flow mediated by additional (geometric) disorder potentials or the existence of a critical line in class A transitions (Gruzberg *et al.*, 2017; Klümper *et al.*, 2019). The appearance of (at least) a second fixed point is explained by the mapping of the structurally disordered model in the continuum limit not only to Dirac fermions coupled to disorder potentials, but to quenched quantum gravity; the latter being absent in regular CC models (Gruzberg *et al.*, 2017).

In the following section a model of the anomalous quantum Hall effect will be presented where disorder is realized also geometrically by breaking up the translational invariance of the underlying lattice randomly. The resulting model can be called amorphous Chern insulator (Agarwala and Shenoy, 2017).[4]

LOCALIZATION LENGTH EXPONENT. The motivation for studying its critical exponent is twofold: Firstly, the model allows for an independent study of the effect of structural disorder in a realization of the anomalous quantum Hall transition, and can be compared to the geometrically disordered CC models, which found a non-universal critical exponent ν. Secondly, an investigation of possible deviations from the conventional lattice model of the Chern insulator is due. This is in particular interesting since a previous study by Ivaki *et al.*, 2020, claims to have found evidence for non-universality within this model, by estimating its critical exponent $\nu = 1 - 1.35$. The authors suggest that the shift in ν is mediated by the vicinity of a percolation transition of the amorphous graph itself close to the topological phase transition. The model belongs to symmetry class D, therefore a thorough study investigating the potentially non-universal

4 There have been studies investigating criticality in models where disorder enters in the lattice structure, for instance in random Voronoi/Delaunay graphs by Puschmann *et al.*, 2015; Puschmann, 2017. Recently, Dresselhaus *et al.*, 2024 suggested an amorphous lattice inspired by a Voronoi/kagomé construction, which would be also highly interesting in terms of its critical properties at quantum Hall transitions.

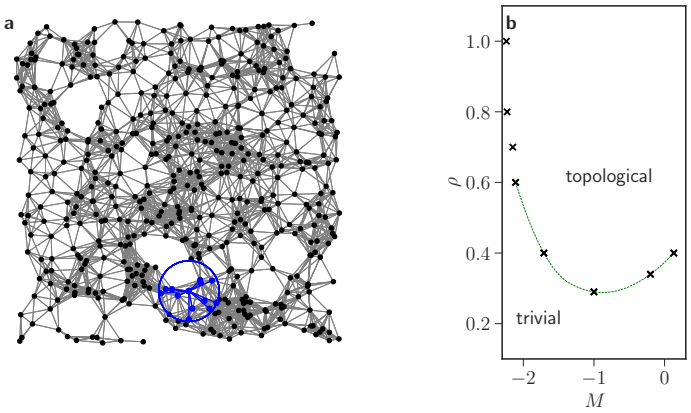

Figure 10: **a** Realization of the lattice of the amorphous Chern insulator. N lattice points (black) are distributed randomly in the $L \times L$ plane, defining the density $\rho = N/L^2$. Hopping is allowed if lattice points have a distance up to a length R as shown in blue around a sample point. Here $L = 32, \rho = 0.5, R = 3$. Construction follows Agarwala and Shenoy, 2017. **b** Qualitative phase diagram of the amorphous Chern insulator, the symbols are estimated critical points, calculated for system size $L = 48, \rho = 0.7, R = 4$, the dotted line is a guide to the eye depicted the approximated phase boundary between topological and trivial phases. The corresponding topological invariant is given by the so-called Bott index (Agarwala and Shenoy, 2017).

behavior in the amorphous realization of class A becomes important. It will be presented in section 4.4.1 .

MULTIFRACTAL ANALYSIS. In the second part of this section a detailed analysis of the multifractal dimensions at the critical point is presented. As introduced in section 3.2 it allows for quantifying the critical fluctuations of wave function amplitudes, by a non-linear dependence of the exponent τ_q on the moment q. The functional form of τ_q strongly constrains the possible analytical theories describing the quantum Hall critical point. Due to Zirnbauer, 1999; Zirnbauer, 2019 suggesting a purely parabolic dependence on q, the investigation of the multifractal properties has gained momentum in recent years once again. In particular there have been studies investigating possible higher order corrections to τ_q, which would exclude the type of theory suggested (Evers *et al.*, 2008; Obuse *et al.*, 2008; Babkin *et al.*, 2023). Its thorough analysis proves highly difficult, because of the very sizeable and slow (in a renormalization group sense, possibly almost logarithmic) irrelevant finite-size corrections present in class A.

Here we attempt to complement previous studies, exclusively realizing the CC model of the quantum Hall effect, with a thorough analysis of a critical point in the amorphous Chern insulator and quantify possible quartic corrections to τ_q in section 4.4.2.

MODEL. By definition crystalline order is absent in an amorphous lattice. Here the construction proceeds as follows: N points, serving as lattice points/atom

positions, are randomly placed in a two-dimensional box of linear size L, characterized by the density $\rho = N/L^2$. The distribution of the real space coordinates is uniform and uncorrelated. Hopping between two pairwise sites, each hosting two orbital degrees of freedom, can occur if their distance is smaller than a length R, cf. Fig. 10 **a**. Hence, the hopping is of short range and the (average) connectivity of the lattice graph is variable and depends on the density ρ and the cut-off length R.

The Hamiltonian realized on this lattice is given by (Agarwala and Shenoy, 2017)

$$\mathcal{H} = -\sum_{ij}\sum_{\alpha\beta} T_{\alpha\beta}(\mathbf{r}_i - \mathbf{r}_j) c^\dagger_{i\alpha} c_{j\beta}, \tag{35}$$

where the hopping matrix reads

$$T_{\alpha\beta}(\mathbf{r}_i - \mathbf{r}_j) = \vec{d}\cdot\vec{\sigma}\; C\, e^{-|\mathbf{r}_i - \mathbf{r}_j|}\, \Theta(R - |\,\mathbf{r}_i - \mathbf{r}_j\,|). \tag{36}$$

$\vec{\sigma}$ denotes the four-dimensional vector of Pauli matrices, $\sigma_0 = \mathbb{1}$, $\sigma_{1,2,3} = \sigma_{x,y,z}$; its prefactors are given by $\vec{d}$ with

$$\begin{aligned} d_0 &= \frac{t_0}{2}, \qquad d_x = -\frac{1}{2}\cos\theta(i + \cos\theta) \\ d_y &= \frac{i}{2}\sin\theta(\frac{i}{2}\sin\theta - 1), \qquad d_z = -1/2, \end{aligned} \tag{37}$$

for $\mathbf{r}_i - \mathbf{r}_j \neq 0$ (inter-orbital hopping) and $(d_0, d_x, d_y, d_z) = (0, 1/2, 1/2, 2 + M)$ for $\mathbf{r}_i - \mathbf{r}_j = 0$. $\mathbf{r}_i$ is the position vector of the ith lattice point in a Cartesian coordinate system and θ the angle between $\mathbf{r}_i - \mathbf{r}_j$ and the positive x-axis. The prefactor is $C = e$ for inter-orbital and $C = 1$ for intra-orbital hopping. Θ denotes the Heaviside function (Agarwala and Shenoy, 2017; Bera *et al.*, 2024). The mass parameter M and the density ρ span the phase diagram in terms of the so-called Bott index (Agarwala and Shenoy, 2017), characterizing topologically trivial and non-trivial phases, cf. Fig. 10 **b**. For $t_0 \neq 0$ the system has none of the fundamental symmetries, rendering it a member of symmetry class A. In this section $t_0 = 1/4$, $R = 4$ are chosen and the scaling behavior is studied as a function of (M, ρ).

Computationally, for the multifractal analysis presented in the following, the linear system size L is increased from 16 to 768, and the Hamiltonian is diagonalized by the implicitly restarted Lanczos method with shift invert at zero energy. The routine is implemented in `ARPACK` (Lehoucq *et al.*, 1998), and calculates the five lowest lying eigenstates of the Hamiltonian matrix. Results are averaged over many disorder configurations, cf. table 5 in appendix B, and checked against convergence when taking only a subset of the calculated eigenstates.

4.4.1 *Localization length exponent in amorphous systems*

EFFECTIVE MULTIFRACTAL DIMENSION. Similarly to the analysis of the quantum Hall transition in the disordered Chern insulator on a square lattice con-

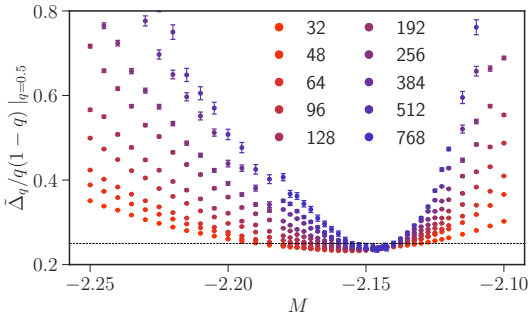

Figure 11: Effective anomalous dimension $\tilde{\Delta}_q$ from the pseudo-derivative in Eq. (22) at $q = 0.5$ for system sizes indicated in the legend. The parameters are $E = 0, \rho = 0.7, R = 4$. In the vicinity of the minima the data is fitted by the ansatz in Eq. (29) up to order $r = 4$ to obtain the effective off-set, the critical point and the curvature. The horizontal line marks the parabolic prediction by Zirnbauer.

sidered in the previous section, the effective multifractal dimension $\tilde{\tau}_q(L; E, M, \rho)$ is calculated across the phase boundary of the topological phase, cf. Fig. 11. Here the parameter subset $(E = 0, M, \rho = 0.7)$ is chosen, and M is varied. Fig. 12 shows the fitted parameters $\Delta^{(0)}, \Delta^{(2)}, M_m$ according to the expansion in Eq. (29) as a function of L, allowing for an extrapolation of the localization length exponent, the critical point and – to limited extent – also of the leading irrelevant exponent y and the critical multifractal dimension. Panel **a** shows that the curvature extracted from the series expansion (29) of the effective dimension across the transition is consistent with $\nu = 2.6$, while $y \sim 0.5$. The critical point $M_c = -2.143(4)$ can be extrapolated assuming leading irrelevant corrections with $y = 0.5$ (panel **b**). Panel **c** shows apex values of the prefactor of the effective anomalous dimension, which is consistently lower than the parabolic prediction by Zirnbauer, 2019. This is in contrast to simulations of the CC model and other realizations of quantum Hall plateau transitions, where extrapolations of the parabolic prefactor of Δ_q^{QH} consistently larger than ~ 0.25 are reported (Evers *et al.*, 2008; Obuse *et al.*, 2008). By itself this is an interesting observation and may allow for confining the numerical value of the parabolic part of the anomalous dimension of the class A universality classes (assuming there is indeed universality) by a multi-model comparison, which has been a notoriously difficult task in the past. A more detailed analysis of the critical multifractal dimension is presented in the next subsection by comparing to the results obtained for the CC network in the literature.

TRANSPORT CALCULATION. Before analyzing the multifractal dimension of the critical point in close detail, additional evidence for the localization length exponent being consistent with universality across different models is presented, using a complementary transport approach. The (dimensionless) conductance, similarly as the Lyapunov exponent of wave function or their multifractal dimension, is highly sensitive to the localization length in finite samples. Therefore, by

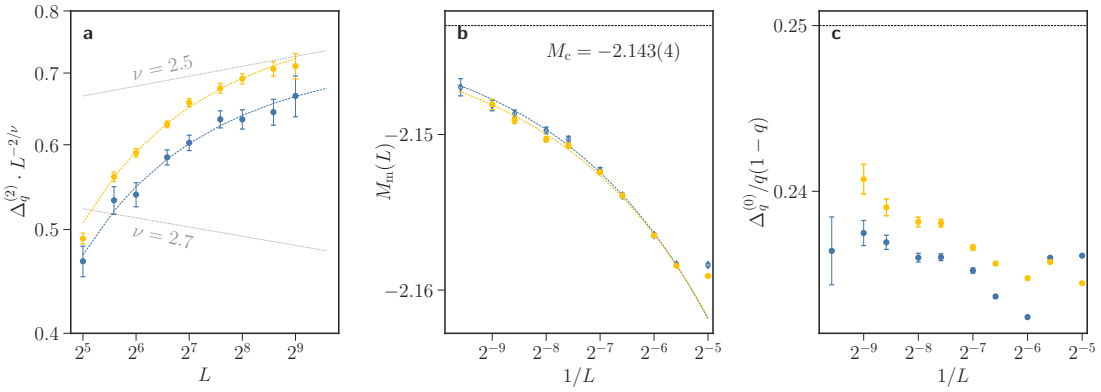

Figure 12: Finite-size scaling of the effective multifractal dimension at the quantum Hall transition of the amorphous model at moments $q = 0.5, 1.5$. **a** Curvature $\Delta_q^{(2)}$ reduced by $L^{-2/2.6}$ obtained from the series expansion (29). Curves are guides to the eye assuming $\nu = 2.6, y = 0.5$. **b** Scaling of the minimum of the effective dimension. The dashed line marks the extrapolation to the critical point M_c. **c** Extrapolated critical multifractal dimension. The numerical values are all below the prediction of Zirnbauer, 2019, $\Delta_q^{(p)} \sim 0.25q(1-q)$, however a stable fit of the finite-size corrections remains difficult. The density of lattice points was chosen to be $\rho = 0.7$ and $R = 4$.

a system size scaling of a sample connected to leads through which a current can flow, and analyzing the asymptotic behavior of the corresponding conductance through the sample, the localization length exponent can be extracted in the vicinity of the topological phase transition of the amorphous Chern insulator.

Technically, the conductance is calculated in a two-terminal transport setup of a tight binding sample connected to two leads modeled by electrons hopping between nearest neighbors on a simple square lattice. By calculating the scattering matrix and applying the Landauer formalism (Landauer, 1957) the dimensionless conductance g is obtained in units of e^2/h. Again an ensemble average needs to be performed which is implied henceforth. The applied transport method is described in more detail in appendix C. The calculations have been performed by S. Bera and N. P. Nayak, using the python transport package `KWANT` (Groth *et al.*, 2014); the data presented is published in Bera *et al.*, 2024.

Fig. 13 **a** shows the raw data of the conductance at the quantum Hall transition at $(E = 0, M, \rho = 0.7)$. The presence of irrelevant scaling corrections is evident from the fact that no unique crossing point is visible. The exponents ν, y, the critical point M_c and expansion coefficients are modeled by Eq. (91) as detailed in appendix C, through a χ^2-minimization. By subtracting the irrelevant scaling contribution according to Eq. (92) the pure relevant conductance scaling is obtained (panel **b**). Only the single relevant scaling parameter $\sim (M - M_c)/M_c \cdot L^{1/\nu}$ remains and a unique crossing point emerges indicating quantum Hall criticality. The corresponding scaling collapse is shown in panel **c**. Complementarily, the analogous scaling collapse of the logarithmic measure of the mean conductance is shown in the inset. The exponents $\nu = 2.58(2), y = 0.35(3)$ emerging

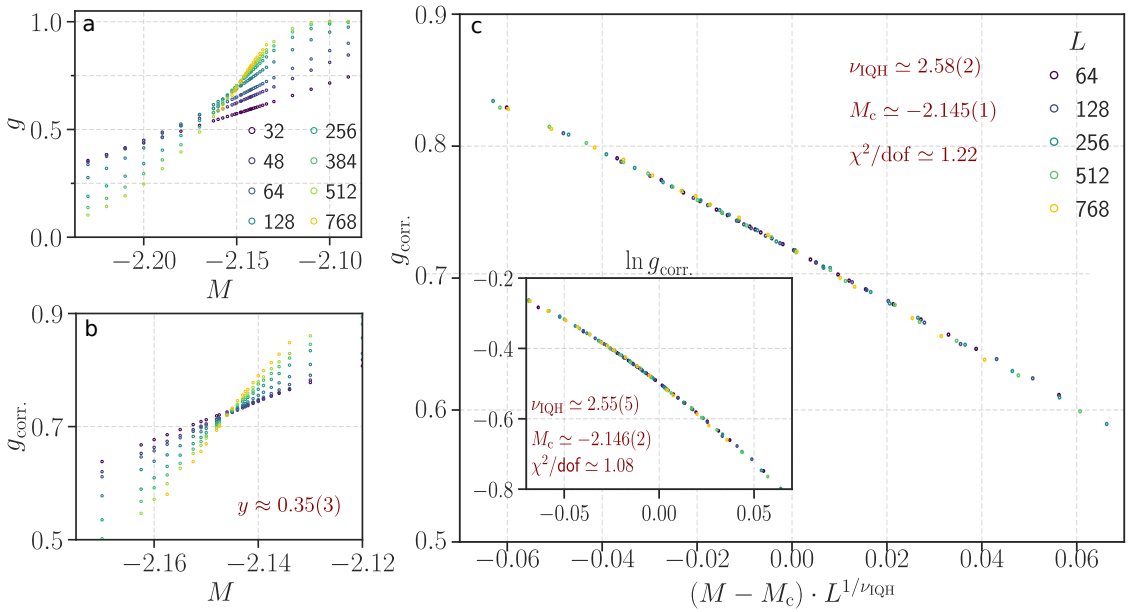

Figure 13: Scaling analysis of the conductance g obtained from Eq. (90), using the scaling ansatz in Eq. (91). **a** Conductance data, averaged over many disorder samples, across the transition at density $\rho = 0.7$ as a function of M. **b** corrected conductance g_{corr}, Eq. (92), where fitted finite-size corrections are subtracted, see appendix C for details. **c** Scaling collapse of the corrected conductance with $\nu \sim 2.58(2)$. (inset) scaling collapse of the logarithmic conductance. The collapse is obtained with an irrelevant scaling exponent $y \sim 0.36$. Adapted from Bera *et al.*, 2024, ©2024 American Physical Society.

from the conductance analysis agree very well with literature results on the Chalker-Coddington network and other models of the integer quantum Hall effect, including the exponents of the transitions in the disordered Chern insulator on a square lattice presented in the previous section.[5]

4.4.2 *Multifractality of the amorphous topological insulator at criticality*

RECIPROCAL SYMMETRY. At the quantum Hall critical point it was shown that the anomalous dimension Δ_q obeys an exact symmetry around $q = 0.5$ (Mirlin *et al.*, 2006), $\Delta_q = \Delta_{1-q}$, which was also checked numerically in Chalker-Coddington network models (Evers *et al.*, 2008). It implies that the function

$$r_q(L) = L^{2(2q-1)} \cdot \frac{P_q}{P_{1-q}}, \tag{38}$$

is a constant in the asymptotic large system size limit. The henceforth called reciprocity relation therefore serves as a a benchmark for the vicinity to the

5 In the original publication Bera *et al.*, 2024 the dependence of the critical exponents on the density of lattice points ρ was checked. Also here consistency with universality has been observed. The expansion orders of the fitting procedure have also been varied to ensure stability of the scaling ansatz.

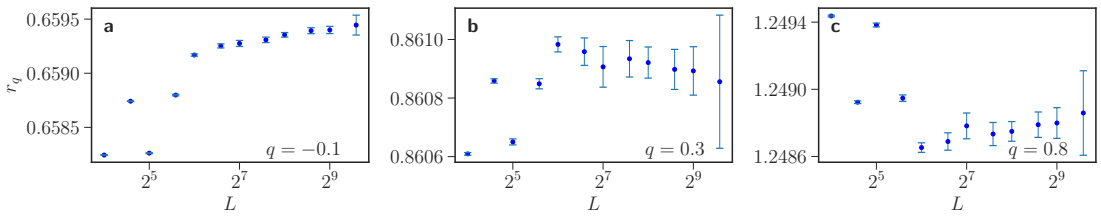

Figure 14: Reciprocity relation at the quantum Hall transition for $q = -0.1, 0.3, 0.8$ at $M_c = -2.144, \rho = 0.7, E = 0$. Convergence is present from $L > 2^7$ onwards. Slight deviations persist $< 0.1\%$, indicating potential remaining irrelevant corrections and residual statistical uncertainty. Adapted from Bera *et al.*, 2024,©2024 American Physical Society.

asymptotic regime: When irrelevant finite-size corrections become small, a constant function of q is approached. However, taking r_q as the benchmark for the asymptotic regime has to be done with caution; recent works suggest that reciprocity is present even before the asymptotic scaling regime develops (Gruzberg *et al.*, 2013).

In Fig. 14 r_q as a function of the linear system size L is presented for different moments q. With increasing L a constant function is approached. Still slight deviations can be observed, indicating residual statistical uncertainty, or potential irrelevant scaling corrections, present up to larger system sizes. However, the corrections must be small, as the deviations are $< 0.1\%$. Again it is unclear if the converged reciprocity relation actually indicates the absence of irrelevant scaling corrections in all other quantities of interest, for instance the curvature of the anomalous dimension Δ_q; there is evidence, that r_q approaches the scaling limit faster than the full function Δ_q.

WAVE FUNCTION MOMENTS. Prominently, Zirnbauer's marginal field theory for the quantum Hall plateau transition connects the prediction of $\nu, y^{-1} \to \infty$ with the necessity of a purely parabolic anomalous dimension Δ_q (Zirnbauer, 1999; Bondesan *et al.*, 2017; Zirnbauer, 2019; Dresselhaus *et al.*, 2021). In light of this development, it is natural to accompany the study of the localization length exponent with the properties of wave functions at criticality itself, i.e. their multifractal dimension. Additionally, as the multifractal spectrum of the quantum Hall plateau transition has been mainly checked in the Chalker-Coddington network before (Evers *et al.*, 2008; Evers and Mirlin, 2008; Obuse *et al.*, 2008), a thorough study in the amorphous Chern insulator may allow for a detailed inter-model comparison, and hence may hint at (non-) universality.

Zirnbauer, 1999; Zirnbauer, 2019 suggested an anomalous dimension

$$\Delta_q^{(p)} = \frac{1}{4} q(1-q). \tag{39}$$

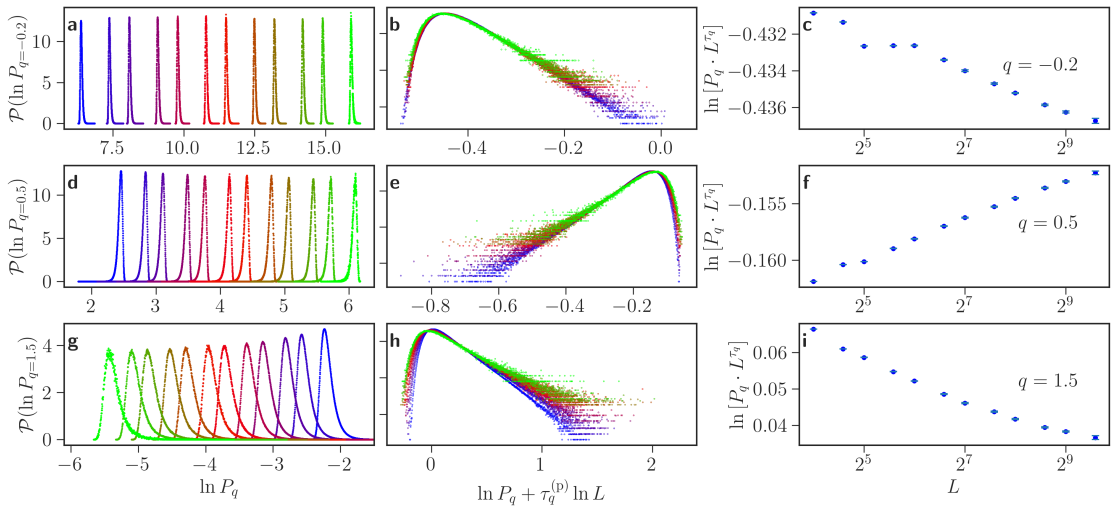

Figure 15: Distribution functions of the wave function moments P_q for increasing system sizes $L = 16 - 768$ (blue to green) at the extrapolated critical point $M_c = -2.144$, on a linear scale for $q = -0.2, 0.5, 1.5$ (**a,d,g**) and a logarithmic scale reduced by the parabolic prediction $\tau_q^{(p)}$ (**b,e,h**). The right column shows the residual flow of the reduced mean of the distribution functions, indicating the remaining corrections (irrelevant or relevant) to the parabolic scaling prediction (**c,f,i**). Adapted from Bera *et al.*, 2024,©2024 American Physical Society.

This result has been questioned by several numerical studies (Evers *et al.*, 2008; Obuse *et al.*, 2008) which found small quartic corrections in Chalker-Coddington networks.

In Fig. 15, first column, the distribution functions of the moments P_q for different values $q = -0.2, 0.5, 1.2$ are shown at the extrapolated critical point $M_c \sim -2.144$[6]. Their shapes become almost invariant for large enough system sizes, and almost collapse when the horizontal axis is rescaled with the system size dependence of the moments, Eq. (19), assuming a parabolic form of the dimension. If Zirnbauer's conjecture is correct the collapse should be perfect when irrelevant corrections do not play a role at large L. However, at closer quantitative inspection a residual shift of the distribution functions is visible. This becomes very clear when showing the means of the distribution functions, reduced by parabolic scaling (right column). All curves should converge to a constant of q, assuming Eq. (39). This clearly is not the case, the corrections are significantly larger than the statistical uncertainty.

However, determining the origin of the corrections remains challenging: A clear curvature is still present, particularly in the data for $q = 0.5, 1.5$ (panels **f,i**), indicating the presence of residual irrelevant finite-size corrections even at the largest system sizes L. Determining their exponent would require larger system sizes, in particular since potentially several interfering power-law corrections may

6 The calculation presented in the following has been repeated for values of M slightly away from ~ -2.144 to exclude a dependence of the result on small systematic errors of the extrapolation of the critical parameter M.

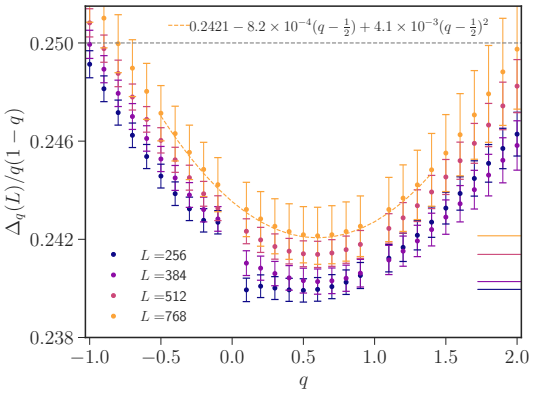

Figure 16: Higher order contribution to the anomalous dimension Δ_q as a function of system size L. No fitting function is assumed, the data is obtained as the pseudo-derivative defined in Eq. (22) at the critical point ($\rho = 0.7, M = -2.144$). The grey dashed line marks Zirnbauer's prediction, Eq. (39), while the orange dashed curve is a fit of the quartic curvature $\sim 4.1 \times 10^{-4}$. The horizontal lines mark the flow of the minima of the curves with system size L. Adapted from Bera *et al.*, 2024, ©2024 American Physical Society.

be in play here. The overall curvature though seems very small, in particular for smaller q's (where the data quality is typically the best (Puschmann *et al.*, 2021)); potentially too small to explain the residual shifts in the attempted collapse using parabolic scaling. This could indicate either a different prefactor of the anomalous dimension in Eq. (39) or higher order corrections all together. This scenario opposes the marginal scaling theory, going along the same lines as the localization length exponent found to be consistent with the exponents in more conventional models of the integer quantum Hall effect. Deviations from parabolic scaling potentially along with deviations from the 1/4 prefactor of the parabolic part in Eq. (39) are also fully consistent with existing studies on the Chalker-Coddington network models (Evers *et al.*, 2008; Obuse *et al.*, 2008). It therefore would be very interesting to quantitatively compare the higher order corrections, in particular the quartic term, to the CC results.

ANOMALOUS DIMENSION. Fig. 16 shows the anomalous part of the multifractal dimension reduced by the parabolic part predicted by Zirnbauer. Δ_q is calculated as a pseudo-derivative between subsequent system sizes, Eq. (22); hence it does not involve fitting functions and is therefore not susceptible to systematic errors originating from underestimating finite-size corrections. Zirnbauer's parabolic prediction, Eq. (39), is marked by the grey dashed line; its flatness resembles the absence of higher order corrections to its parabolic form. Several things stand out: (i) We do not observe convergence of the anomalous dimension with the system size L. (ii) Nevertheless, the shape of the anomalous dimension, including its (quartic) curvature remains stable for the shown sys-

tem sizes, while (iii) the off-set on the vertical axis is still significantly shifting upwards.

These observations are fully consistent with previous studies on the multifractal dimension of the CC network model (Evers *et al.*, 2008; Obuse *et al.*, 2008), which were able to obtain much higher numerical precisions due to the favorable structure of the CC network. It may therefore be plausible that the corrections to parabolicity are actually due to deviations from Zirnbauer's theory, and not only due to residual finite-size corrections. A definite statement about the presence or absence of such corrections is however not possible, as long as a full convergence of the anomalous dimension is not achieved.

Interestingly, one aspect of the data presented in Fig. 16 compares differently to previous studies on the CC network; the off-set shift tends to *larger* values for increasing system sizes, in contrast to the dimensions observed in CC networks (Evers *et al.*, 2008; Obuse *et al.*, 2008). As these previous studies experienced the same difficulties in converging the off-set of the multifractal dimension, the combination of the two models – assuming universality of Δ_q in class A across those models – may allow for establishing a strict upper and lower bound, which was not possible so far.

Partially motivated by Puschmann *et al.*, 2021 the quartic curvature in Fig. 16 can be characterized by a χ^2-minimization procedure; using the ansatz

$$\Delta_q = \gamma_q \, q(1-q), \tag{40}$$

with

$$\gamma_q = b_0(L) + b_1(L)(q - \frac{1}{2}) + b_2(L)(q - \frac{1}{2}). \tag{41}$$

While the asymptotic behavior of $b_0(L)$ is unclear and may potentially even converge to Zirnbauer's prediction, the quartic term $b_2(L)$ seems converged already at the system sizes available, and can be estimated to be $b_2(L = 768) = 4.1(8) \times 10^{-3}$. This value is quantitatively consistent with the studies of the CC network by Evers *et al.*, 2008; Obuse *et al.*, 2008. It is noteworthy that also a slight violation of the symmetry relation around $q = 0.5$ is observed, quantified by a finite b_1. It was not possible to faithfully judge whether its origin is statistical noise or for instance transient finite-size scaling corrections.

MULTIFRACTALITY. In the last section evidence has been presented supporting a non-parabolic anomalous dimension Δ_q. Since the data presented does not match previous studies on the CC model in its statistical accuracy, due to its non-ideal properties for computational simulations, there is a chance that the true asymptotic limit has not been reached. Given this consideration the main achievements of the multifractal analysis of the amorphous Chern insulator can be summarized as follows: We observe a non-vanishing quartic curvature in the anomalous dimension, which is consistent with the literature on the CC network. First, this hints towards a rejection of the theory by Zirnbauer, crucially building on the parabolicity of the dimension. Second, it is an instance of a universal feature of the quantum Hall critical point across vastly different models, i.e. the amorphous realization of the anomalous quantum Hall effect presented in the last section and the well studied model of the lowest Landau level, the Chalker-Coddington network model. In both models however, the fate of the quartic contribution in the thermodynamic limit eventually remains inconclusive. Additionally, the prefactor of the quadratic term in Δ_q converges to larger values; as opposed to the CC network models where the opposite tendency was observed. By a cross-model comparison this may allow for establishing strict upper and lower bounds for the prefactor in the thermodynamic limit, which has been a notoriously difficult task in the past. A non-parabolic multifractal dimension

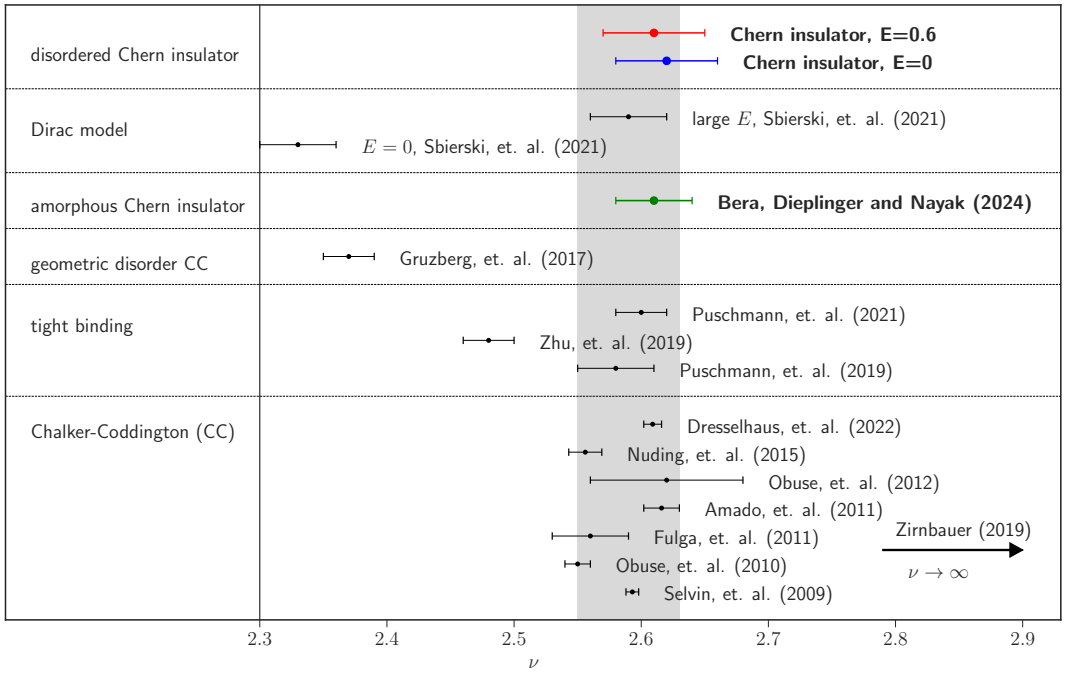

Figure 17: Literature overview of localization length exponent ν including the analysis of the anomalous quantum Hall transitions presented in this thesis.

τ_q would imply serious restrictions on the nature of possible candidate theories describing the critical point of the quantum Hall transition, which is unknown to date. The consequences of non-parabolicity are an active matter of research (Zirnbauer, 1999; Bondesan *et al.*, 2017; Zirnbauer, 2019; Karcher *et al.*, 2022).

Adding to the study of the leading multifractal exponents, we have presented a first study of parts of the generalized multifractal properties of correlation functions in the Chern insulator on a square lattice. In the future a detailed study of such exponents might enable a high-precision estimate of quartic corrections in the generalized MF spectrum, which could exhibit a more favorable signal-to-noise ratio than the leading exponents.

LOCALIZATION LENGTH EXPONENTS. In this chapter the localization length exponent of different realizations of the anomalous quantum Hall effect has been quantified. In both models there have been serious doubts that ν, y are consistent with universality of the quantum Hall transition. The disordered Chern insulator on a square lattice has been expected to show an energy dependence in its exponents, suggesting non-universality even within the model (Sbierski *et al.*, 2021). This observation was not corroborated in the study presented in this chapter. Similarly, structural or geometric disorder has been hypothesized to lead to a second renormalization group fixed point, with a possibly distinct set of critical exponents (Gruzberg *et al.*, 2017). Additionally, in related amorphous topological insulators, a dependence on the density of lattice points has been observed, reasoned to be due to the vicinity of a percolation transition (Ivaki *et al.*, 2020). Both considerations have not manifested in the amorphous realization of the Chern insulator.

In contrast, even when lacking crystalline structure all together, the localization length exponent ν is perfectly consistent with previously studied models of quantum Hall criticality. The current status of the literature on the exponent ν in different models of the integer quantum Hall effect is summarized in Fig. 17, including the results presented in this chapter on the square lattice and amorphous realization of the anomalous quantum Hall transition, cf. Slevin and Ohtsuki, 2009; Obuse *et al.*, 2010; Fulga *et al.*, 2011; Amado *et al.*, 2011; Obuse *et al.*, 2012; Nuding *et al.*, 2015; Gruzberg *et al.*, 2017; Zirnbauer, 2019; Puschmann *et al.*, 2019; Zhu *et al.*, 2019; Puschmann and Vojta, 2021; Sbierski *et al.*, 2021; Dresselhaus *et al.*, 2022; Bera *et al.*, 2024.

To conclude it is due to emphasize another time the importance of a proper consideration of irrelevant finite-size corrections and the corresponding exponents. As can be seen from the data presented in this chapter, misinterpretation of the localization length exponents, as well as the multifractal dimension, are likely. Therefore, also here it needs to be emphasized that even if the data presented here is perfectly compatible with the fitting models used, and takes into account several sources of irrelevant finite-size corrections, we cannot exclude the existence of further corrections which are not possible to be resolved at the system sizes and the statistical quality of the data available.

5

LOCALIZATION VS. SPECTRUM-WIDE CRITICALITY AT THE SURFACE OF TOPOLOGICAL INSULATORS

The results presented in this chapter were developed in collaboration with A. Altland, P. W. Brouwer, M. S. Foster, M. Moreno-Gonzalez, L. Trifunovic, S. Bera and M. Puschmann, and are partly published in Altland et al., 2024. The analytical theory in the publication was derived by A. Altland, P. Brouwer, M. Foster, M. Moreno-Gonzalez, L. Trifunovic, while the numerical simulations and analysis were carried out by the author of this thesis.

5.1 SPECTRUM-WIDE QUANTUM HALL CRITICALITY IN TOPOLOGICAL INSULATORS?

Critical states at the quantum Hall plateau transition are a glaring exception of generic Anderson localization in two dimensions. They are robustly extended and carry current even in the thermodynamic limit. Usually however, the critical fixed points in parameter space are unstable with respect to perturbations in a renormalization group sense. In reality due to the presence of imperfections one is primarily confronted with the quantum Hall insulating phases. To experimentally observe quantum Hall critical currents (beyond the edge states) in an actual sample it is necessary to fine-tune the parameters to the critical point, for instance the energy, the magnetic field or other system parameters.

Strikingly, a recent study by Sbierski *et al.*, 2020 has presented evidence that there may be more stable quantum Hall criticality with respect to parameter changes on the surface of three-dimensional topological insulators in models of the chiral symmetry class AIII. It has been debated if finite energy states localized to the surface, namely those away from the high symmetry point protected by chiral symmetry, may be critical states effectively belonging to class A, namely of the quantum Hall type. This feature has been reported to be surprisingly stable with respect to changes in the energy. The phenomenon has therefore been called *spectrum-wide criticality*.

This prediction, for which an effective Dirac surface theory and numerical evidence have been presented (Sbierski *et al.*, 2020; Karcher and Foster, 2021), suggests that the unstable integer quantum Hall critical fixed point is promoted to a stable phase by the bulk-boundary principle of the three-dimensional topological bulk material. The chiral symmetry present in the bulk Hamiltonian of class AIII is hereby broken explicitly away from the high symmetry point around which

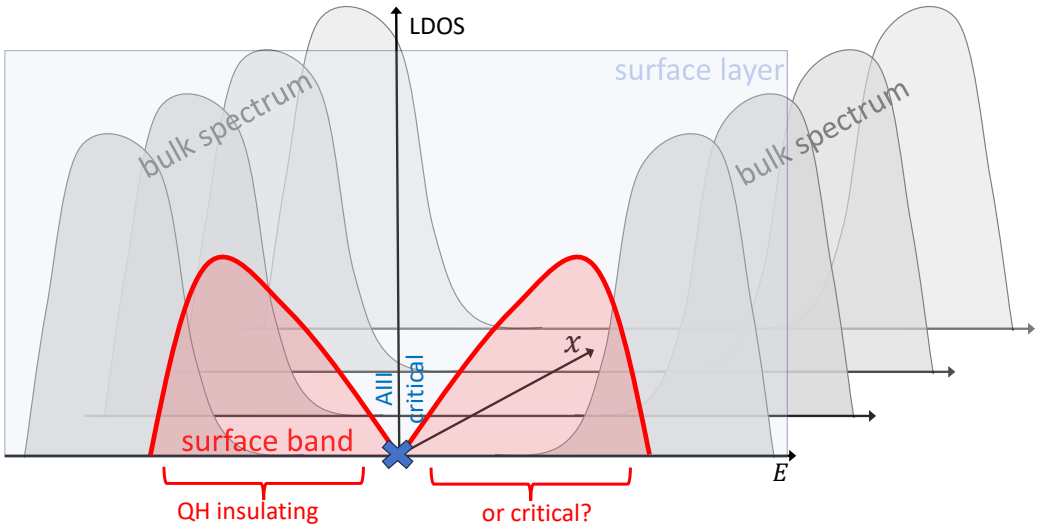

Figure 18: Schematic local density of states (LDOS) of the AIII topological insulator Eq. (42). The surface layer, where the boundary conditions are opened, is placed in the visual plane (blue shaded), orthogonal to the x-axis. The clean bulk spectrum is gapped; the gap is populated by few scattering states in the presence of disorder. The surface layer hosts an additional surface band (red), which fills the bulk gap. At the high symmetry point ($E = 0$) wave functions are AIII critical according to the bulk-boundary correspondence and protected. The finite energy surface states (red) break the AIII symmetry, their fate is the subject of this chapter.

the spectrum is symmetric, rendering finite energy surface states effectively in class A. However, strict topological arguments protecting the boundary states of an AIII bulk from localization only apply to the zero energy state, not to the entire finite energy surface spectrum (Essin and Gurarie, 2015). Therefore, the result presented by Sbierski *et al.*, 2020 is highly non-trivial.

In the present section we revisit the conclusion presented by Sbierski *et al.*, 2020 and present high-precision numerical data supporting the claim of quantum Hall critical states at a range of energies inside the bulk gap in a concrete model of a AIII topological insulator. We show that the results are somewhat robust with respect to the choice of system parameters. In the following sections the limits of generic quantum Hall criticality without fine-tuning are shown; the critical "phase" does not survive certain perturbations within class AIII, which are able to localize the surface spectrum with the sole exception of the AIII protected energy at the high symmetry point. The theory classifying finite energy states of symmetry-broken parts of the spectrum of chiral and particle-hole symmetric Hamiltonians is discussed together with numerical evidence for various interesting examples.

MODEL: THREE-DIMENSIONAL AIII TOPOLOGICAL INSULATOR. The starting point of the present chapter is the symmetry class AIII which is characterized by the absence of time-reversal and particle-hole, but the presence of chiral symmetry. Chiral symmetry manifests itself for instance in a mirror symmetric spectrum around a specific energy, referred to as zero energy. Consequently, in a topological phase, if present, the topological protection derived from the bulk-boundary principle only strictly refers to surface states at this high symmetry point. The rest of the surface states explicitly break chiral symmetry and hence are demoted to class A states; naively one would expect quantum Hall insulating states without fine-tuning.

The precise model of a three-dimensional topological insulator in class AIII studied in the following is the lattice Hamiltonian

$$\begin{aligned}\mathcal{H}_{\mathrm{AIII}} &= \mathcal{H}_0 + \sum_{a=1}^{3} \mathcal{H}_a,\\ \mathcal{H}_0 &= M \sum_{x,y,z} \psi^\dagger_{x,y,z} \tau_2 \sigma_0 \psi_{x,y,z},\\ \mathcal{H}_a &= \frac{1}{2} \sum_{x,y,z} \left[t^a_{x,y,z} \psi_{(x,y,z)+\mathbf{e}_a} (\tau_2 \sigma_0 - i\tau_1 \sigma_a) \psi_{x,y,z} + \mathrm{h.c.} \right], \end{aligned} \tag{42}$$

introduced by Ryu *et al.*, 2010.

Here, σ_μ, τ_μ represent the 2×2 Pauli matrices for $\mu = a = 1,2,3 = x,y,z$ and the identity matrix for $\mu = 0$. $\psi^\dagger_{x,y,z}, \psi_{x,y,z}$ represent the four dimensional fermionic spinors in real space basis at lattice site $\mathbf{r} = (x,y,z)$. $\mathbf{e}_a$ are the lattice basis vectors in direction $a = 1,2,3 = x,y,z$. Disorder enters in the hopping elements via a Peierls phase $\phi^a_{x,y,z}$,

$$t^a_{x,y,z} = e^{-i\phi^a_{x,y,z}}. \tag{43}$$

M is a mass-like parameter controlling the topological phase. $\mathcal{H}_{\mathrm{AIII}}$ anticommutes with the antiunitary $\tau_3\sigma_0$ following from the basic properties of the Pauli matrices, realizing the chiral symmetry. In the clean case, $t^a_{x,y,z} = 1$, the system is lattice periodic on a cubic lattice and can be diagonalized by a band structure with four bands. The topological phases realized in the clean case are the following: the Chern number $\nu = 1$ for $1 <| M |< 3$, $\nu = -2$ for $| M |< 1$ and $\nu = 0$ for $| M |> 3$. At the critical points the Hamiltonian experiences a band closing in the form of a Dirac cone for small energies, where the Dirac point at zero energy is protected by the bulk-boundary principle of the topological phase for $| \nu |> 0$. The boundary conditions are chosen as follows: While in y,z direction the lattice is periodic, it is open in the remaining x-direction. Here, at the borders of the sample the topological bulk results in surface states filling the bulk gap according to the bulk-boundary principle. The local density of states of such a sample is sketched in Fig. 21.

Throughout the chapter we choose two approaches to construct the disordered phases $\phi^a_{x,y,z}$. Analytical results for the high symmetry point, $E = 0$, concerning AIII criticality, have been obtained using a disordered vector potential, defined with a small correlation length ξ_A (Evers and Mirlin, 2008; Sbierski *et al.*, 2020),

$$\langle A_a(\mathbf{r}) A_b(\mathbf{r}')\rangle_{\text{ens}} = \frac{W_A^2}{(2\pi\xi_A^2)^{3/2}} \delta_{ab} e^{-|\mathbf{r}-\mathbf{r}'|/2\xi_A^2}, \tag{44}$$

where $\mathbf{r} = (x, y, z)$. The random phase is hence calculated like a Peierl's phase,

$$\phi^a_{\mathbf{r}} = \int_{\mathbf{r}}^{\mathbf{r}+\mathbf{e}_a} d\mathbf{r}' \mathbf{A}(\mathbf{r}'). \tag{45}$$

Alternatively, the phase can be chosen randomly directly with a correlation length ξ_ϕ[1], as

$$\langle \phi^a_{\mathbf{r}} \phi^b_{\mathbf{r}'}\rangle_{\text{ens}} = \frac{W_\phi^2}{(2\pi\xi_\phi^2)^{3/2}} \delta_{ab} e^{-|\mathbf{r}-\mathbf{r}'|/2\xi_\phi^2}. \tag{46}$$

The latter definition of disorder is more direct and optimal to verify that qualitative results are not depending on the finite correlation length ξ_A. The disorder strength in units of the hopping is quantified by the parameters W_A, W_ϕ, respectively.

SURFACE MULTIFRACTALITY. Similarly to chapter 3 we employ the method of multifractal analysis to identify (quantum Hall) critical states. In practice we calculate the anomalous multifractal dimensions Δ_q for surface states at different energies and parameter sets and compare to the approximate parabolic shape of Δ_q known from analytical and numerical considerations of more conventional models of quantum Hall plateau transitions. The goal is hence not to pinpoint the deviations from said parabolic prediction Eq. (39), as demonstrated in the previous chapter, but to use it as an approximate benchmark for quantum Hall criticality. Apart from the different objective in comparison to the previous chapter where we characterized the transition itself (now we are merely interested in the question if there is criticality, not in its precise characteristics), the reason for this is simply the increased complexity of the model system: Instead of a two-dimensional square lattice with two orbitals per spatial site, we now have a model of three dimensions with four orbitals, where, however, the studied physics manifests only in the two surface directions of the three spatial dimensions. The accessible linear system sizes of the surface of the topological insulator are hence much smaller than previously and a thorough finite-size scaling analysis of irrelevant corrections becomes almost impossible, making a high-precision estimate of critical properties comparable to more conventional numerical models unfeasible.

1 In practice disorder is artificially enhanced by a factor of $\times 5$ on the surface layers to enhance surface multifractality, while keeping the bulk gap largely clean of scattering states. Since this is naturally still a local potential it is a topologically allowed alteration of the disordered sample.

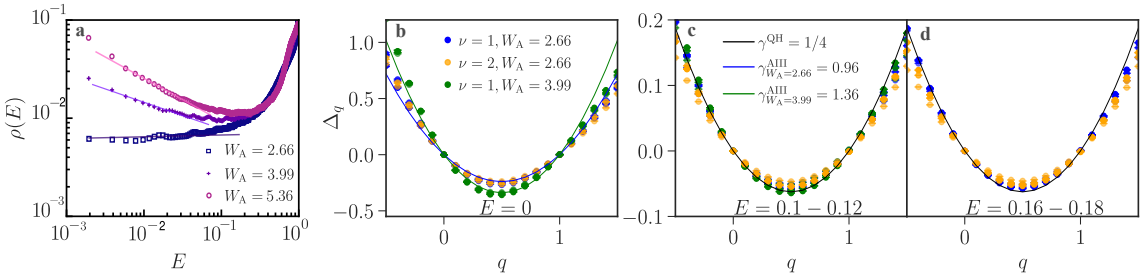

Figure 19: Multifractality and criticality of surface states at zero and finite energy of the AIII model with vector potential disorder ($\xi_A \sim 1.2$) with winding number $\nu = 1$ ($M = 2$). **a** Density of states close to zero energy, with corresponding power-law fits, obtained by the Kernel Polynomial Method method (appendix C) with 8192 Chebyshev moments on the $\nu = 1$ surface. The system size is $L = 192$ in the periodic directions y, z and $L_x = 32$ in the transverse direction. Data shown with permission by S. Bera. **b** Multifractal dimension Δ_q, according to the numerical derivative as in Eq. (22) for the largest linear surface system sizes $L = 64, 96, 128$ (from transparent to opaque colors, partly overlapping) and slab thickness $L_x = 8$. The lines correspond to the prediction by Eq. (48) using the power law fit from **a**. **c,d** Average multifractal dimension over energy windows $E > 0$, compared to the parabolic prediction for QH criticality, Eq. (39).

As in this chapter only surfaces of a three-dimensional sample are investigated, and are expected to show two-dimensional multifractality, the definition of the wave function moments needs to be reconsidered, as the surface localization is not perfect and hence the wave functions are not fully normalized with respect to their surface weight. A natural way to generalize the moments is[2]

$$P_q \to P_q^{\text{surface}} = \frac{\sum_{\mathbf{r}\in\text{surface}} |\psi_\mathbf{r}|^{2q}}{\left[\sum_{\mathbf{r}\in\text{surface}} |\psi_\mathbf{r}|^2\right]^q}, \tag{47}$$

reestablishing (surface) normalization by the denominator.

AIII CRITICALITY. In previous sections the multifractal fingerprint of quantum Hall criticality has been discussed extensively. First and foremost here the Hamiltonian of interest belongs to class AIII; it is therefore necessary to comment on the critical properties of the AIII critical state at zero energy. Here chiral symmetry is present; the critical properties have been described by a Wess-Zumino (WZ) field theory (Evers and Mirlin, 2008; Sbierski *et al.*, 2020) for short range correlated vector potential disorder (W_A). The critical state at zero energy,

2 Even though the surface weight fluctuates, it is both constant and very large $\geqslant 90\%$ for the samples studied, such that the numerical values of the extracted multifractal dimension do not depend on the choice of the normalization within the statistical errorbars of the ensemble average. At most it is expected that a different choice of normalization may alter the prefactor of irrelevant finite-size corrections. As the analysis of this three-dimensional model is computationally highly demanding a high-precision study of the irrelevant corrections goes beyond the scope of currently available computational technology.

localized to the surface, is multifractal in the two in-plane surface dimensions, with a parabolic multifractal dimension

$$\Delta_q^{\mathrm{AIII}} = \gamma_{W_A}^{\mathrm{AIII}}\, q(1-q), \tag{48}$$

similarly to the quantum Hall critical multifractal dimension. However, here the prefactor is non-universal and depends on the disorder strength W_A. Additionally, field theory predicts a singularity of the density of states $\rho(E)$ at zero energy,

$$\rho(E) \sim E^{(2-z)/z}, \tag{49}$$

where the exponent z is supposedly related to the MF spectrum by $z = 1 + \gamma_{W_A}^{\mathrm{AIII}}$ (Evers and Mirlin, 2008; Sbierski *et al.*, 2020) for bulk winding number one. By comparing the density of states with this prediction a parameter-free model of the anomalous dimension of the AIII critical point at zero energy is obtained.

In panel **a** of Fig. 19 the density of states of the mid-gap states of $\mathcal{H}_{\mathrm{AIII}}$ is shown, where disorder enters as a disordered vector potential with strength W_A and correlation length $\xi \sim 1.2$ (in units of lattice spacing). Close to zero energy the data approximately follows a power law, with exponents depending on W_A. This allows for a prediction of $\gamma_{W_A}^{\mathrm{AIII}}$ for the critical zero energy state, namely $\gamma_{2.66}^{\mathrm{AIII}} \sim 0.96, \gamma_{3.99}^{\mathrm{AIII}} \sim 1.36$. The corresponding theoretical anomalous dimension according to Eq. (48) is shown in panel **b** (solid lines). In panel **b** the anomalous dimension as a function of linear surface system size L (transparent to opaque colors, largely overlapping) is shown for the disorder strengths W_A corresponding to panel **a** at zero energy. The dimension is obtained by a fit-free calculation using a pseudo-derivative as in Eq. (22). For the system sizes shown and the statistical precision available the data is almost converged, and agrees well with the prediction from WZ field theory. The critical exponents of the anomalous dimension and the density of states close to zero energy (AIII criticality) are hence consistent with each other.

Even though the numerical verification of the critical properties of surface states in an AIII topological insulator represents an important result, the emphasis of this chapter lies on the finite energy surface states, which are not AIII critical but break the defining chiral symmetry explicitly.

QUANTUM HALL CRITICALITY. In panels **c,d** the system size dependent anomalous dimension is shown for two windows of energies inside the bulk gap but away from the high symmetry point of the spectrum at $E = 0$. There is no trend towards localization when observing the dependence of Δ_q on L. Instead both energies and all three shown parameter sets exhibit universal behavior: The functional form of Δ_q follows approximately a parabola with prefactor $\gamma = 1/4$, i.e. has the same fingerprint as the quantum Hall plateau transition in more conventional QH models, such as those studied earlier in this thesis. Even though, as discussed, the numerical precision of the study is not sufficient to quantify possible corrections to Zirnbauer's prediction of parabolic multifractality similar to

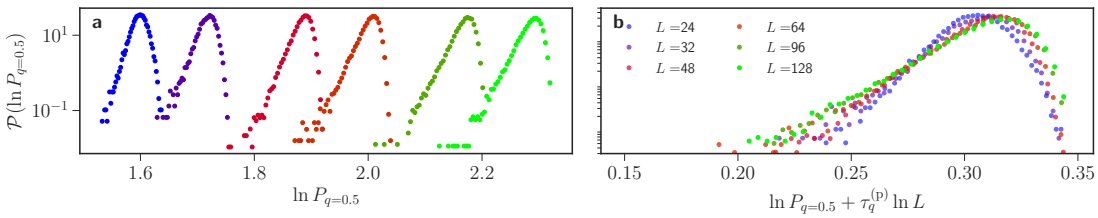

Figure 20: **a** Distribution functions of the moments P_q of wave functions with $W_A = 2.66, M = 2, L_x = 8$ in the energy window $0.1 < E < 0.12$. **b** Distribution functions rescaled with the quantum Hall multifractal dimension assuming parabolicity, $\tau_q^{(p)}$.

the study in the previous chapter, this fingerprint is a smoking gun that contrary to naive expectations finite energy states do not become quantum Hall insulating but critical; this seems to be true across a wide range of parameter choices of the present model, supporting the possibility of spectrum-wide quantum Hall criticality by Sbierski *et al.*, 2020 at least for the present three-dimensional lattice model, $\mathcal{H}_{\text{AIII}}$.

Additional support for the presence of quantum Hall criticality away from zero energy on the surface of the AIIII insulator is offered by the full distribution functions of the wave function moments P_q. Fig. 20 shows the distribution function of P_q across many samples and within an energy window $0.1 < E < 0.12$, at $\nu = 1, W_A = 2.66$ for several system sizes from $L = 24 \to 128$. The shape of the distribution becomes almost invariant for larger L, residual changes can be attributed to irrelevant finite-size corrections (which however cannot be quantified precisely due to the relatively small computational limit in linear system sizes). When reducing the moments by the effective dimension $\tau_q^{(p)}$, the distributions corresponding to larger L (brighter colors) almost collapse. Again finite-size corrections generate deviations from the expected scaling as can be seen from the imperfect collapse for small system sizes ($L < 64$). Additionally, there may be deviations from the paraobolic shape of the anomalous dimension $\tau_q^{(p)}$, which however cannot be resolved here due to numerical precision and available system sizes.

The presented data suggests that indeed spectrum-wide criticality can be observed in this model of an AIII topological insulator. Quantum Hall criticality is present without fine-tuning the energy. Within the Hamiltonian (42), this phenomenon seems to be robust; upon changes of E, M, W_A, ν the multifractal fingerprint of finite energy states resembles more conventional quantum Hall plateau transitions. However, the origin of this phenomenon remains mysterious at this point. Chiral symmetry in class AIII only protects the zero energy state; away from which generic class A Anderson localization is naively expected. In the following section the theory capturing localizability vs. spectrum-wide criticality for such surface states is summarized; it is originally published and explained in more detail and mathematical rigour in the original publication Altland *et al.*, 2024.

Topological insulators in any symmetry class generically owe their popularity to the bulk-boundary principle; the existence and robustness of conducting edge or boundary states. In the context of disorder this robustness is usually translated to protection from Anderson localization, even at effective one- or two-dimensional boundaries, where generic states would localize.

In this thesis we extensively discussed the famous example of the anomalous quantum Hall effect; edge modes form conducting bands even inside the bulk gap. Other instances of this principle are the quantum spin Hall effect or the three-dimensional topological insulator in class AII. In the very beginning of this thesis we saw that the quantization and the robustness of the conduction properties with respect to perturbations in the microscopic details of the underlying material or model of such system can be topologically explained by Laughlin's gauge argument, essentially relying on a topological pump. A key ingredient to this argument is the principle of spectral flow, which connects the conducting boundary modes at the Fermi energy inside the bulk gap spectrally with extended bulk states deep in the spectrum and by that with the opposite boundary. There is hence a spectral connection between extended surface states on opposite boundaries.

Spectral flow itself however relies crucially on the topological equivalence of all energies in the bulk gap (Altland *et al.*, 2024).

For instance suppose the opposite, an exponentially localizable bulk with localized eigenstates $|\psi(\mathbf{r})\rangle$ with localization centers $\mathbf{r}$. Then the Hamiltonian of the full system can be written as the direct sum of a boundary part $\mathcal{H}_\partial$ and a bulk part $\mathcal{H}_{\text{bulk}}$, up to corrections of maximally exponential size, where $\mathcal{H}_{\text{bulk}}$ is the projection of the full Hamiltonian $\mathcal{H}$ on the eigenstates $|\psi(\mathbf{r})\rangle$ with $\mathbf{r}$ further from the boundary than a cut-off distance (Altland *et al.*, 2024). Due to $\mathcal{H}_{\text{bulk}}, \mathcal{H}_\partial$ being local operators it is possible to define energies $E_{\text{gap}}, E_\partial$, such that the eigenvalues of $\mathcal{H}_{\text{bulk}}$ are larger than $> E_{\text{gap}}$ and of $\mathcal{H}_\partial$ smaller than $< E_\partial$. Then there exists a continuous deformation of $\mathcal{H}$,

$$\mathcal{H}' = \left(\frac{E_{\text{gap}}}{2E_\partial}\mathcal{H}_\partial\right) \oplus \mathcal{H}_{\text{bulk}}. \tag{50}$$

This Hamiltonian now has a spectral gap between energies $E_{\text{gap}}/2 < E < E_{\text{gap}}$ which separates the surface part of the spectrum from the bulk part, cf. Fig. 21 **a,b**. This contradicts the requirement of equivalent surface states within the bulk gap.

Now, particle-hole and chiral symmetries generate a special energy inside the bulk gap, namely the one around which the spectrum is mirror symmetric. By that the assumption of topologically equivalent in-gap surface states becomes violated. In contrast to the standard Wigner-Dyson classes, the principle of spectral flow, and by that, the protection of *all* in-gap surface states has to be reconsidered. Essentially, this leaves us with three possible scenarios for non-Wigner-Dyson classes, where non-equivalent special energies exist in the bulk

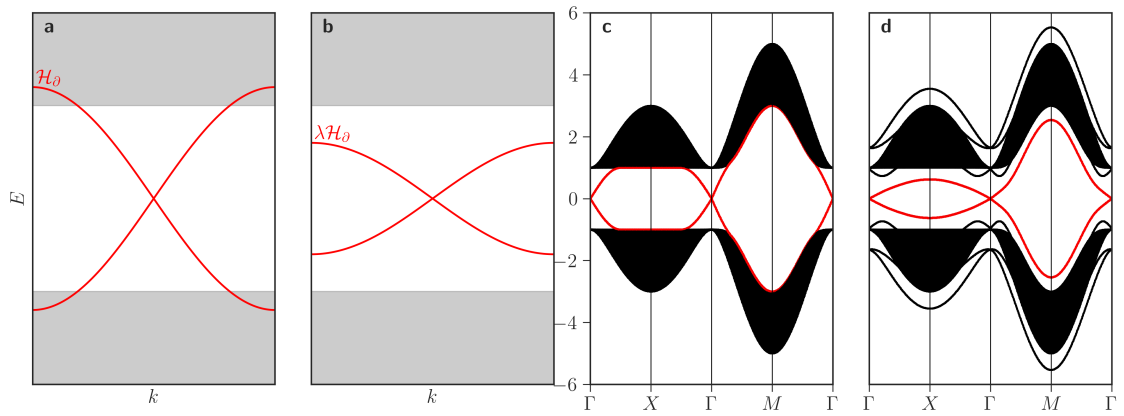

Figure 21: Schematics of surface (red) and bulk (grey) spectra of an Hamiltonian which is separable into bulk and surface part, $\mathcal{H} = \mathcal{H}_\partial \oplus \mathcal{H}_{\text{bulk}}$, **a** before and **b** after rescaling, opening a gap between surface and bulk spectra. **c-d** spectrum of $\mathcal{H}_{\text{AIII}}$ without disorder with open boundaries in x-direction and $M = 2$ **c** without and **d** with ($u_f = 0.9$) the fragmenting surface potential opening an indirect gap. Adapted from Altland *et al.*, 2024, ©2024 American Physical Society.

gap: (i) Spectral flow is still guaranteed topologically by a different mechanism than the chiral or particle-hole symmetry. In this case the surface states remain delocalized and the topological insulator may behave as a Wigner-Dyson class. (ii) Spectral flow is not guaranteed by topology but it is uninterrupted nevertheless for a specific class of models. In this case finite energy surface states may still be extended and one could observe spectrum-wide criticality nevertheless. However, it would be topologically fragile, (iii) since a symmetry-conserving perturbation may open a gap between surface and bulk spectra and localize the finite energy surface states. We will explore these possibilities in a case study of the model defined by Eq. (42), which is in symmetry class AIII.

5.3 CASE STUDY OF AIII TOPOLOGICAL INSULATORS

Both the study by Sbierski *et al.*, 2020 as well as the data presented for the three-dimensional lattice Hamiltonian (42) suggest that finite energy states away from the topologically protected zero energy state are still extended; indeed they behave as a continuum of quantum Hall critical wave functions. In panel **c** of Fig. 21 the band structure along high symmetry cuts of the Brioullin zone of the clean Hamiltonian is shown. Indeed the surface bands (red) are connected to the bulk spectrum; spectral flow to the bulk and in between the separated surface can be present and an extended band of boundary states in the bulk gap exists, just as in the class A Chern insulator as argued by Laughlin.

DISRUPTING SPECTRAL FLOW. We here present a construction how to interrupt spectral flow between bulk and surface spectra and by that localize the

surface states away from the high symmetry point at $E = 0$, which is protected by chiral symmetry.

We add the potential term to the AIII lattice model,[3]

$$\mathcal{H}'_{\mathrm{AIII}} = \mathcal{H}_{\mathrm{AIII}} + u_f \sum_{(x,y,z)\in\mathrm{surface}} \psi^\dagger_{x,y,z}\tau_2\sigma_1\psi_{x,y,z}, \tag{51}$$

where u_f quantifies the strength of this fragmenting surface potential. $\mathcal{H}'_{\mathrm{AIII}}$ is still chirally symmetric and its bulk properties, i.e. its topology is not changed, since the added potential is local (it is non-zero only on the surface layers).

Fig. 21 **d** shows the band structure of this model with a surface potential imposed on the two outer lattice layers. We observe an indirect gap opening between the surface bands (red) and the bulk (black), similar to the schematic picture shown in panel **b**. Spectral flow is hence interrupted.

The localization properties of finite energy surface states can be assessed by calculating the Berry curvature of the surface bands (Moreno-Gonzalez *et al.*, 2023). When these are connected to the bulk it is necessarily zero, while in the detached case it is finite. The latter implies surface localization, the former extended states. All studied AIII topological models in literature had zero Berry curvature on their surfaces; cf. Ryu *et al.*, 2010; Ghorashi *et al.*, 2018; Sbierski *et al.*, 2020; Ghorashi *et al.*, 2020; Karcher and Foster, 2021. Only upon imposing an additional surface potential the fragility of delocalized finite energy surface states is revealed.

When the surface band is fully detached from the bulk spectrum it is possible to define a non-zero Chern number of a surface by integrating over the Berry curvature of the band.[4] The numerical value of the Chern number depends on the sign of the potential u_f, $\mathrm{Ch} = -\mathrm{sgn}(u_f)$ (its parity is fixed by the winding number, here $\nu = 1$). Hence, detaching the surface and bulk bands necessarily implies a finite surface Chern number.

SURFACE CHERN NUMBER. Let us consider a fragmenting surface potential which has domain walls on the surface at which the sign of u_f changes. This leads to puddles of opposite Chern numbers. As we may think of the finite energy surface band as a two-dimensional class A system, these domains between opposite Chern numbers come with counter propagating chiral edge modes, equivalently to a quantum Hall insulator. For those once again Laughlin's gauge argument applies implying that the chiral modes must hybridize with extended states both at $E = 0$ but also at high energies. At the latter the hybridization must happen either with delocalized bulk states or with delocalized surface states; both contradicting a full localizability of the high-energy spectrum.

3 The localizing potential has a different form when the surface is defined in a different direction of the three-dimensional cubic lattice Altland *et al.*, 2024.

4 For details on the definition and calculation of the surface Chern number when the fragmenting surface potential is present, the reader is referred to the original publication Altland *et al.*, 2024. The focus of this thesis lies on the numerical study of the AIII insulator; this paragraph is solely intended to provide the relevant analytical context.

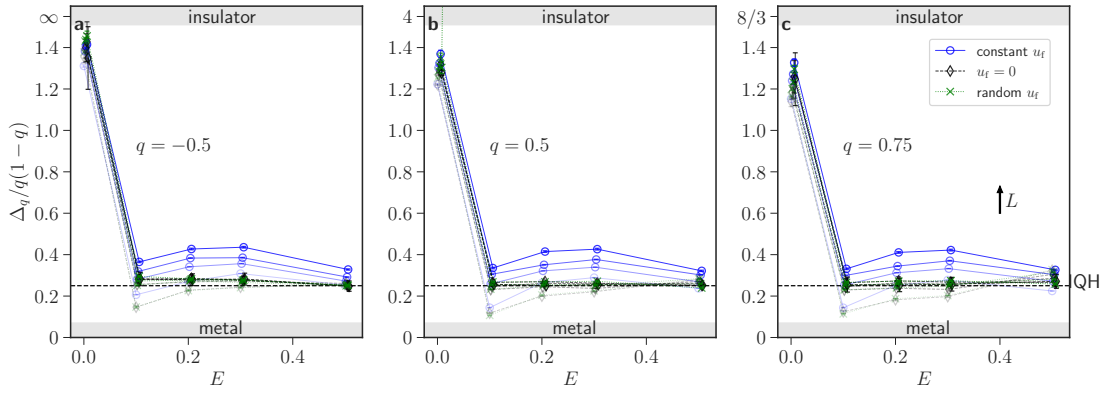

Figure 22: Anomalous multifractal dimension Δ_q for $q = -0.5$ (**a**), $q = 0.5$ (**b**), $q = 0.75$ (**c**) of surface states for increasing system sizes (transparent to opaque colors, $L = 24 \to 128, L_x = 8$), as a function of energy inside the bulk gap. Disorder is uncorrelated, and chosen as random phases $\phi^a(\mathbf{r})$ with correlation length $\xi_\phi = 1$ and strength W_ϕ. The data sets correspond to $W_\phi = 0.1, u_f = 0.3$ (blue), $W_\phi = 0.15, u_f = 0$ (black), $W_\phi = 0.15$ and random u_f with zero mean and standard deviation $\sigma_{u_f} = 0.3$. The dashed line marks the value of quantum Hall criticality $\gamma^{QH} \approx 1/4$, the localization limit $\tau_q|_{q>0} = 0$ corresponds to $\Delta_q/q(1-q) \to \infty, 4, 8/3$ for $q = -0.5, 0.5, 0.75$. (The value ∞ reflects the formal divergence of the moments in the localized limit for negative q.) Adapted from Altland *et al.*, 2024, ©2024 American Physical Society.

Going one step further, let us imagine puddles of opposite sign of u_f, Ch with equal probability distributed on the surface. A network of propagating chiral edge modes must form, which percolate critically through the entire surface. Topologically this represents the Chalker-Coddington network at criticality, protected from Anderson localization. This mechanism explains the observation of spectrum-wide criticality. As soon as a non-vanishing average between puddles of opposite sign u_f appears we expect localization of finite energy states (Altland *et al.*, 2024).

LOCALIZING FINITE ENERGY SURFACE STATES. Similarly to Fig. 19 we analyse the anomalous dimension using the numerical pseudo-derivative (22) for the disordered three-dimensional AIII model with fragmenting surface potential $\mathcal{H}'_{AIII}$. As our primary focus lies on the finite energy states and we skip another detailed analysis of the zero energy AIII critical wave functions it is not required to construct the disordered phases $\phi^a_{x,y,z}$ from a vector potential. Instead they are directly sampled from Eq. (46), with a small correlation length ξ_ϕ and amplitude W_ϕ.

The modified (surface) wave function moments are averaged over many disorder realizations and over small windows of energy. The system sizes are varied from $L = 24 \to 128$, with $L_x = 8$.[5]

5 The convergence with the slab thickness L_x has been verified, cf. appendix A.2 and Altland *et al.*, 2024.

Fig. 22 shows the system-size dependent anomalous multifractal dimension as a function of energy for different moments q, with constant (blue), vanishing (black), and random (green) fragmenting potential u_f. The data is consistent with an approximately parabolic shape of the AIII critical state for $E = 0$ with a prefactor $\gamma^{\mathrm{AIII}} \sim 1.3$ for all three cases. Thus, it exhibits much stronger multifractality than the quantum Hall critical states known from the previous chapters, but is comparable to the values obtained in the very beginning of this chapter for correlated vector potentials.

For vanishing fragmenting surface potential $u_f = 0$ we observe consistency with the quantum Hall critical multifractal dimension, with a parabolic prefactor of around $\gamma^{\mathrm{QH}} \sim 1/4$ (black curves). As seen above this is the signature of spectrum-wide criticality for $\mathcal{H}_{\mathrm{AIII}}$, and further confirms the results by Sbierski *et al.*, 2020.

A constant fragmenting potential $u_f = 0.3$ however leads to a clear tendency away from QH criticality for $E > 0$, towards localization when system size L is increased (transparent to opaque, blue). This is expected because $u_f \neq 0$ – as argued above – distrupts spectral flow and induces a finite surface Chern number on the finite energy surfaces.

Motivated by the scenario of puddles of different Chern numbers inducing percolating chiral domain wall modes across the surface a random fragmenting potential with zero mean and variance $\langle u_f(x,y,z)u_f(x,y',z)\rangle_{\mathrm{ens}} = u_f^2\,\delta_{xx'}\delta_{yy'}$, is simulated (green) curves. This perturbation again leads to quantum Hall delocalization and an agreement with the approximate quantum Hall critical form of the anomalous dimension Δ_q. This observation is in perfect consistency with the qualitative considerations of the previous section.

An alternative diagnostic of quantum Hall criticality vs. localization are the distribution functions of the wave function moments P_q for different disorder configurations directly. The distribution functions should become shape invariant and scale with the multifractal dimension of the quantum Hall critical point in the former case, while in the latter scenario they do not collapse. An analysis of the distribution functions is presented in appendix A.2.

5.4 Generalization and conclusion: ten-fold way and localizability

Conclusion and implications. In this chapter a theory has been presented how the observation of spectrum-wide criticality plays together with the topological properties of surfaces of non-Wigner-Dyson topological insulators, here namely in class AIII.

Apart from the very interesting phenomenology itself – in particular the observation of relatively robust quantum Hall criticality upon statistical properties of the discussed perturbations, and localization of surface states when a gap between surface and bulk is induced – some very general but just as interesting remarks are in order.

Cartan label	T	P	C	$d = 1$	$d = 2$	$d = 3$
A (unitary)	0	0	0	0	$\mathbb{Z}^{\checkmark}$	0
AI (orthogonal)	+1	0	0	0	0	0
AII (symplectic)	−1	0	0	0	$\mathbb{Z}_2^{\checkmark}$	$\mathbb{Z}_2^{\checkmark}$
AIII (ch. unit.)	0	0	1	$\mathbb{Z}^{\times}$	0	$\mathbb{Z}^{\times}$
BDI (ch. ortho.)	+1	+1	1	$\mathbb{Z}^{\times}$	0	0
CII (ch. sympl.)	−1	−1	1	$2\mathbb{Z}^{\times}$	0	$\mathbb{Z}_2^{\times}$
D (BdG)	0	+1	0	$\mathbb{Z}_2^{\times}$	$\mathbb{Z}^{\checkmark}$	0
C (BdG)	0	−1	0	0	$2\mathbb{Z}^{\checkmark}$	0
DIII (BdG)	−1	+1	1	$\mathbb{Z}_2^{\times}$	$\mathbb{Z}_2^{\checkmark}$	$\mathbb{Z}^{\checkmark/\times}$
CI (BdG)	+1	−1	1	0	0	$2\mathbb{Z}^{\times}$

Table 3: Localizability of topological materials. The classification of Table 1 is extended by a superscript $\times$ indicating localizable, or ✓non-localizable topological phases. For class DIII in three dimensions, phases with even bulk winding number can be localized, while those with odd winding number cannot. Spectral flow is only robust in non-localizable classes. Adapted from Altland *et al.*, 2024, ©2024 American Physical Society.

In literature surface states of topological insulators are often described by minimal models, linearized around the Dirac points, for instance by Sbierski *et al.*, 2020. Even though this approach is very simple and has been incredibly successful in describing certain phenomena, it is fundamentally insufficient to describe even as basic properties as wave function localization: A minimal Dirac model of the AIII surface would always result in a zero Chern number and therefore predict delocalization. As we saw, in certain cases this is wrong. In the study presented here and in the original publication Altland *et al.*, 2024 this problem is cured by the inclusion of the full lattice dispersion; it allows to explore spectral flow to the bulk explicitly. In the language of minimal Dirac models this can be achieved complementarily by including trivial bulk bands, cf. Altland *et al.*, 2024 for details.

OUTLOOK: TEN-FOLD WAY OF LOCALIZABILITY. A key ingredient of evaluating the stability or fragility of extended states is the exploration of spectral flow of a certain Hamiltonian. If spectral flow can be interrupted by some local potential, for instance u_f in the case discussed, a Chern number is induced on the surface bands and finite energy states localize. The disruption of spectral flow in turn crucially relies on the possibility of separating the bulk and surface in local operators (up to exponentially small corrections). The relevant criterion for the fragility of surface states hence can be formulated as the localizability of the bulk spectrum. This can be in principle generalized beyond symmetry class AIII to the entire ten-fold way of topological insulators.

To this end three cases need to be considered: (i) Wigner-Dyson classes are in principle non-localizable. As soon as there are edge states, extended bulk states appear due to spectral flow guaranteed by the equivalence of energies inside the bulk gap. (ii) Non-Wigner Dyson classes have a special energy around which the spectrum is typically symmetric. Therefore spectral flow need not be robust. However, if upon the explicit breaking of the symmetry related to this special energy, i.e. particle-hole or chiral symmetry, the then symmetry broken system (now in a Wigner-Dyson class) still can host a topological phase, spectral flow is still protected. Spectral flow here is then robust due to the Wigner-Dyson sibling and not due to the additional chiral or particle-hole symmetry. (iii) If such a topological phase in the Wigner-Dyson sibling does not exist, the bulk spectrum generically is localizable and spectral flow is fragile. For this we saw the example of the three-dimensional AIII insulator; the sibling class A does not have a topological phase in three dimensions, hence spectral flow is not robust. These considerations are summarized in a full characterization of the ten-fold way with respect to its localizability in Table 3.

Part II

MANY-BODY LOCALIZATION AND ERGODICITY

6

THERMALIZATION AND MANY-BODY LOCALIZATION

6.1 THERMALIZED SYSTEMS AND ERGODICITY

The overarching theme of the first part of this thesis is universality: Properties of the quantum Hall effect, for instance its conductance quantization, the appearance of boundary states or the characteristics of the critical point of topological phase transitions have been shown to have the same fingerprint despite of their vastly different microscopic origins; at least for the models studied in this thesis.

By that reasoning, the theory of the integer quantum Hall effect or – more general – the theory of disordered topological materials is an *effective* theory, which separates irrelevant degrees of freedom (microscopic details) from relevant effective degrees of freedom (for instance the topological winding number, or the surface Chern number determined in chapter 5).

Beyond topological materials a concept to describe and understand generic physical systems is (equilibrium) statistical mechanics. The goal is similar, namely to resolve the dilemma of the infinite number of microscopic degrees of freedom in nature, obscuring physical insight into its most important emergent phenomena. It offers highly successful and generically applicable ways to coarse-grain from a microscopically exact physical system or model towards a tractable effective theory of relevant and interesting properties.

The following chapter is intended to give a brief phenomenological overview over interacting many-body dynamics and the conditions of thermalization. A detailed account of the underlying mathematical foundations is not provided. Parts of the following paragraphs loosely follow the review articles by Nandkishore and Huse, 2015; Tikhonov and Mirlin, 2021b.

What is thermalization?

At the heart of statistical mechanics lies the concept of thermal equilibrium, as detailed in the introduction to this thesis. It defines the final, thermodynamic state of the time evolution of generic interacting many-body systems, which – due to coarse-graining – "forget" all the details of their microscopic nature and their initial state. The physical descriptors necessary to understand the majority of phenomena of such systems are restricted to generic averaged quantities like temperature, particle density or the energy density; they define so-called

macroscopic states. This theory not only successfully describes physical systems of different microscopic origin but even classical and quantum mechanical physics on equal footing.[1]

Classical many-particle systems can realize the process of equilibration so as to evolve to a universal thermal state in different ways. Conceptually, the simplest mechanism is to consider the system of interest A coupled to an environment B. Through the coupling system A can interact with the bath B, and spread information about the initial state of A where A and B may have been uncoupled, e.g. the initial momentum of a specific particle, on all degrees of freedom of the combined system $A + B$. In this way energy and possibly also particles can be exchanged between A and B, defining the so-called *canonical* and *grand canonical ensembles*.

If we now measure properties of system A after long times without access to or interest in the bath B, one is not able to extract the information about the original initial microscopic state, e.g. the energy or exact particle number, of A. Only average quantities such as the average energy and particle number are accessible to local measurements. Information about the initial state is hidden in the full system $A + B$ and is only accessible to global measurements.

Thermalization in closed quantum systems

Considering now a system which is not in contact with an external bath – called *micro canonical ensemble* – the notion of thermalization and the associated forgetting of information has to be adjusted conceptually, in particular in a closed *quantum* system.

Considering a general, initial mixed state density matrix ρ_0 of some closed quantum system with many degrees of freedom, its time evolution (in the Schrödinger picture) is given by

$$\begin{aligned} i\hbar\frac{d\rho}{dt} &= [\mathcal{H}, \rho]\,, \\ \rho(t) &= e^{-i\mathcal{H}/\hbar t}\rho_0 e^{i\mathcal{H}/\hbar t}. \end{aligned} \tag{52}$$

It is one of the main dogmas of quantum mechanics that the time evolution is unitary, meaning that information present at $t = 0$ is also present at $t \to \infty$ (Sakurai and Napolitano, 2020). A closed quantum system cannot loose information.

The obvious question is how to reconcile this fact with our daily observation of nature, where we almost exclusively see thermal states, at least locally. The answer is that the information is not really lost on a global level. Instead it becomes hidden more and more by the time evolution which spreads the entanglement

1 The different nature of classical and quantum mechanics is captured in the definition of the objects entering the theory, most prominently the density operator of a quantum, or the ensemble probabilities of a classical system.

throughout the entire system. Consequently, to recover the initial local information at long times it would be necessary to measure global operators, which in general are not accessible to experiments. For local measurement, however, the time evolved quantum state looks thermal. This process is called *decoherence* (Nandkishore and Huse, 2015).

Eigenstate thermalization hypothesis

Consider the density matrix at time $t = 0$ to be initialized in a many-body eigenstate of the system of interest. The time evolution of said system with its Hamiltonian hence is trivial, $\rho(t) = \rho(0)$. A very instructive concept is the eigenstate thermalization hypothesis (ETH) which suggests that thermalization of all initial states consequently must imply that all eigenstates of the system must be thermal to begin with. Studying the thermalization properties of a many-body quantum system it is thus sufficient to understand the many-body eigenstates (Deutsch, 1991; Srednicki, 1994; Tasaki, 1998; Rigol *et al.*, 2008). The validity of this hypothesis is difficult to assess because it is typically not possible to access all eigenstates of a many-body system (except for very small ones). Still it is very useful when studying thermalization properties, because it allows us to define thermodynamic ensembles containing just a single many-body eigenstate in order to study its thermalizing properties.

Thermalization in the language of the ETH happens along the following lines: the density matrix of the many-body system is prepared in its eigenbasis; making its diagonal elements, the probability densities, trivially time-independent. The coherences in the off-diagonals of the density matrix aquire a phase which is given by the energy differences between the many-body levels. The ETH in this context now translates to the corresponding phase oscillations of the coherences contributing to local observables effectively randomly due to their fast and diverse frequencies, such that they interfere destructively and eventually cancel. The coherences decay for long times, giving rise to the mechanism of decoherence. The mechanism of thermalization in this language is thus dephasing of the off-diagonal entries in the density matrix (Nandkishore and Huse, 2015).

The ETH allows us to focus on single eigenstates when assessing thermalization characteristics. Therefore, another class of ensembles can be introduced to the theory of statistical mechanics, adding to the microcanonical, canonical and (generalized) grandcanonical ensembles: Defining the single eigenstate ensembles as containing only a single wave function of a many-body Hamiltonian at a certain energy (somewhat similarly to the microcanonical ensemble) it is possible to extrapolate the correct thermodynamics information of the system in its thermal equilibrium; just as in the traditional ensemble types (Nandkishore and Huse, 2015). These single eigenstate ensembles play an important role in studying statistical properties of many-body problems numerically, for instance when calculating the wave function moments, as shown in the next chapters.

This consideration suggests to connect the concept of thermalization – the loss of memory of initial conditions during time evolution – with *ergodicity*, or ergodic wave functions, respectively. Such wave functions uniformly explore the entire Fock or Hilbert space and thus serve as a quantum analogy to classically ergodic trajectories which uniformly cover the entire available phase space of a classical system. Investigating ergodicity of wave functions now can be addressed on the level of single eigenstate ensembles and in that sense this concept is again closely related to the ETH.

Exceptions: integrable systems

Generically, not all quantum systems thermalize. Most prominently integrable system, exhibiting an extensive number of local conservation laws, evade thermalization and keep memory of their initial state forever[2]. However, in general integrable systems are rare and require fine-tuning, while a slight perturbation in the system's parameters can drive them back to a thermalizing behavior.

Consider for instance the famous example of classical or quantized billiards: A perfectly circular shape of the boundary results in regular, integrable dynamics, while already a small deviation from that, for instance a cardioid billiard results in eventual thermalization and ergodic behavior (Robnik, 1983; Bäcker *et al.*, 1995).

Therefore, an interesting question in the context of thermalization vs. integrability is if there exists a class of systems which exhibit non-thermal behavior without fine-tuning, i.e. a finite, stable phase in the space spanned by Hamiltonian parameters. If so, a natural extension of this question is, if one can observe and characterize the transition between the thermal and the localized phases.

Ergodicity breaking: Localization

A candidate for a generic class of physical systems which do evade quantum thermalization appears to be certain disordered systems[3]. If there was localization of wave functions in a random potential – analogously to single-particle Anderson localization which we encountered in the first part of this thesis, however *with interactions* – such a class of systems would have been found.

Theory and experiment have been attempting to judge if such a *many-body localized* (MBL) quantum phase exists, and – if the answer is yes – under which circumstances it arises.

In the following section the basic concept and some selected recent developments and their status within the field of MBL will be introduced.

2 Integrable systems are argued to have their own version of the ETH and thermalization within the constraints of extensive local conservation laws (Nandkishore and Huse, 2015).

3 There are more ways to break ergodicity. For instance so-called quantum many-body scarring describes the phenomenon that a many-body system relaxes to equilibrium for most initial conditions, while for specific states non-thermalizing behavior is observed (Serbyn *et al.*, 2021).

Some of the most studied models in the context of many-body localization and ergodicity are short-range interacting spin-less fermions, for instance formalized by

$$\mathcal{H} = -\frac{1}{2}\sum_{i=1}^{N_{\mathcal{B}}-1} c_i^\dagger c_{i+1} + \text{h.c.} + \sum_{i=1}^{N_{\mathcal{B}}} \epsilon_i \left(n_i - \frac{1}{2}\right) + V \sum_{i=1}^{N_{\mathcal{B}}-1} \left(n_i - \frac{1}{2}\right)\left(n_{i+1} - \frac{1}{2}\right), \quad (53)$$

with $n_i = c_i^\dagger c_i$, and $c_i, c_i^\dagger$ fermionic annihilation and creation operators. $N_{\mathcal{B}}$ represents the number of real space lattice sites in one dimension and V the strength of the nearest-neighbor density interaction, which is set to unity. The onsite potentials are chosen randomly from an uncorrelated box-distribution $\epsilon_i \in [-W, W]$, where W represents the interaction strength (Evers *et al.*, 2023). Identifying or discarding a localization transition as a function of W at a critical disorder strength W_c is one of the main goals of the field of many-body localization and ergodicity.

Recap: single-particle localization

To introduce the concept of many-body localization and highlight its differences to conventional single-particle Anderson localization we briefly recapitulate the latter. To this end we reconsider the non-interacting disordered model Hamiltonian from Eq. (5).

In one or two dimensions all eigenstates of this Hamiltonian localize due to constructive interference of particles scattered at the disorder potential. A key ingredient to this argument is coherence: If the particle dephases, due to the coupling to external degrees of freedom, or interaction with another particle, before it is able to scatter back to its original position in a closed path, coherence is lost and the pattern of constructive and destructive interference giving rise to weak and eventually Anderson localization ceases to exist. Essentially, the coherence length has to be larger than the scattering length (Nandkishore and Huse, 2015).

Of course upon transforming Eq. (5) into its eigenbasis one can extend this picture easily into a many-body problem (however still non-interacting), by filling up the localized orbitals to a Fermi energy. Most many-body wave functions – being product states of the single-particle orbitals – then violate the ETH as soon as at least some single-particle eigenstate are localized.

What happens now upon introducing interactions? Since then dephasing definitely enters the picture due to electron-electron interactions, coherence is lost and the original mechanism which localized the single-particle orbitals in general fails. Can interactions stabilize a localized phase nevertheless?

Many-body localization: selected models and their status

For the sake of brevity the focus of this section lies on the numerical understanding of MBL and the current status of research there. As there are interesting developments also in analytical theory[4] *and modeling as well as experiments the reader is referred to recent reviews, e.g. by Nandkishore and Huse, 2015; Abanin* et al.*, 2019; Sierant* et al.*, 2024.*

Generally, most approaches to MBL have in common that investigations are carried out at high or infinite temperature [5]. This is due to the fact that high-energy/temperature thermal states are those to which initial states far from equilibrium tend to at long times. Since those are also the states for which we expect MBL to be more abundant, it is natural to study high temperature properties. From this consideration derives the common belief that it does not really matter too much which kind of statistics underlie the theoretical models. This is why all, fermion, boson and spin, models are common tools in the study of MBL (Nandkishore and Huse, 2015). In the remainder of this paragraph some of these models and approaches are introduced.

As the field still lacks a controlled analytical approach to microscopic models of many-body localization, e.g. the disordered Heisenberg spin chain, numerical studies serve as the most direct way to tackle the problem. However, also that comes with obvious restrictions: the Fock space of many-body basis states becomes exponentially large as the system size is increased. Therefore, exact simulations are very challenging compared to single-particle Anderson localization studies, where the Hilbert space is only polynomial in linear system size. Effectively, exact diagonalization (ED) studies are restricted to around ~ 20 spin-1/2 like degree of freedoms.

Within these studies there has been evidence of MBL or MBL-like regimes, their exact nature is still under activate debate. The same holds for the presence or absence of a phase transition between extended and localized phases for the thermodynamic limit, as finite-size corrections are very large in particular when trying to determine the position of a possible critical disorder strength. For ED studies it is also essentially impossible to estimate critical exponents, systems larger than > 100 spin degrees of freedoms would be necessary (Tikhonov and Mirlin, 2021b).

A way to reach such large systems are methods from the family of matrix product states. However, here only moderately long time scales can be simulated

4 In particular the popular phenomenological theory of l-bits as well as the details around the developments concerning so-called avalanches and associated instabilities in the context of rare region effects in disordered spin chains (Nandkishore and Huse, 2015; Thiery *et al.*, 2018; Morningstar *et al.*, 2022) are not touched upon in the following chapters. They are not essential for the specific context of this thesis, however important when attempting to grasp an overview over the full field of many-body localization.

5 for instance by studying the central part of the many-body spectrum of a finite system

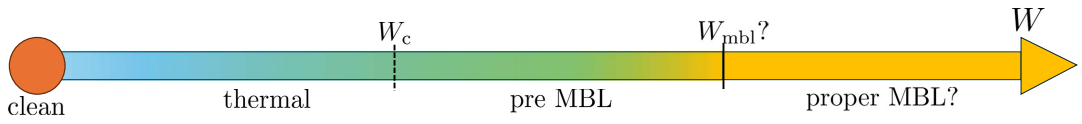

Figure 23: Schematic phase diagram of disordered spin chains (for instance the isotropic Heisenberg model). The thermal/pre-MBL regime is characterized by power laws for instance for the density imbalance or the entanglement entropy. At $W_c \geqslant 4.5$ a cross-over to decelerating dynamics, characterized by a decreasing effective diffusion exponent happens. The regime above W_{mbl} is largely unexplored but believed to host the actual MBL phase, fully evading thermalization in the long time limit, Evers *et al.*, 2023.

which are often not sufficient to estimate the long time and infinite system size asymptotic properties.

The status quo: many open questions

After numerical studies suggested a critical disorder strength $W_c \sim 3-4$ (referring to models of the type described in Eq. (53)) – cf. Luitz *et al.*, 2015; Macé *et al.*, 2019 – in recent years the number has shifted to ever increasing values (Bera *et al.*, 2017; Doggen *et al.*, 2018; Weiner *et al.*, 2019; Sierant *et al.*, 2020; Lezama *et al.*, 2019; Doggen *et al.*, 2021; Sierant and Zakrzewski, 2022; Morningstar *et al.*, 2022; Sels, 2022). This is a manifestation of the strong finite-size effects related to the believed localized character of a potential critical point. Most recently it has been hypothesized that $W_c \geqslant 20$ which is out of reach of numerical studies at the moment (Tikhonov and Mirlin, 2021b; Evers *et al.*, 2023).

Therefore, recent studies focused on the regime of $W \sim 2-10$, i.e. the regime where the critical disorder strength was believed to lie earlier (Evers *et al.*, 2023). Currently a common belief is that in this regime the onset of many-body localization can be observed, while the thermodynamic asymptotic behavior is still thermal. This is seen for instance in a strongly reduced rate of thermalization, caused by the need for a collective organization of quantum particles in such strongly disordered potential landscapes during time evolution. This regime has been dubbed *pre-MBL* while the actual MBL phase for $W > W_c$ is referred to as *proper MBL* (Weiner *et al.*, 2019; Morningstar *et al.*, 2022; Evers *et al.*, 2023).

A current interpretation of the phase diagram of the MBL transition is summarized in Fig. 23, according to Evers *et al.*, 2023.

Anderson localization on random regular graphs

Analytical approaches to the problem of many-body localization have proven to be notoriously difficult. The extension to an interacting many-body problem complicates theoretical investigations strongly: The corresponding Hilbert space grows exponentially with the number of particles while the interaction induces a

huge degree of correlations between the matrix elements in this high-dimensional Hilbert space. This is why to date there are no efficient exact ways to systematically capture the quantitative physics of the MBL problem (Nandkishore and Huse, 2015; Tikhonov and Mirlin, 2021b).

Several approaches to tackle its qualitative features have been put forward. Analytically for instance, perturbative expansion has been used to search for a transition between localized and ergodic/thermal behavior. However, such and other approaches suffer fundamental qualitative shortcomings: Rare region effects of unusually high and low disorder can be missed, which turn out to have significant qualitative influence on the scaling of the MBL transition and the critical behavior in the limit of large system sizes. Additionally, some approximations were shown to enhance delocalization and thus are not useful to study localization properties (Gornyi *et al.*, 2005; Basko *et al.*, 2006; Gornyi *et al.*, 2017a; Agarwal *et al.*, 2017; Thiery *et al.*, 2018; Tikhonov and Mirlin, 2021b). With some success phenomenological renormalization group schemes have been introduced which capture the effect of rare regions of anomalous disorder (Dumitrescu *et al.*, 2019; Morningstar *et al.*, 2020; Tikhonov and Mirlin, 2021b; Morningstar *et al.*, 2022).

A conceptual alternative to microscopic theories in understanding the qualitative physics are toy models. The following paragraph is devoted to Anderson localization on so-called random regular graphs and its connection to the MBL problem.

The model is fairly simple, we consider nearest neighbor hopping between lattice sites and an uncorrelated random potential just as in the d-dimensional Anderson model on a square lattice (5). However, the role of the underlying lattice is now taken by a random regular graph (RRG). An RRG is a finite graph with a fixed coordination number $p = m + 1$, which has a local tree-like structure without a boundary.

The motivation for this structure comes from considering an interacting many-body problem in the Fock space in the basis of its single-particle eigenstates. Those also form a graph which is not represented by a simple crystalline lattice. The single-particle orbitals now take the role of the vertices of the RRG while the interaction-induced couplings are represented by its links (Tikhonov and Mirlin, 2021b). Due to its conceptual simplicity the model has gained significant popularity in recent years, cf. De Luca *et al.*, 2014; Tikhonov *et al.*, 2016; García-Mata *et al.*, 2017; Metz and Castillo, 2017; Biroli and Tarzia, 2017; Kravtsov *et al.*, 2018; Bera *et al.*, 2018; Tikhonov and Mirlin, 2019a; Tikhonov and Mirlin, 2019b; García-Mata *et al.*, 2020; Tikhonov and Mirlin, 2021a.

Obviously, this is not more than a greatly simplified model of the interaction structure in the Fock space of an actual microscopic Hamiltonian. First, the Fock space graph of a physical system will not have the structure of an RRG, and second, correlation effects between matrix elements are completely neglected in this model. This can already be seen from the difference in the number of

parameters between the two models, which is polynomial in system size in a Hamiltonian model and exponential in the RRG problem.

The big advantage of this toy model is its analytical accessibility: Using a field theoretical approach one gains access to key properties, such as level statistics and the scaling of the many-body eigenfunctions which allow to distinguish between localization and ergodicity, as well as characterize the transition as a function of the disorder strength. This allows, by solving self-consistency equations resulting from field theory numerically with a high efficiency, to access Hilbert space sizes of $\mathcal{O}(10^{19})$ compared to ED studies of microscopically defined Hamiltonians which are limited to $\mathcal{O}(10^6)$. This leads to a very precise numerical estimate of the critical disorder strength. For coordination number $m+1=3$ and box-distributed potential disorder – the most studied case – the critical disorder strength is $W_c = 18.17(1)$ (Tikhonov and Mirlin, 2021b).

Even though such drastic simplifications have been made Anderson localization on RRGs shows remarkable similarities to known or suspected properties of MBL:

(i) the thermal side of the transition at disorder strengths smaller than the critical value W_c is ergodic, meaning wave functions spread over the entire Hilbert space;

(ii) in contrast to metal-insulator transitions in single-particle physics for instance in the d-dimensional Anderson model the critical point has localized properties. This manifests itself both in Poissonian level spacing statistics as well as an inverse participation ratio of order $\mathcal{O}(1)$.

(iii) The latter point causes strong finite-size corrections close to the critical point on the ergodic side $W < W_c$. This is because at the small system sizes which are usually available to numerical investigations wave functions which are extended in the thermodynamic limit appear localized and reveal their ergodic character only for large systems. Therefore, the critical point determined by numerics appears to "shift" strongly to larger disorder strengths as the system sizes are increased (Tikhonov and Mirlin, 2021b).

Apart from those striking similarities to MBL the interest in RRGs within this thesis additionally derives from the close relation to a different model, which actually is defined microscopically, but still is a drastic simplification of the MBL problem.

The toy model of interest is a quantum dot with random all-to-all interactions between a finite but large number of fermions. It is a variant of the Sachdev-Ye-Kitaev model, which is introduced in the following section. The surprisingly close connection to Anderson localization on random regular graphs is discussed then later in section 6.4.

6.3 EXCURSION: SACHDEV-YE-KITAEV (SYK) MODEL

This section is intended to provide a very short introduction to the Sachdev-Ye-Kitaev model for complex fermions, focusing solely on aspects important for the remainder of this thesis. The interested reader is referred to recent comprehensive reviews such as

Maldacena and Stanford, 2016; *Gu* et al., *2020*; *Chowdhury* et al., *2022*.

In a number of sub-fields of theoretical physics the Sachdev-Ye-Kitaev (SYK) model in several of its variants has received a fair amount of attention. Although the original model introduced by Kitaev, 2015 – after a proposal in the context of spin-glasses by Sachdev and Ye, 1993 – was given for Majorana fermions and many of its properties have been proven first in the Majorana version, this thesis will solely refer to the complex version of the SYK model. Although slightly more complicated, since particle number conservation is present and some of its properties depend on the respective symmetry sector, the basic physics is identical. Its Hamiltonian reads

$$\mathcal{H}_{\mathrm{cSYK}} = \sum_{i,j,k,l}^{N_{\mathcal{B}}} J_{ijkl} c_i^\dagger c_j^\dagger c_k c_l, \tag{54}$$

where $c_i, c_i^\dagger$ denote the fermionic annihilation and creation operators at site i. The interaction kernel J_{ijkl} represents a complex valued matrix with randomly distributed elements sampled from a Gaussian distribution with zero mean and variance $\langle J_{ijkl}^2 \rangle = J^2/(2N_{\mathcal{B}})^3$ subject to the condition of Hermiticity (Gu *et al.*, 2020).

After choosing J as the unit of energy, the Hamiltonian (54) features only two parameters: the size of the single-particle basis $N_{\mathcal{B}}$ and the number of fermions N. The temporal and spatial dynamics thus mediated is structureless in the thermodynamic limit in the sense that per time two particle-hole pairs are redistributed with the only constraint of particle-number conservation. The SYK model can thus be thought of as an artificial zero-dimensional interacting quantum dot.

The interest in the SYK model derives from this simplicity causing it to be exactly solvable at large (but finite) $N_{\mathcal{B}}$. Solubility in this context means that it is possible to obtain all two- and four-point correlators exactly by resummation of a special class of perturbative diagrams, or alternatively by solving the path integral for its partition function directly. Conceptually, these calculations are fairly simple; they will however not be repeated here. The reader is referred to recent reviews, e.g by Maldacena and Stanford, 2016; Gu *et al.*, 2020; Chowdhury *et al.*, 2022.

Despite the aforementioned conceptual simplicity the SYK model reveals a number of interesting phenomena.

When first discussed in the present (Majorana) form the SYK model triggered particular interest in the community of quantum gravity. This is due to the fact that in the strong coupling limit at low temperature T and large fermion number, $1 < J/T < N_{\mathcal{B}}$, its correlation functions become scale invariant and resemble the Green's function of black holes in two-dimensional gravity in Anti-de Sitter space also known as Jackiw-Teisselbloem (JT) gravity. The duality between SYK and

JT gravity is a very prominent instance of the famous holographic duality or Anti-de Sitter/ Conformal field theory (AdS/CFT) principle, according to which a strongly coupled conformal quantum field theory in d space-time dimensions corresponds to a weakly coupled gravity theory in $d+1$ space-time dimension. Here the role of the CFT is taken by $0+1$ dimensional quantum mechanics of the SYK model in the aforementioned strong coupling limit, and the gravity side by the $1+1$ dimensional JT gravity theory. Interesting consequences of the SYK model and the aforementioned duality have been revealed by e.g. Sachdev, 2015; Kitaev and Suh, 2018; Maldacena and Stanford, 2016; Maldacena *et al.*, 2016b; Fu *et al.*, 2017; Cotler *et al.*, 2017; Bagrets *et al.*, 2017; Stanford and Witten, 2017; Moitra *et al.*, 2019; Sachdev, 2019; Iliesiu and Turiaci, 2021; Heydeman *et al.*, 2022.

Connected with this duality several stunning properties of the SYK model have been discovered. It has been shown, for instance, that local information subject to time evolution of the SYK model is transported and mixed within the many-body system with the fastest rate possible; the so-called quantum Lyapunov exponent λ_L – named in analogy to the classical Lyapunov exponent in the phase space of a classical chaotic system – saturates its upper bound $\lambda_L \leqslant 2\pi T$ (Maldacena *et al.*, 2016a). This fact is responsible for the SYK model being called "maximally chaotic" or "scrambling". By this we can estimate the typical relaxation times of excitations within the SYK model to be of the order of $\tau_{relax} \sim 1/\lambda_L \sim 1/T$. This linear-in-temperature scaling translates also to transport coefficients such as resistivity (for instance using the Drude formula), and is in striking contrast to Fermi liquid theory which has been extremely successful in describing the properties of most metals. Instead this linear-in-temperature resistivity observed in the SYK model and its relatives (for instance coupled SYK quantum dots on a square lattice, cf. Patel and Sachdev, 2019) closely resembles the so-called strange metal phase of cuprates above the critical temperature of superconductivity. Therefore, the SYK model and its lattice extensions are thought of as useful toy models of non-Fermi liquids which could play an essential role in understanding some properties of high-temperature superconductors (Parcollet and Georges, 1999; Georges *et al.*, 2001; Sachdev, 2011; Grissonnanche *et al.*, 2021; Hartnoll and MacKenzie, 2022). Partly in this context it has been attempted to reproduce signature characteristics of strange metals, like the linear-in-temperature resistivity in SYK derived models on real space lattices, see for instance Zhang, 2017; Haldar *et al.*, 2018; Chowdhury *et al.*, 2018; Patel and Sachdev, 2019; Guo *et al.*, 2019.

Last but not least the SYK model has gained significant attention in the context of chaos-integrable transitions and – closely related – the many-body localization problem (García-García *et al.*, 2018; Micklitz *et al.*, 2019; Monteiro *et al.*, 2021a; Monteiro *et al.*, 2021b; Dieplinger *et al.*, 2021; Dieplinger and Bera, 2023). This application of the SYK model and its properties will play the most important role in the remainder of this thesis and is therefore elaborated upon in the following sections.

A great consensus on the existence, the position and the nature of a potential phase transition between a localized and an ergodic phase as a function of the strength of a disordered potential in interacting systems has not emerged.

This is greatly due to the immense complexity of the problem: spatial extension and the form of the Hamiltonian structure the huge Hilbert or Fock space in an intractable way. Both numerical simulation and analytical description are essentially uncontrolled at the moment in the relevant parameter regimes.

Therefore, it turns out to be useful to take a very different, in some sense radical, approach to the problem: We completely give up the microscopic structure of our model system and with it its connection to experiment and microscopic reality, but try and keep the only problem-specific important feature: the existence of both localized and extended states as a function of disorder.

This approach has prominently been taken by Monteiro *et al.*, 2021a and is discussed in the following paragraph.

Giving up realistic microscopic Hamiltonian structure allows us to consider the most generic and maximally entropic version of the form

$$\mathcal{H} = \mathcal{H}_2 + \mathcal{H}_4, \tag{55}$$

where $\mathcal{H}_2$ contains two fermionic operators representing a single-particle term, and $\mathcal{H}_4$ four fermionic operators, representing generic two-particle interaction.

In the Majorana representation this leads to the Hamiltonian

$$\mathcal{H} = \frac{1}{2}\sum_{ij} J_{ij}\chi_i\chi_j + \frac{1}{4!}\sum_{ijkl} J_{ijkl}\chi_i\chi_j\chi_k\chi_l, \tag{56}$$

with random zero-mean couplings with variances $\overline{J_{ij}^2} = \delta^2/2N_{\mathcal{B}}$ and $\overline{J_{ijkl}^2} = 6J^2/(2N_{\mathcal{B}})^3$. χ_i are Majorana operators.

The maximum entropy requirement (imposing the least possible structure on the matrix elements of (55)) directly implies that $\mathcal{H}_2, \mathcal{H}_4$ are variants of the Sachdev-Ye-Kitaev model with randomly distributed matrix elements of the interaction kernels. Changing to the basis of eigenstates of $\mathcal{H}_2$ it is clear that (55) then supports a fully localized single-particle spectrum and by extension then a trivially localized many-body spectrum. Additionally, we know that $\mathcal{H}_4$ hosts a fully chaotic phase, reminiscent of random matrix theory (RMT). By changing the relative strength of both parts of (55) it should be possible to observe a transition between the two regimes. Studies in this direction have gained significant interest in recent years, e.g. by García-García *et al.*, 2018; Haque and McClarty, 2019; Lunkin *et al.*, 2018; Altland *et al.*, 2019; Haldar *et al.*, 2020; Nandy *et al.*, 2022; Larzul and Schiró, 2022. The big advantage of this approach is that understanding this model analytically is possible *exactly*, as the Sachdev-Ye-Kitaev model can be solved exactly and mapped to well-understood random matrix theories (Monteiro

et al., 2021a). Studying the properties of the transition/cross-over may then be possible in much better detail and – more importantly – with higher precision.

Still we need to hope that some of the properties of the model and its chaotic-integrable transition or cross-over can be extended to models with more structure and are thus more relevant for experiments and the theory of many-body localization in finite dimensions.

Even though the (thermodynamic) localization properties of interacting quantum materials in principle have to be determined in the limit of infinite system size, or at least estimated by an appropriate extrapolation, the study of localization properties in mesoscopic systems of intermediate size has gained significant attention in recent years. The motivation is twofold: Partly driven by pragmatism, mesoscopic systems such as SYK and its relatives offer more analytic control while at the same time they can be dealt with numerically as well. Additionally, the localization properties of smaller systems are still not well understood, but highly relevant for a number of mesoscopic devices (Monteiro *et al.*, 2021a), such as quantum dot or qubit arrays (Altshuler *et al.*, 1997; Silvestrov, 1997; Silvestrov, 1998; Gornyi *et al.*, 2016; Gornyi *et al.*, 2017b; Xu *et al.*, 2018; Roushan *et al.*, 2017) and small size optical lattices (Rubio-Abadal *et al.*, 2019; Choi *et al.*, 2016; Schreiber *et al.*, 2015).

The main result of Monteiro *et al.*, 2021a in the SYK quantum dot problem is the analytical identification of the transition point between localized and extended states, which is given by[6]

$$\delta_c \sim J N_{\mathcal{B}}^{5/2} \ln N_{\mathcal{B}}, \tag{57}$$

where δ represents the variance of the single-particle couplings in Eq. (56).

Interestingly, here the relationship to the RRG calculations described earlier appears: It has a similar structure as the RRG model with a Hilbert space volume of $\mathcal{V} = 2^{N_{\mathcal{B}}}$ and coordination number $m + 1 \sim N_{\mathcal{B}}^4$. Considering this RRG setting one again arrives at the same scaling of the critical point δ_c, showing the close connection between the two toy models (Tikhonov and Mirlin, 2021b).

Additionally, a prediction for the wave function moments, defined as

$$P_q = \sum_{\nu} \overline{|\langle \nu \mid \psi \rangle|^{2q}}, \tag{58}$$

where the sum is over the Fock space basis $|\nu\rangle$ in occupation number representation of real space orbitals, is given:

While in the localized limit and in the limit of infinite interaction strength J the situation is clear, namely P_q is unity or represents the ergodic limit, at $\delta \sim \delta_c$ close to the critical point the moments are non-trivial: On the ergodic side of the transition they scale with a power law of the effective interaction strength

6 Actually, Monteiro *et al.*, 2021a chose a normalization of the many-body energy which is not extensive in $N_{\mathcal{B}}$, and therefore cite an expression of the form $\sim J N_{\mathcal{B}}^2 \ln N_{\mathcal{B}}$.

δ/J. This behavior was interpreted as a sign of a regime of non-ergodic extended states, since they do not have full Fock space support. However, in the following discussion it turned out that this is actually a misinterpretation: In fact these state also are ergodic, however only on a subspace of Fock space, namely only on a finite energy-shell around the wave function under consideration (Tikhonov and Mirlin, 2021b; Monteiro *et al.*, 2021b).

In summary, the models and results offered in this and the previous sections offer insightful toy models where theory can actually provide microscopic predictions for the nature of wave functions in the vicinity of a localization transition. It is therefore hoped that these results may be useful also for more complex models with a more realistic structure such as disordered spin chains.

7

THE SYK MODEL AND DENSITY-DENSITY INTERACTIONS: SPECTRAL & WAVE FUNCTION STATISTICS ACROSS THE FINITE-SIZE ERGODICITY-INTEGRABILITY TRANSITION

This chapter is largely based on the publication Dieplinger et al., 2021.

7.1 MOTIVATION: TOWARDS A MORE REALISTIC INTERACTION STRUCTURE

By construction the SYK model Eq. (54) has a very different structure than systems studied in more conventional investigations of many-body localized and ergodic phases, for instance the spinless Fermi-Hubbard model. This is true for theoretical studies but much more importantly also for experimental settings, e.g. in optical lattices.

Usually, electronic many-body Hamiltonians realized in experiments and studied in theory have the real space form

$$\mathcal{H} = \mathcal{H}_{\text{kin}} + \sum_{i,j} U_{ij} n_{\mathbf{r}_i} n_{\mathbf{r}_j}, \tag{59}$$

where the interaction kernel is usually motivated by the Coulomb repulsion between electrons (screened or unscreened). Importantly, in contrast to the SYK model, the interaction term commutes with all local densities in real space. Most famously the celebrated Fermi-Hubbard model takes this form (when including spin as an additional local degree of freedom) and hosts many electronic phases, such as BCS superconductivity or magnetically ordered ground states, which are prominent also in nature.

The structure of actual electronic Hamiltonians realized in experiments is therefore much less general than the SYK model since it is missing all off-diagonal matrix elements (in real space). Even effective low-energy models with more complex "off-diagonal" electronic interactions, such as the famous t-J model, eventually capture only physics already present in (59).

Coming back to the question of thermalization vs. localization and possible phase transitions between these two extremes, we therefore need to address the question how results obtained for SYK-related systems translate to these actually microscopically more realistic Hamiltonians of the form of (59).

In the following we will address this question by restoring the density-density form of the interaction part while still keeping the structureless nature of the

corresponding interaction kernel. We show the presence of similar regimes as observed in Monteiro *et al.*, 2021a between two localized and a chaotic, thermal regimes. To this end we compare the statistics of both the energy levels as well as the wave functions of the different models.

MODEL. Inspired by Eq. (59) we study a model of the form

$$\mathcal{H}_{tU} = \sum_{ij}^{N_{\mathcal{B}}} t_{ij} c_i^\dagger c_j + \sum_{ij}^{N_{\mathcal{B}}} U_{ij} n_i n_j, \tag{60}$$

where $n_i = c_i^\dagger c_i$. In contrast to the SYK Hamiltonian (54) its interaction commutes with all local densities n_i in the real space occupation number basis.

All other possible structure, such as a spatial dependence of the kernels t_{ij}, U_{ij} is omitted in accordance with the SYK model: The matrix elements t_{ij}, U_{ij} are zero-mean Gaussian random numbers with variance $\langle t_{ij}^2 \rangle = t^2/(64 N_{\mathcal{B}})$ and $\langle U_{ij}^2 \rangle = U^2/(64 N_{\mathcal{B}})$, chosen such that $\mathcal{H}_{tU}$ is Hermitian. The scale factor in the variance ensures volume scaling of the many-body energy, analogously to the definition of the matrix elements in (54).

METHOD. To access thermodynamic properties of this model the Hamiltonian is written and diagonalized in matrix form exactly for a finite $N_{\mathcal{B}} = 12, 16, 20$, using a Jordan-Wigner transformation to a spin system

$$c_i^\dagger = \left[\prod_{j=1}^{i-1} \sigma_j^z \right] \sigma_i^+, \tag{61}$$

where $\sigma_i^\pm = 1/2(\sigma_i^x \pm i\sigma_i^y)$ and $\sigma_i^{x,y,z}$ the Pauli-matrices in x, y, z direction at site i (Jordan and Wigner, 1928; Fu and Sachdev, 2016; García-Álvarez *et al.*, 2017). By that the Hamiltonian is represented as a matrix in Fock space in the occupation number basis of n_i. Due to particle number conservation of (60) a block diagonal form can be found with blocks of reduced Fock space dimension of symmetry sectors at a specific filling. In this chapter a filling of 1/4 is chosen throughout; the qualitative results are independent of this choice.

7.2 CHAOTIC AND INTEGRABLE PHASES WITH DENSITY-DENSITY INTERACTIONS

The approach to identifying the integrable and chaotic phases (corresponding to localized and thermal in the language of many-body localization) is threefold: First, we study the level spacing statistics of the many-body spectrum, namely by identifying the distribution function of the spacings of subsequent (many-body) energy levels. This approach however is blind to the structure of wave functions in Fock space. Additionally, we investigate the spectral form factor, which again is

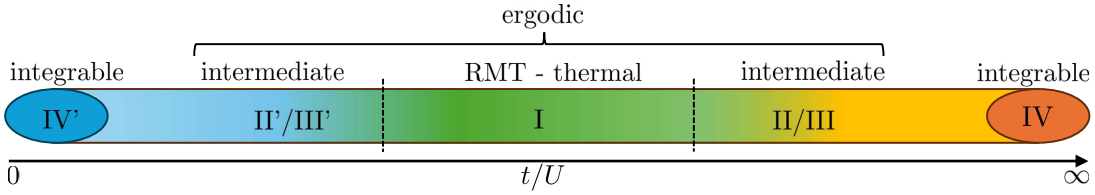

Figure 24: Phase diagram of the SYK inspired density-density model, Eq. (60). The regions I, II/III, IV refer to the regimes identified by Monteiro *et al.*, 2021a in the full extended SYK model. The integrable limits are expected to collapse to $t/U \to 0, \infty$, Dieplinger *et al.*, 2021.

a measure of energy level correlations in the many-body spectrum. This measure is able to discriminate to some degree between different integrable phases in its intermediate time behavior. Last but not least we study the wave function statistics directly, giving access to the complex statistical structure of wave functions in Fock space. This allows us to differentiate between different ergodic regimes in the vicinity of the chaotic-integrable transition. In summary these statistical measures allow us to make detailed statements about the properties of localized and ergodic regimes of (60) as a function of the relative interaction strength and compare to the deformed SYK model studied in Monteiro *et al.*, 2021a.

We find five different regimes, some of which can be identified with the regimes found by Micklitz *et al.*, 2019; Monteiro *et al.*, 2021a: a fully ergodic regime with wave function support in the entire Fock space, reminiscent of the RMT phase of the SYK model (regime I), two ergodic regimes with support only on shells of constant energy in Fock space, on either side of regime I (regimes II/III, II'/III') and finally two fully localized regimes in the limiting cases $t \to 0, U \to 0$ (IV' and IV, respectively). This structure is depicted in Fig. 24.[1]

7.2.1 *Energy level correlations*

DISTRIBUTION FUNCTION $P(s)$. The distribution function of subsequent energy level spacings is defined as

$$\mathcal{P}(s) = \langle \delta(s - s_l) \rangle_{\text{ens,spectrum}}, \tag{62}$$

where $s_l = (E_l - E_{l-1})/\Delta$ denotes the spacing between two neighboring eigenvalues of the Hamiltonian (60) in units of the corresponding mean level spacing Δ (Guhr *et al.*, 1998; Mehta, 2014) and the average runs over energy levels in the spectrum of a given realization of (60) and ensembles of different realizations.

This quantity is a hall-mark measure of random matrix theory. A Poissonian distribution $P(s)$ of this quantity corresponds to an integrable system while

1 In Refs. Monteiro *et al.*, 2021a; Dieplinger *et al.*, 2021 the intermediate finite support ergodic regimes have been dubbed "non-ergodic". This is a misleading naming, since the wave function in this regime actually are ergodic, however only on a subset of Fock space sites (Tikhonov and Mirlin, 2021b; Monteiro *et al.*, 2021b).

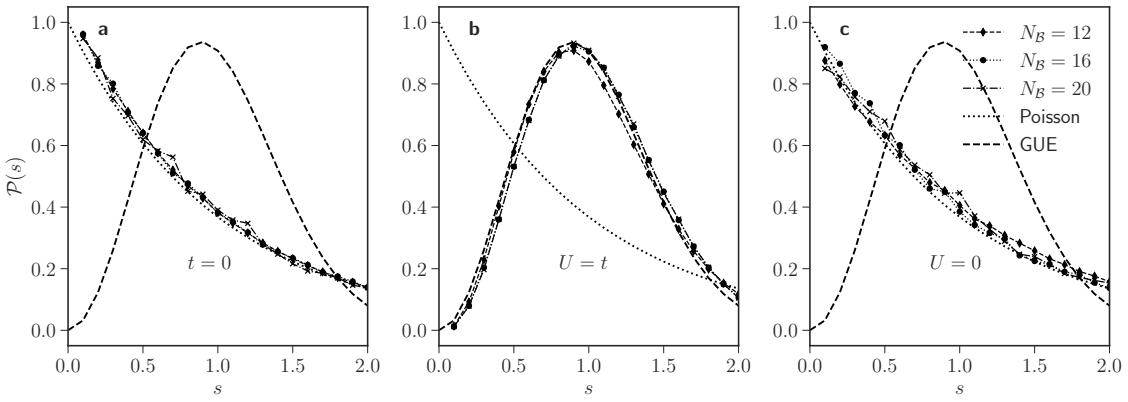

Figure 25: Level spacing distribution in selected interesting parameter settings of model (60), compared to the theoretical curves of a Gaussian unitary ensemble (Wigner-Dyson) and an integrable system (Poisson). Adapted from Dieplinger *et al.*, 2021, ©2021 Elsevier.

a Wigner-Dyson distribution for a Gaussian unitary, Gaussian orthogonal or Gaussian symplectic RMT ensemble correspond to quantum chaos (Mehta, 2014; Bohigas *et al.*, 1984). For the Gaussian unitary ensemble the Wigner-Dyson distribution of level spacings reads

$$\mathcal{P}_{\mathrm{GUE}}(s) = \frac{32}{\pi^2} s^2 e^{-\frac{4}{\pi}s^2}. \tag{63}$$

It was observed that for instance the level spacings of heavi nuclei follow the characteristic RMT distribution (Weidenmüller and Mitchell, 2009).

The qualitative difference in particular refers to the limit $s \to 0$, i.e. the probability of finding two energies infinitesimally close to one another: While in the integrable, Poissonian case the probability is finite, even maximal, in chaotic systems it goes to zero for all ensembles. This phenomenon is called *level repulsion* and often appears as avoided crossings in spectral analyses. The SYK model (54) – being a prime example of a many-body quantum chaotic system – prominently follows the predictions from random matrix theory (Kitaev, 2015; Maldacena and Stanford, 2016; García-García and Verbaarschot, 2016; García-García and Verbaarschot, 2017; García-García *et al.*, 2018; Haque and McClarty, 2019; Gu *et al.*, 2020; Behrends and Béri, 2020; Kobrin *et al.*, 2021). To probe the infinite temperature thermodynamics of the model Hamiltonian we only take into account the central part ($\sim 60\%$) of the many-body spectrum of the finite-size system.

Fig. 25 shows the level spacing distribution for the density-density model (60) at different relative interaction strengths t/U. In the intermediate case, i.e. $t = U$, in panel **b** $\mathcal{P}(s)$ resembles the Gaussian unitary random matrix ensemble. This is a clear signature of a quantum chaotic system. In the limiting cases $t = 0$ (**a**) and $U = 0$ (**c**) the system is trivially integrable, which is reflected by the clear Poissonian fingerprint of $\mathcal{P}(s)$. The quantum chaotic behavior in the intermediate interaction regime resembles the SYK model (54) away from half filling.

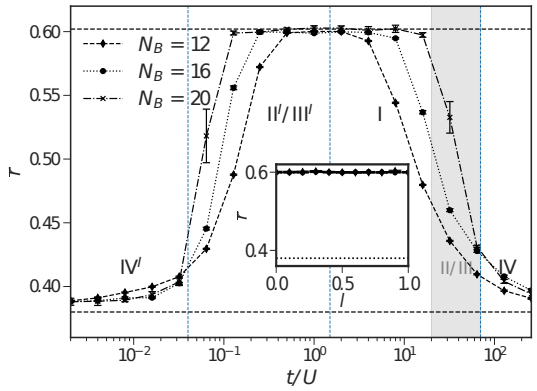

Figure 26: Transition between integrable (Poisson) and ergodic (Wigner-Dyson) level spacing statistics for different interaction strengths t/U. The corresponding RMT predictions are indicated as dashed horizontal lines. The labelling of the regime is defined in analogy to Monteiro *et al.*, 2021a. The nature of some of the subregimes is not resolved in the level statistics; it can only be disentangled when analyzing the corresponding wave functions. (inset) Level spacing ratios of the interpolation between SYK and the density-density model (60) at $t = U$ as a function of the interpolation parameter λ. Adapted from Dieplinger *et al.*, 2021, ©2021 Elsevier.

LEVEL SPACING RATIOS. Closely related to $\mathcal{P}(s)$ one can define the level spacing ratios,

$$r_l = \frac{\min(s_l, s_{l+1})}{\max(s_l, s_{l+1})}, \tag{64}$$

and its average $\bar{r} = \langle r_l \rangle_{\text{ens,spectrum}}$ (Oganesyan and Huse, 2007; Cuevas *et al.*, 2012; García-García *et al.*, 2018). This definition has the additional benefit that (i) it is valid also for strongly varying spectral densities and avoids unfolding[2] (Oganesyan and Huse, 2007) and (ii) allows to track the resemblance of $\mathcal{P}(s)$ to the Wigner-Dyson or Poissonian limit using a single parameter. $\bar{r} \sim 0.388$ corresponds to Poissonian statistics while $\bar{r} \sim 0.599$ for a GUE Wigner-Dyson distribution (Oganesyan and Huse, 2007; Atas *et al.*, 2013; Cuevas *et al.*, 2012; García-García *et al.*, 2018).

In Fig. 26 $\bar{r}$ is shown as a function of relative interaction strength t/U for the density-density model (60). The level spacing ratio indicates two transitions between two integrable regimes in the limiting cases $t \ll 0, U \ll 0$ (corresponding to panels **a** and **c** in Fig. 25, indicated by IV′ and IV) and a non-integrable one in between at $t \sim U$.

The limit where $U \ll t$ – resembling the structure of the SYK model, however in a quadratic operator form – has been studied by Liao *et al.*, 2020; Winer *et al.*, 2020. Integrability was expressed in terms of a large SU(2) symmetry group which destroys energy level correlations.

2 As the spectrum is smooth and roughly constant in the regime studied here, this is not relevant for this chapter.

In order to identify the RMT phase of Fig. 26 of the model (60) with the original SYK model we define a new family of Hamiltonians which interpolate between SYK and the density-density interacting variant (60)

$$\mathcal{H}(\lambda) = \lambda \cdot \mathcal{H}_{\text{cSYK}} + (1-\lambda) \cdot \mathcal{H}_{\text{tU}}, \tag{65}$$

with $\lambda \in [0, 1]$. If a phase transition – to which $\bar{r}$ is sensitive – occurs it should be visible upon varying λ. The inset of Fig. 26 shows $\bar{r}(\lambda)$ for $t = U$. It stays at the GUE value for all λ indicating a RMT phase. No phase transition is crossed suggesting that the two RMT phases of the SYK model and the intermediate interaction regime of (60) can be identified with each other; at least on the level of the infinite temperature level correlations.

SPECTRAL FORM FACTOR. The so-called spectral form factor is an alternative descriptor of quantum chaos (Brézin and Hikami, 1997; Müller *et al.*, 2004). Similarly to measuring the level spacing statistics directly it quantifies correlations between subsequent energy level spacings. Part of the interest in this form of measuring level correlations in the field of quantum chaos derives significantly from its accessibility in semiclassical periodic orbit theory (Sieber and Richter, 2001; Müller *et al.*, 2005) and field theories, including the the gravity duals, for instance JT gravity (Cotler *et al.*, 2017; Saad *et al.*, 2018).

We here take the simple definition of the spectral form factor $K(T)$ to be

$$K(T) = \langle\mid Z(\beta + iT) \mid^2\rangle_{\text{ens}}, \tag{66}$$

where $Z(\beta+iT)$ is the partition function taken at (inverse) temperature β and observation time T.

Level repulsion – being the primary indicator of quantum chaos in the distribution of level spacings as seen above – translates to a so-called linear ramp feature, which can be most easily seen when visualizing $K(T)$ for a set of random matrices for instance of the Gaussian unitary ensemble (GUE). Fig. 27 **a** shows the infinite temperature spectral form factor of a GUE, defined as $\mathcal{H}^{\text{GUE}}$ with Hilbert space dimension L and complex Gaussian uncorrelated matrix elements

$$\langle \mathcal{H}^{\text{GUE}}_{ij}\ \mathcal{H}^{\text{GUE}}_{i'j'}\rangle_{\text{ens}} = \frac{1}{L}\delta_{ii'}\delta_{jj'}, \tag{67}$$

under the constraint of Hermiticity of the Hamiltonian.

Here, for a wide range of times T, after an initial system dependent behavior up to a time of order one, $K(T)$ grows linearly up to times of the order of the inverse level spacing (Heisenberg time, vertical dashed line). After that the spectral form factor saturates to the so-called plateau (horizontal dashed line) (Saad *et al.*, 2018).

$K(T)$ encodes many of the interesting quantities of quantum chaotic systems and even its gravitational duals, for instance JT gravity. Additionally, it is

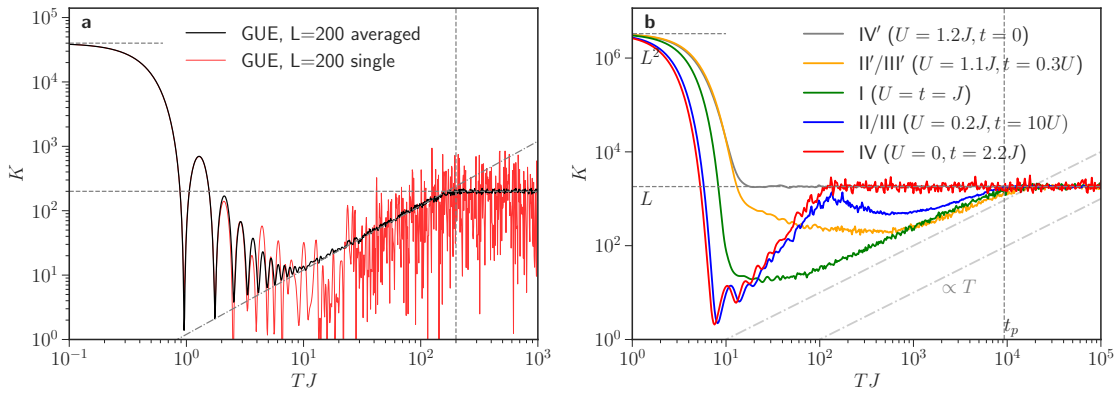

Figure 27: Spectral form factor for **a** an ensemble of Gaussian unitary random matrices of size $L = 200$ and ensemble size 400 and **b** different regimes of model (60). The linear ramp behavior is sketched as a dashed grey line. Here, $N_{\mathcal{B}}$ averaged over 2000 disorder realizations. The plateau time is $t_p \sim 5L/J$. Adapted from Dieplinger *et al.*, 2021, ©2021 Elsevier.

conjectured that any two point correlator of the SYK model Eq. (54) can be expressed in terms of $K(T)$, stressing its universal features and significance.

Here, we use the spectral form factor only to discriminate between different regimes, resembling integrable and chaotic/ergodic parameter regions. As it turns out its sensitivity of characterizing the regimes of different t/U is enhanced compared to the distribution of the nearest neighbor level spacing statistics.

In panel **b** of Fig. 27 $K(T)$ is calculated at infinite temperature for different values of the interaction parameter t/U. The many-body bandwidth is kept approximately constant and comparable to the energy scale J of the bare SYK model (54), which can be seen from the fact that the plateau is reached at the same (Heisenberg) time for all curves. The plateau-/Heisenberg time is a measure of the inverse level spacing and by that of the many-body energy scale.

Before the plateau develops, at $TJ \geqslant 10$ the different parameter regimes can be distinguished by the qualitative form of the "ramp": In the case we found to be reminiscent of the RMT case before, $t = U$ (green) a wide range of linear behavior can be observed, similar to the GUE in panel **a**.

For smaller t/U the linear part of the ramp becomes shorter and develops a shallower initial slope (yellow) until it vanishes completely and assumes the plateau value immediately (grey, regime IV'). This is consistent with the study by Prakash *et al.*, 2021 which observed a similar regime, when localizing an ergodic system by adding a strong disordered Fock space diagonal term in the Hamiltonian.

Contrasting that, in the opposite case, $U = 0$, when the model becomes quadratic and non-interacting (blue to red, regime IV), Liao *et al.*, 2020; Winer *et al.*, 2020 reported a very steep slope of the ramp feature, resulting in an exponential growth until the plateau value is reached. We confirm their finding

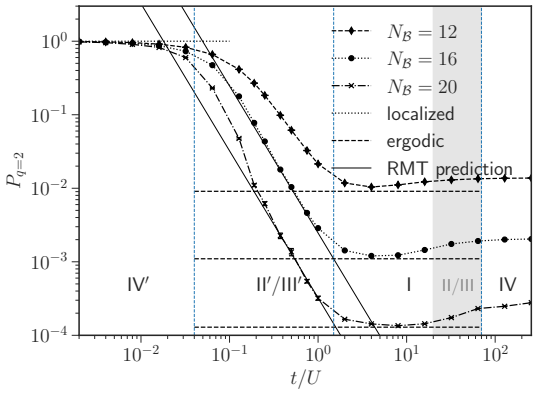

Figure 28: Inverse participation ratio $P_{q=2}$ for different relative interaction strengths t/U. The dashed lines mark ergodic behavior over the entire Fock space. The solid curve marks the the energy-shell RMT prediction by Micklitz *et al.*, 2019; Monteiro *et al.*, 2021a, (69), with the constant $c = 0.5$. Adapted from Dieplinger *et al.*, 2021, ©2021 Elsevier.

qualitatively; the slope is significantly steeper than linear in T. However, in our model the exponential character cannot be uniquely resolved.

Interestingly, $K(T)$ is able to discriminate between the two extreme limits which are both integrable. This is not possible using the nearest neighbor level spacing statistics as seen in Fig. 26 — there both regimes have the same characteristics.

Here, analyzing the energy correlations at infinite temperature, a rich structure of qualitatively different parameter regimes could be identified, including an RMT phase connected to the bare SYK model.

Additionally, it would be interesting to study $K(T)$ also in the low temperature regime. Studies of SYK models equipped with a single-particle term have been shown a cross-over to a renormalized Fermi liquid at small temperatures (Song *et al.*, 2017; Parcollet and Georges, 1999).

7.2.2 *Wave function statistics*

To further analyze possible substructures of the integrable and in particular of the ergodic regime – already hinted at by Fig. 27 and observed in the deformed SYK model by Monteiro *et al.*, 2021a – we study statistical properties of the wave functions of model (60).

A common statistical measure to quantify properties of wave functions of disordered systems are the wave function moments or inverse particpation ratios. Analogously to the analysis of quantum Hall criticality, where the moments were analyzed in a single-particle setting, cf. Eq. (18), they are defined as

$$P_q = \sum_\nu |\langle \nu \mid \Psi \rangle|^{2q}, \tag{68}$$

where the sum runs over the real space occupation number basis $|\nu\rangle$ in $L = \binom{N_\mathcal{B}}{N_\mathcal{B}/4}$ dimensional Fock space. P_q here is averaged over disorder ensembles as well as all energies in the center of the spectrum, analogously to the level spacing statistics as seen above.

The two extreme limits result in $P_{q>0} = 1$ for fully localized (to a single Fock space site) and the Porter-Thomas distribution $P_q = q!L^{1-q}$ for fully ergodic wave functions (on the entire Fock space volume), resembling independently distributed Gaussian random matrix ensembles.

Fig. 28 shows the inverse participation ratio $P_{q=2}$ as a function of the parameter t/U for the density-density model $\mathcal{H}_{tU}$. Several substructures which can be identified with the regimes found in Fig. 25,26 and 27 reappear, while additional differences can be resolved:

REGION IV'. When the kinetic energy vanishes ($t = 0$), $\mathcal{H}_{tU}$ is diagonal in the occupation number basis of real space orbitals. Its eigenstates therefore become trivially localized to a single Fock space site. This comes with a clear Poissonian level statistics and a largely flat ramp in the spectral form factor, diagnosing trivial integrability, since the local occupations form an extensive set of local conservation laws.

REGION I. This regime is reminiscent of standard RMT, the IPR follows the Porter-Thomas distribution for fully ergodic wave functions with support on the entire Fock space and level correlations corresponding to GUE, featuring Wigner-Dyson level spacings and linear ramp feature in the spectral form factor.

REGION IV. In this limit, when U approaches zero, $\mathcal{H}_{tU}$ becomes non-interacting. The quadratic part of the Hamiltonian can be diagonalized and the occupation of its orbitals forms again an extensive set of conservation laws. The system is integrable. Since the Hamiltonian is not diagonal in the basis in which P_q is measured here, the IPR does not approach unity.

REGION II/III. An intermediate regime with neither fully ergodic, over the full Fock space support, nor localized character emerges, which on the level of the eigenenergies follows the GUE prediction. This was observed for the first time by Micklitz *et al.*, 2019; Monteiro *et al.*, 2021a in the deformed SYK model (56). As the deformed SYK model is accessible easily these authors have been able to disentangle two subregimes with different characteristics. These are obscured by finite-size effects in numerical investigations, cf. Monteiro *et al.*, 2021a. This regime is remarkable because of the following reason: Even though according to the level correlations – there are clear signs of level repulsion and a linear ramp feature in Fig. 26 and 27 – the states do not cover the entire Fock space uniformly/ergodically, i.e. do not follow the Porter-Thomas distribution, cf. dashed horizontal lines in Fig. 28. In the past this regime has therefore been said to host *non-ergodic extended states* (Micklitz *et al.*, 2019; Monteiro *et al.*, 2021a;

Tikhonov and Mirlin, 2021b). This term is misleading: In fact the reason for this is that only a finite number of Fock space basis states have a finite overlap with the eigenstates of energy E, by that defining an energy shell. The wave function of energy E now only has support on this energy shell in Fock space on which it is ergodic. In that sense also the states in this regime are ergodic however with a different effective Fock space size. Consequently, in this regime the level spacing statistics P(s) is of the random matrix type. As was already the case in region IV, the precise dependencies on t/U and its nature cannot be resolved with the choice of the occupation number basis in real space in Fig. 28. A study in the basis of the occupations of the single-particle orbitals of t_{ij} would be in order. Our main interest however lies the next regime;

REGION II′/III′. In our model $\mathcal{H}_{tU}$ a dual region emerges. In analogy to II/III it separates the fully ergodic regime I from the second integrable region IV′. The IPR P_q varys strongly with increasing t/U, cf. Fig. 28; similarly to II/III this can be interpreted as the wave function occupying ever increasingly large energy shells ergodically, until it distributes uniformly across the entire Fock space in regime I. We compare the scaling of $P_q(t/U)$ with the regimes II/III found by Monteiro *et al.*, 2021a; which predicts a power law in the relative interaction strength with an exponent $\alpha = 1$ for regime III and $\alpha = 2$ for II. The adapted prediction for the dual region II′ reads

$$P_2 = c \cdot 8\sqrt{N_{\mathcal{B}}}\frac{U^2}{\pi t^2 \binom{N_{\mathcal{B}}}{N_{\mathcal{B}}/4}}, \tag{69}$$

which has been obtained for the extended SYK model (56) analytically using random matrix theory considerations by Monteiro *et al.*, 2021a. In an extended parameter range of t/U the parametric scaling in $t/U, N_{\mathcal{B}}$ fits well the data presented in Fig. 28. The prefactor c is an open fit parameter but expected to be of order unity; a high quality description of the numerical data is obtained for $c \sim 0.5$.

7.3 CONCLUSION: MINIMAL MODEL OF ERGODIC-INTEGRABLE TRANSITIONS FROM A DENSITY-DENSITY INTERACTION MODEL

In summary, we defined a model featuring the appealing lack of structure of the SYK model, which simplifies numerical and analytical treatment signficantly, allowing for detailed analytical predictions, e.g. (69) by Monteiro *et al.*, 2021a. However, we restricted the interaction Hamiltonian to a density-density form, as observed in nature for instance in the Coulomb interaction. Interestingly, we observed that – by analyzing three key diagnostics of statistical characteristics of (many-body) wave functions and spectra – the rich, but tractable, substructure of integrable and ergodic regimes observed in the deformed SYK model by Monteiro *et al.*, 2021a survives this rather drastic restriction. Moreover, dual ergodic regimes

References	model	α, β	$\tilde{t}_{ij}$	$\tilde{U}_{ij}$	ϵ_i
Ref. Kitaev, 2015; Maldacena and Stanford, 2016	majorana	$\alpha, \beta{=}0$	o	SYK	nr
Ref. Gu *et al.*, 2020; Fu and Sachdev, 2016	fermion	$\alpha, \beta{=}0$	o	SYK	nr
Ref. Monteiro *et al.*, 2021a; García-García *et al.*, 2018; Haque and McClarty, 2019; Lunkin *et al.*, 2018; Dieplinger and Bera, 2023; Nandy *et al.*, 2022	majorana	$\alpha, \beta{=}0$	r	SYK	nr
This work, Dieplinger *et al.*, 2021	fermion	$\alpha, \beta{=}0$	r	r	nr
Ref. Burin, 2015a	spin	$\alpha, \beta \in (d, 3)$	r	r	r
Ref. Tikhonov and Mirlin, 2018	spin	$\alpha{=}\beta \in (d, 2d)$	r	r	r
Ref. Thomson and Schiró, 2020	fermion	$\alpha, \beta \in (0, 2.5)$	r	r	r
Ref. De Tomasi, 2019	fermion	$\alpha \in (1, 4), \beta{=}\infty$	r	nr	r
Ref. Nag and Garg, 2019	fermion	$\alpha{=}\beta \in (0.5, 3)$	nr	nr	r
Ref. Safavi-Naini *et al.*, 2019	spin	$\alpha{=}\beta \in (0.5, 2.5)$	nr	nr	r
Ref. Kloss and Bar Lev, 2020	spin	$\alpha{=}\beta \in (1.75, \infty)$	nr	nr	r
Ref. Modak and Nag, 2020	fermion	$\alpha \in (1.2, 4), \beta{=}\infty$	nr	nr	r
Ref. Roy and Logan, 2019	spin	$\alpha, \beta \in (0, \infty)$	nr	nr	r
Ref. Deng *et al.*, 2020	boson	$\alpha, \beta \in (0, \infty)$	nr	nr	r

Table 4: Selection of models appearing in literature which conncect the model proposed in this chapter (60) with fermion, spin and boson models in the context of SYK and many-body localization; from fully structureless (SYK-type, top rows) to more realistic Hamiltonians (bottom) which partly are realizable for instance in cold atom experiments. Some form of disorder enters the models in the kinetic energy, $t_{ij}{=}\tilde{t}_{ij}/|i-j|^{\alpha}$, with randomized hoppings $\tilde{t}_{ij}$ and similarly in the density-density interaction matrix elements, $U_{ij}{=}\tilde{U}_{ij}/|i-j|^{\beta}$, and as random potential energies, ϵ_i. In Safavi-Naini *et al.*, 2019; Deng *et al.*, 2020 power-law correlated disorder is realized in t_{ij}, U_{ij} by random site positions. Abbreviations: r for random and nr for non-random matrix elements; $\beta{=}\infty$ refers to nearest-neighbor interactions; SYK denotes an interaction as in Eq. (54), i.e. deviating from the density-density form. Adapted from Dieplinger *et al.*, 2021, ©2021 Elsevier.

on energy shells in Fock space emerge due to the existence of a second integrable limit at $U \to \infty$ (Dieplinger *et al.*, 2021). We found that contrary to intuition – this dual regime does not exist in the original deformed SYK model – its wave function moments P_q can be described using an analogous analytical form.

The model and the results presented offer another puzzle piece in the connection between the well understood SYK model and its rich physics when including a single-particle term (studies summarized at the top of table 4); and the much less understood but microscopically much more relevant models of many-body localization/ergodicity in real space (bottom of table 4).

Computationally – by an analysis of spectral and wave function statistics – we found five qualitatively different regimes of $\mathcal{H}_{tU}$; two integrable limits, which differ in their nature qualitatively, cf. Fig. 27, a fully ergodic phase with support in the entire Fock space, reminiscent of the RMT phase of the bare SYK model 54; and two corresponding ergodic regimes with support only on a fraction of the Fock space – they separate the SYK type from the integrable regimes. While we do not have high resolution access to the regime on the strongly interacting side of the RMT phase due to our choice of the basis (Monteiro *et al.*, 2021a), we have found that the dual phase, which has arisen due to the restriction on density-density interactions, follows a similar law. Its wave function moments scale with power laws as a function of the relative interaction strength; their exponents and amplitude can almost fully be predicted by Eq. (69). The latter is a modification of the RMT prediction for the deformed SYK model by Monteiro *et al.*, 2021a once more highlighting the close connection of our model $\mathcal{H}_{tU}$ to the Sachdev-Ye-Kitaev model even though the interaction is restricted to the density-density type.

The proposed model, (60), therefore represents a significant step to put SYK physics – here in the context of ergodicity breaking – closer to experimentally realizable systems, such as those at the bottom of table 4. Table 4 puts our work in context with literature results from the conventional SYK field dealing with quantum chaos to the more microscopically relevant models of many-body localization, which can for instance be realized in cold-atom set-ups. A future direction of research in this context would be the study of the evolution of the phase diagram shown in Fig. 24 when moving down in the table, i.e. towards the actual many-body localization problem for instance in disordered spin-chains.

8

DYNAMICS IN MINIMAL MODELS OF ERGODICITY AND INTEGRABILITY: FINITE-SIZE PRE-THERMALIZATION

This chapter is largely based on the publication Dieplinger and Bera, 2023.

8.1 MOTIVATION: DYNAMICS CLOSE TO THE TRANSITION

The previous chapter focused solely on the statistical properties of the many-body energy spectrum of (de)localized phases. Specifically, the spacings of energy levels as well as the distribution of wave functions in Fock space has been investigated; by that the identification of integrable and ergodic phases was possible. This translates to the properties of the system in the limit of infinite time $t \to \infty$.

In actual experiments, as well as in many numerical investigations, however, physicists usually have access to finite time properties, such as density correlations. The time evolution in such experiments or simulations is limited either by experimental constraints, such as dephasing times of cold atom experiments, or by finite-size effects, which become relevant when the time evolved state has explored the finite boundaries of a model system after a finite time. Therefore, investigating the effect of (de)localization, integrability and ergodicity on finite time properties close to a possible MBL transition is an important task in understanding the interplay of thermodynamic properties and actual observable phenomena in simulations and experiments.

The present chapter is dedicated to exploring the finite time dynamics of toy models of ergodicity breaking; in particular we will focus on a variant of the mass-deformed SYK model, Eq. (56) considered by Monteiro *et al.*, 2021a. As detailed in section 6.4, Eq. (56) hosts a finite-size ergodicity-integrability transition, which can be interpreted as a toy model of a MBL transition. Here the goal is to understand not only the infinite time, statistical properties of such a model, but rather its finite time dynamics which could in principle be accessed by experiments.

The main quantity of interest in this chapter is the density-density correlator at finite times and – complementarily – the real time dynamics of a propagating wave function in Fock space. The finite-size transition between localized and ergodic regimes occurs as a function of the relative interaction strength, as seen above. At intermediate times a per-thermal regime emerges, before eventually the system thermalizes. This regime exhibits signatures of the localized phase at

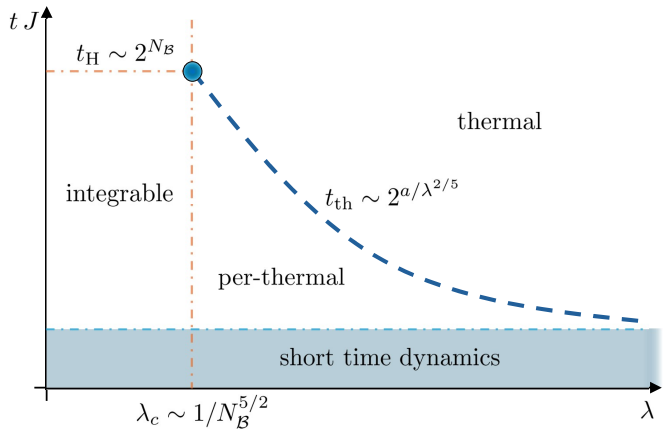

Figure 29: Finite time phase diagram of the minimal model Hamiltonian (70) for increasing interaction strength λ. $N_{\mathcal{B}}$ denotes the real space sites in the SYK quantum dot. t_H is the Heisenberg time, and the thermalization time t_{th} (dashed line) depends on λ. Adapted from Dieplinger and Bera, 2023, ©2023 American Physical Society.

the opposite side of the transition which can similarly be observed in the Fock space dynamics of single wave functions. Fig. 29 shows a qualitative "dynamical" phase diagram for finite times.

MODEL AND METHOD. To study dynamical properties of an ergodic-integrable transition we employ the deformed SYK model introduced by Monteiro *et al.*, 2021a. Its definition is adjusted to complex fermions,

$$\mathcal{H} = \lambda \mathcal{H}_{SYK_4} + (1-\lambda)\mathcal{H}_{SYK_2}, \tag{70}$$

where $\lambda \in [0,1]$ denotes the relative interaction strength of the two Hamiltonian terms and

$$\mathcal{H}_{SYK_4} = \sum_{ijkl}^{N_{\mathcal{B}}} J_{ijkl} c_i^\dagger c_j^\dagger c_k c_l, \tag{71}$$

and

$$\mathcal{H}_{SYK_2} = \sum_{ij}^{N_{\mathcal{B}}} t_{ij} c_i^\dagger c_j. \tag{72}$$

As before $c_i^\dagger (c_i)$ indicate complex fermions at site i and $N_{\mathcal{B}}$ the number of sites. Analogously to the structureless Hamiltonians dealt with so far in this thesis, Eq. (54), (56), (60), the couplings are zero mean random numbers with variances given by

$$\langle t_{ij}^2 \rangle_{ens} = \frac{J^2}{64 N_{\mathcal{B}}} \text{ and } \langle J_{ijkl}^2 \rangle_{ens} = \frac{J^2}{2 N_{\mathcal{B}}^3}, \tag{73}$$

with constraints to ensure Hermiticity of $\mathcal{H}$. This model conserves the global particle number, in contrast to the original Majorana version by Monteiro *et al.*, 2021a, Eq. (56). Since properties of SYK are qualitatively independent of the particle number sector chosen we henceforth restrict all simulations to half filling, $n_{\text{fill}} = 1/2$, without loss of generality.

Similarly to the model studied in the previous chapter as well as the Majorana version of Monteiro *et al.*, 2021b $\mathcal{H}$ hosts an ergodic and an integrable phase depending on the parameters $\lambda, N_{\mathcal{B}}$. For $\lambda = 1$ the model is identical to the SYK Hamiltonian which is known to be (maximally) chaotic, while at $\lambda = 0$ the Hamiltonian becomes non-interacting, Therefore, it is many-body integrable, due to the set of occupations of the single-particle orbitals forming an extensive set of local integrals of motions. In the presence of both terms, $0 < \lambda < 1$ a transition between both qualitative limits is expected to happen as a function of λ for given $N_{\mathcal{B}}$ (García-García *et al.*, 2018; Monteiro *et al.*, 2021a); in this regime we will probe the dynamical properties in form of the density-density correlator and the wave function propagation in real space.

Models of the type SYK_4 + SYK_2 have been studied in recent years in diverse contexts, see for instance Monteiro *et al.*, 2021a; García-García *et al.*, 2018; Haque and McClarty, 2019; Lunkin *et al.*, 2018; Altland *et al.*, 2019; Haldar *et al.*, 2020; Nandy *et al.*, 2022; Larzul and Schiró, 2022. In particular, Nandy *et al.*, 2022 have examined the spectral form factor of a mass-deformed SYK model, which is closely related to Eq. (70); however in the eigenbasis of the single-particle hopping term $\mathcal{H}_{SYK_2}$[1]. They found a time scale (Thouless time), which is scaling with the system size supporting an ergodic regime for long times at large enough system sizes.

In the following a numerical investigation of the density correlations is presented which supports the notion of a cross-over time scale for large enough time scales to an ergodic behavior. Additionally, a semi-analytical scaling argument is presented for the associated time scale. The latter is verified by exact numerical simulations of the time evolution of Eq. (70).

OBSERVABLES. Numerically, we calculate the infinite temperature density-density correlator and its sample-sample fluctuations[2],

$$\mathcal{C}_i(t) = \langle | \langle n_i(t) n_i(0) \rangle_\infty - n_{\text{fill}}^2 | \rangle_{\text{dis}}. \tag{74}$$

The time evoloved densities at site i are given by

$$n_i(t) = e^{-i\mathcal{H}t}\, c_i^\dagger c_i\, e^{i\mathcal{H}t}, \tag{75}$$

1 In Nandy *et al.*, 2022 the single-particle energies are uncorrelated, in contrast to the spectrum of $\mathcal{H}_{SYK_2}$. It is believed that this does not affect the ergodic-integrable characteristics qualitatively (Monteiro *et al.*, 2021a).

2 The average density-density correlator is known to be qualitatively similar to the spectral form factor which was for instance studied by Nandy *et al.*, 2022. An exact relation is known for the bare SYK model. Both the effect of the mass deformation, and the behavior of the ensemble fluctuations on this correspondence is not known precisely.

where $i = 0$ is chosen without loss of generality due to the structureless nature of the model (70); all sites are equivalent up to fluctuations. $\langle \cdot \rangle_T = \mathrm{Tr}(e^{-\mathcal{H}/T} \cdot)/\mathrm{Tr}(e^{-\mathcal{H}/T})$ is the quantum mechanical expectation value at temperature T (Dieplinger and Bera, 2023).

The computational method used to calculate the time evolved operators $n_i(t)$ is provided by the kernel polynomial method (KPM), where the time evolution operator $e^{-i\mathcal{H}t}$ is expanded in Chebyshev polynomials (Weiße *et al.*, 2006). Quantum typicality is used by evaluating quantum mechanical expectations values stochastically (Weiße *et al.*, 2006; Bera *et al.*, 2017). Some details about KPM and Chebyshev expansions are delegated to appendix C; for a detailed review the reader is referred to the article by Weiße *et al.*, 2006. Infinite time, $t \to \infty$, calculations have been performed using exact diagonalization, analogously to chapter 7.

8.2 RESULTS: PRE-THERMAL PLATEAUS AT FINITE TIMES

The main result of the present chapter is the existence and the quantification of a (long) finite time window on the ergodic side of the ergodic-integrable transition, reminiscent of the integrable phase. The thermalization process is qualitatively different from the sub-diffusive regimes observed e.g. in disordered spin models in the vicinity of the MBL transition. The slow power-law process governing for instance the return probability towards thermal equilibrium (Weiner *et al.*, 2019) is replaced by the formation of a finite-time plateau, where the dynamics are reminiscent of the integrable regime. As the system parameters approach the transition this plateau becomes longer before it eventually thermalizes quickly (qualitatively similar to the bare SYK model (54)). The cross-over time scale to the thermodynamic limit can be quantified by a simple scaling argument, and physical intuition regarding the Fock space wave function propagation is provided on both sides of the ergodic-integrable transition (Dieplinger and Bera, 2023).

8.2.1 *Density correlations*

LIMITING CASES. The dynamics of both limiting cases $\lambda = 0, 1$ can be understood quite easily. The purely interacting case, i.e the proper SYK model (54) is studied in Fig. 30 **a** for different numbers of basis sites $N_\mathcal{B}$. The densities n_i are expected to become uncorrelated and uniformly distributed when ergodicity is present, decoupling the density-density correlator in the limit $t \to \infty$. Therefore,

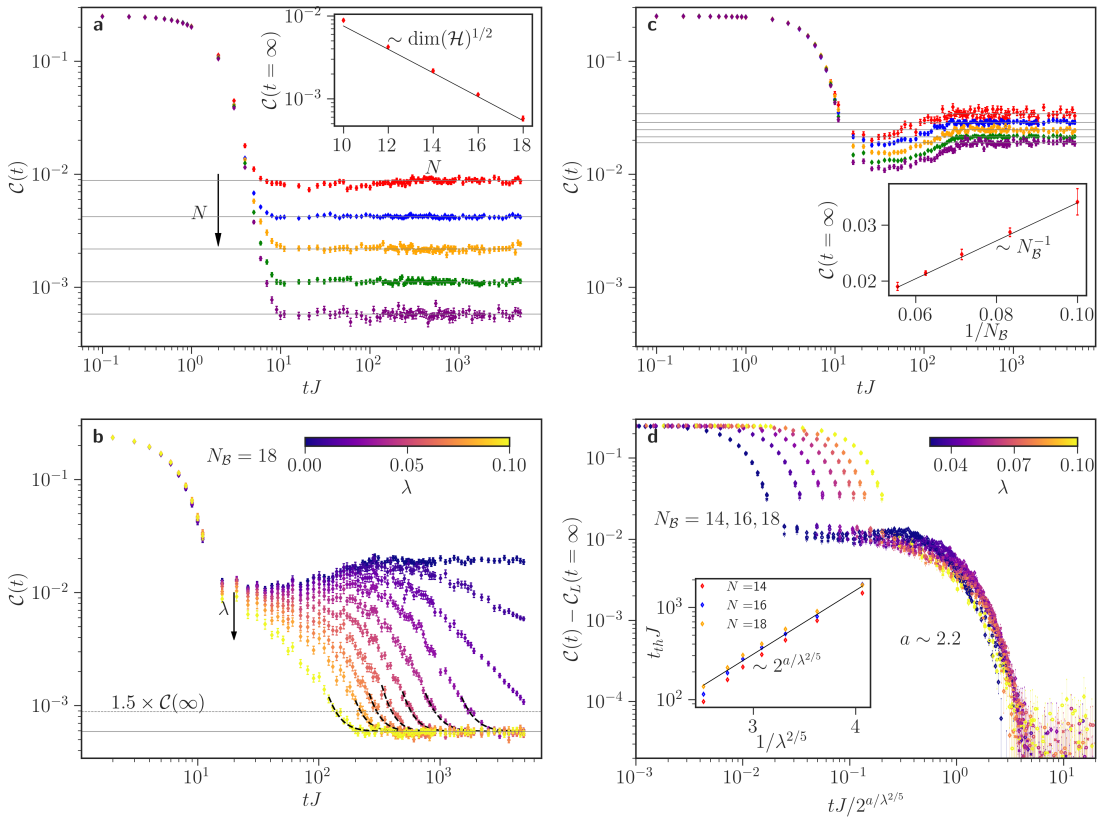

Figure 30: Infinite temperature density-density correlator fluctuations Eq. (74) of the modified SYK model with random single-particle kinetics, Eq. (70). Limiting cases of $\lambda = 1$, i.e. the bare SYK model (**a**) and $\lambda = 0$, the non-interacting limit (**c**) of $\mathcal{C}(t)$ for several system sizes $N_{\mathcal{B}} = 10, 12, 14, 16, 18$ as a function of time t. In both limits the curves saturate to (different) plateaus at $t \to \infty$; its numerical value $\mathcal{C}(t = \infty) = \langle \mathcal{C}(t > t_{\text{thresh}}) \rangle_t$ is shown as black horizontal lines and in the insets of **a, c** as a function of $N_{\mathcal{B}}$, with $t_{\text{thresh}}J = 10^3$. **b** $\mathcal{C}(t)$ for different relative interaction strengths $\lambda = 0.0, 0.02, 0.03, 0.04, 0.05, 0.06, 0.07, 0.08, 0.1$ at $N_{\mathcal{B}} = 18$. Depending on λ a finite time plateau can be observed, which eventually thermalizes to the bare SYK saturation value (black horizontal line). For numerical purposes we define the system thermalized when an exponential fit of $\mathcal{C}(t)$, marked in the dashed curves, crosses a threshold $\mathcal{C}_{\text{thresh}} = 1.5\mathcal{C}_\infty$ (black dashed line) at the thermalization time t_{th}, cf. Eq. (78). **d** Approximate scaling collapse of $\mathcal{C}$ for different $N_{\mathcal{B}}$ in a time window $\mathcal{O}(10^{-1}) - \mathcal{O}(10^0)$, where the $N_{\mathcal{B}}$ dependent SYK plateau value has been subtracted from $\mathcal{C}(t)$ and t is rescaled by the analytical estimate $t^a_{\text{th}}(\lambda)$. (inset) thermalization time from **b** as a function of the interaction strength λ and the analytical estimate Eq. (77). Adapted from Dieplinger and Bera, 2023, ©2023 American Physical Society.

$\mathcal{C}$ should tend towards zero.[3] Since the system at hand is always finite, fluctuations of $\mathcal{C}$ do not decay completely resulting in a finite $\mathcal{C}(t \to \infty)$ for a given finite

3 Numerically, the infinite time correlations have been defined as

$$\mathcal{C}(t = \infty) = \langle \mathcal{C}(t > t_{\text{thresh}}) \rangle_t, \tag{76}$$

$N_{\mathcal{B}}$ even in a fully ergodic phase. Ergodicity can be diagnosed by the scaling of the fluctuations with the basis size $N_{\mathcal{B}}$ (inset). The sample-to-sample fluctuations of the density correlations $\mathcal{C}(t)$ decay exponentially with $N_{\mathcal{B}}$, i.e. with a power $1/2$ of the Fock space dimension $\dim(\mathcal{H})$. The full Fock space is explored by the wave function at long times, implying ergodicity.

A different picture emerges for the non-interacting limit $\lambda = 0$, cf. panel **c**: Another plateau forms whose value is also depending on $N_{\mathcal{B}}$. Upon a careful examination two qualitative difference to the former case can be observed: (i) The values of the plateaus are orders of magnitude larger than in the SYK case (**a**), and (ii) the scaling of the plateau value $\mathcal{C}(t = \infty)$ proceeds with a power-law of the number of real space sites $N_{\mathcal{B}}$ instead of the Fock space dimension, which is exponential in $N_{\mathcal{B}}$ (inset). Absolutely speaking, also states which evolve governed by the non-interacting Hamiltonian explore ever larger parts of Fock space due to its extensive connectivity. Relatively speaking, however, the fraction of the explored Fock space to its total size decreases exponentially. In the thermodynamic limit $N_{\mathcal{B}} \to \infty$ the dynamics is integrable in this sense.

CROSS-OVER DYNAMICS. Having understood both limits, now finite λ, mixing ergodic and integrable evolution, is considered. Following García-García *et al.*, 2018; Monteiro *et al.*, 2021a; Dieplinger *et al.*, 2021 a transition from an ergodic regime to an integrable one in the statistics of the spectrum of $\mathcal{H}$ is expected. Monteiro *et al.*, 2021a predicted a critical interaction strength $\lambda \sim 1/N_{\mathcal{B}}^{5/2} \ln N_{\mathcal{B}}$; above which ergodicity and below which integrability emerges for a given $N_{\mathcal{B}}$. Due to the exponential size of Fock space and the associated computational complexity of exact simulations using KPM or exact diagonalization, the range of $N_{\mathcal{B}}$ accessible is limited ($N_{\mathcal{B}} < 20$) making it impossible to resolve the logarithmic part of the scaling of the critical point. We here henceforth focus on the leading power, $\lambda_c \sim 1/N_{\mathcal{B}}^{5/2}$, to benchmark numerical results.

Fig. 30 **b** depicts the correlator $\mathcal{C}(t)$ in the intermediate interaction regime $0 < \lambda < 1$. For the largest values of λ the curve looks qualitatively similar to the SYK case at $\lambda = 1$ (**a**) with slightly altered short time behavior. When λ becomes smaller, a qualitative change occurs; a plateau develops which has even a local maximum at intermediate times when λ is small enough. At these times, cf. for instance $\lambda = 0.04$, at times $t < 5 \times 10^2/J$, the data resembles the *non-interacting* cases shown in panel **c**; the system looks integrable. However, at longer times a second drop in $\mathcal{C}(t)$ is observed after which the thermal plateau, reminiscent of the bare SYK model (**a**) is assumed. Apparently, a time scale exists before which the system looks integrable – dubbed pre-thermal – and after which the system eventually thermalizes, indicating a finite-time cross-over.

If λ is decreased further and eventually crosses the critical value λ_c, the system eventually becomes truly integrable, as expected from Monteiro *et al.*, 2021a. Here

with t_{thresh} a threshold time scale at which the finite-size density correlator $\mathcal{C}(t)$ does not change any more up to fluctuations. $\langle \cdot \rangle_t$ denotes a long time average.

the time traces eventually qualitatively follow the non-interacting limit, cf. Fig. 30 **c**.

THERMALIZATION TIME SCALE. Next we would like to quantify the cross-over time scale at which the behavior of the time-evolved states changes from pre-thermal to thermal in the vicinity of the transition at $\lambda_c \sim 1/N_{\mathcal{B}}^{5/2}$. One can find an analytical estimate from the following qualitative argument: In finite systems the smallest energy scale is typically the level spacing of the many-body spectrum. In a disordered system the mean level spacing typically is a sufficient measure; it usually scales inversely with the number of levels, i.e. the Fock space dimension; so exponentially in $N_{\mathcal{B}}$.

The smallest energy scale available translates to the largest time scale at which dynamics can still be non-trivial. This time scale is often referred to as the Heisenberg time t_H, and scales inversely with the level spacing, so $t_H \sim \mathcal{O}(1) \times \binom{N_{\mathcal{B}}}{N_{\mathcal{B}}/2}$ at half filling. This can for instance also be seen when studying the spectral form factor of a chaotic system, e.g. Eq. (60) shown in Fig. 27; the plateau time is the latest time at which a change in the dynamics happens in the finite system, and it is roughly given by the Heisenberg time.

Now we assume that there is a thermalization time as observed in Fig. 30. This time scale has to be smaller than the Heisenberg time for state evolutions on the ergodic side of the ergodic-integrable transition and larger than the Heisenberg time on the integrable side, to be consistent with the pre-thermal plateau. In this case it is plausible to assume that *exactly at the critical point* λ_c the two time scales coincide, i.e. $t_{th}^a(\lambda = \lambda_c) = t_H$. Adding the scaling of the critical point, i.e. $\lambda_c \sim 1/N_B^{5/2}$, and approximating the level spacing scaling by an exponential, $t_H \sim 2^{b \times N_B}$, a consistent analytical form for t_{th}^a is

$$t_{th}^a(\lambda) \propto 2^{a/\lambda^{2/5}}, \tag{77}$$

where $a = \mathcal{O}(1)$.

Fig. 30 **d** a verification of this analytical idea is attempted. The time axis is rescaled by t_{th}^a, while the ergodic plateaus, shown in panel **a**, are subtracted from $\mathcal{C}(t)$. Many data traces corresponding to $\mathcal{C}(t)$ with system sizes from $N_{\mathcal{B}} = 14, 16, 18$ and interaction strengths from $\lambda = 0.03$ to 0.1 are shown, which are all expected to show a pre-thermal behavior according to the previous analysis.

Assuming Eq. (77) a collapse of all data to a single curve is expected, however limited to the intermediate time regime, where the plateau was observable in panel **b**. Upon setting the open constant in Eq. (77) to $a = 2.2$ an approximate collapse of the data traces can be observed around $tJ \sim \mathcal{O}(1)$.

Additionally, we quantify the numerically observed thermalization directly. For that a threshold value $\mathcal{C}_{\text{thresh}}$ is defined slightly higher than the thermal value, cf. panel **a**, below which the system is said to be thermal (black horizontal line in panel **c**). In the vicinity of $\mathcal{C}_{\text{thresh}}$ the correlator $\mathcal{C}(t)$ is fitted by an exponential

to reduce statistical noise (black dashed curves). Their crossing of the threshold $\mathcal{C}_{\text{thresh}}$ defines t_{th},

$$t_{\text{th}} = t\,|_{\mathcal{C}<\mathcal{C}_{\text{thresh}}}\,. \tag{78}$$

t_{th} is shown in the inset of Fig. 30 **d**. The theoretical prediction t^{a}_{th} (black line) is a reasonably good description of the simulated data across a wide range of parameters $\lambda, N_{\mathcal{B}}$. Deviations both in the imperfect collapse in panel **d** and in the scaling analysis is the inset may be explained by logarithmic corrections, according to Eq. (57), which are impossible to resolve in detail in exact numerics. Additionally, the different regimes of the wave function moments observed by Monteiro *et al.*, 2021a and in a related model in the previous chapter may affect the scaling of the thermalization time close to the transition; it is conceivable that different regimes of distinct scaling emerge in the finite time dyanmics which correspond to the parameter regions II/III in Monteiro *et al.*, 2021a and chapter 7. To resolve these details an energy-resolved study of Eq. (70) may be in order. The analytical form of t_{th} and its numerical verification is the second main result of this chapter.

Recent studies cited a Thouless time scale in system such as the one studied in this chapter; it is defined as the time at which the dynamics of a many-body system approaches universal behavior and loses memory of its initial conditions (Schiulaz *et al.*, 2019). It is conceivable that the observed thermalization time can be interpreted in this context. t_{th} approaches t_{H} when the interaction strength λ becomes almost critical at finite $N_{\mathcal{B}}$. A similar observation has been made in disordered spin chain models, where strong disorder prohibits thermalization, cf. Schiulaz *et al.*, 2019. The role of disorder is taken by the relative interaction strength λ in the present study.

8.2.2 *Wave function propagation in Fock space*

The Fock space of many-body models can be interpreted as high-dimensional graphs where Fock space sites are the nodes and the connections are mediated by Hamiltonian matrix elements in a fixed basis. Typically the connectivity is highly complex, in particular when the model has a high degree of (spatial) structure. There is a variety of works which attempt at modeling many-body properties, e.g. localization transitions, in simplified graph models of Fock space, cf. section 6.2 and Tikhonov and Mirlin, 2021b. The model (70) connects the two extremes on some level; the Fock space connectivity is much more complex than in simple random regular graphs (Tikhonov and Mirlin, 2021b), while its general structure is still relatively simple compared to e.g. disordered spin chains. While a fully analytic time-dependent study is beyond the reach of the available method, it is possible to understand the dynamics of the extended SYK model better by analyzing its wave functions propagating through Fock space.

In the ergodic regime of Eq. (70) the wave functions are expected to eventually distribute over the entire volume of the Fock space uniformly; while on the integrable side of the transition finite support only on a smaller fraction is expected, which is not scaling with the lattice size.

Computationally, we consider the time evolution of initial states which are fully localized on a single Fock space site in occupation number basis, i.e.

$$\psi(t) = e^{-itH}\psi_0 = e^{-itH}\,|0,0,0,\ldots,1,1,1\ldots\rangle\,, \tag{79}$$

at half filling. The choice of the initial basis state is not relevant since all Fock space basis states are equivalent up to disorder fluctuations. Here the Fock space is structured according to the local occupations of the sites $i = 1,\ldots,N_{\mathcal{B}}$; the basis states are denoted

$$\psi_a = |n_1^a, n_2^a, \ldots, n_{N_{\mathcal{B}}}^a\rangle\,, \tag{80}$$

where $n_i^a = 0,1$ are fermionic occupations. Structure of propagating wave function can hence be quantified by the distance[4] between two basis states contributing to a time evolved wave function,

$$d_H(\psi_a,\psi_b) = \frac{1}{2}\sum_{i=1}^{N_{\mathcal{B}}} |\, n_i^a - n_i^b \,|, \tag{81}$$

with maximum length $d_H^{max} = N_{\mathcal{B}}/2$.

For the remainder of this section an important quantity is the probability to find a many-body wave function at a certain "distance" d away from the initial state. It can be defined as

$$\mathcal{P}_d(t) = \sum_{\psi_a,\ \text{for}\ d_H(\psi_a,\psi_0)=d} |\,\langle\psi(t)\,|\,\psi_a\rangle\,|^2\,. \tag{82}$$

When starting with a wave function localized at a single Fock space site, $d = 0$, the probabilities for different distances d from that basis site are governed mainly by the available Fock space sites at these distances; for instance the Fock space volume of sites with a distance $d = N_{\mathcal{B}}/4$ is always much larger than at $d = 1$. As this effect obscures possible alterations due to the relative interaction strength λ, the probability densities as a function of d are normalized by the respective Fock space volumes, which can be determined combinatorically,

$$\mathcal{P}_d^{th} = \frac{1}{\mathcal{N}_{th}}\binom{N_{\mathcal{B}}-n}{d}\cdot\binom{n}{n-d}, \tag{83}$$

4 The defined distance d_H is not necessarily quantifying the shortest possible path in the Fock space lattice. For the purpose of this study it is sufficient to measure propagation through Fock space using d_H. The connectivity of the Fock space graph is scaling with the system size $N_{\mathcal{B}}$ due to the SYK interaction.

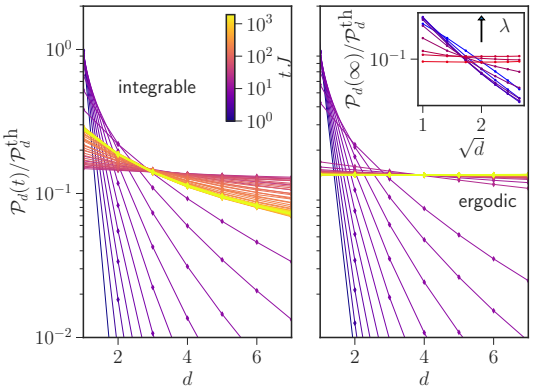

Figure 31: Normalized probability density as a function of the Fock space distance to the fully localized initial state for different times (color scale) for the non-interacting (left) and fully interacting (right) limits. The yellow curves and the inset represent the infinite time extrapolation of the probability distribution; the color scale in the inset encode the varying interaction strength λ, increasing from blue to red. The system size is $N_{\mathcal{B}} = 16$. Adapted from Dieplinger *et al.*, 2021, ©2023 American Physical Society.

for filling factor $n_{\mathrm{fill}} = n/N_{\mathcal{B}}$ and normalization constant

$$\mathcal{N}_{\mathrm{th}} = 2^{N_{\mathcal{B}}}\Gamma(N_{\mathcal{B}} + 1/2)/\sqrt{\pi}\Gamma(N_{\mathcal{B}} + 2/2), \tag{84}$$

at half filling. This distribution also corresponds to the equilibrium distribution at which a wave function is uniformly occupying the entire Fock space lattice.

Fig. 31 shows the normalized time-dependent distribution functions $\mathcal{P}_d(t)/\mathcal{P}_d^{\mathrm{th}}$ as a function of time t in the two limits $\lambda = 0, 1$ for the same time range as shown in Fig. 30. Initially in both cases the probability broadens from a localized peak at $t = 0$ and eventually reaches to all distances d. However, a clear distinction is offered by the late time behavior: While in the integrable case the distribution always retains some imbalance towards small distances, in the ergodic case it eventually becomes flat and uniform. This means that using the distance defined in Fock space the non-interacting limit is not only integrable but one can even associate a notion of "localization" in Fock space, while the ergodic limit trivially is delocalized. For the first time in this work the ergodic-integrable transition studied in these many-body models can actually be associated with a (finite-size) localization-delocalization transition. This offers an important puzzle piece to bridge our results to the problem of actual many-body localization. Fock space localization has been diagnosed similarly by Creed *et al.*, 2023 in a disordered spin chain; the authors investigated – similar to the study presented here – probability transport as a function of the Fock space distance for many-body wave functions subject to a disordered spin Hamiltonian. They, too, observed homogeneity of the probability distribution in the long time limit on the ergodic, and a residual imbalance on the integrable side of the transition. The inset of Fig. 31 extends the analysis of the long time limit to finite interaction strengths λ. The distributions

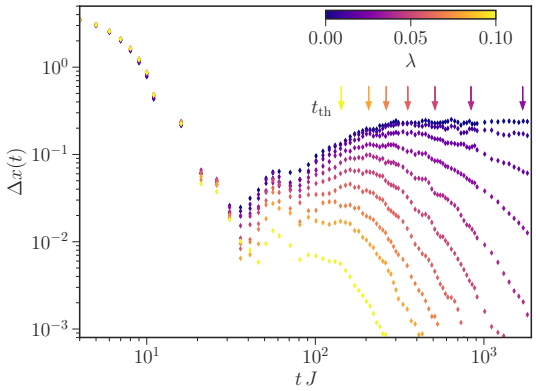

Figure 32: The first moment of the probability distribution $\mathcal{P}_d$ as a function of time t, according to Eq. (86). The interaction strength is varied analogously to Fig. 30; the curves resemble qualitatively the density-density correlations. The arrows indicate the respective thermalization time $t_{th}(\lambda)$, shown in Fig. 30 **d** in the inset. The system size is $N_{\mathcal{B}} = 18$. Adapted from Dieplinger and Bera, 2023, ©2023 American Physical Society.

are calculated by a exact time evolution to a time $t \gg t_H$. The localized character of the distribution functions as a function of the distance to the initial basis state d appears to be a stretched exponential with

$$\mathcal{P}_d(t \to \infty) \sim e^{-\sqrt{d/\xi}} \times \mathcal{P}_d^{\mathrm{th}}, \tag{85}$$

with ξ defining a localization length in Fock space using the distance d_H. Interestingly, all data sets belonging to the localized side of the transition collapse to the same stretched exponential with identical localization length ξ, while the ergodic regime collapses to a uniform flat distribution as expected.

FINITE TIME PROPAGATION OF FOCK SPACE WAVE FUNCTIONS. Next we define the first moment of the distribution $\mathcal{P}_d$ to quantify the finite time behavior of the wave function propagation, starting from a fully localized initial state,

$$\Delta x(t) = \sum_d \left[\mathcal{P}_d(t)\, d\right] - \frac{4}{N_{\mathcal{B}}}, \tag{86}$$

the term $4/N_{\mathcal{B}}$ referring to the equilibrium distribution $\mathcal{P}_d^{\mathrm{th}}$.

$\Delta x(t)$ is calculated for increasing interaction strengths λ, cf. Fig. 32, for the same parameter range and time window as in the calculation of the density correlations in Fig. 30 **b**. First a – for quantum chaotic many-body systems universally expected – initial decay of the form $\Delta x(t) \sim e^{-\Gamma^2 t^2}$ (Schiulaz *et al.*, 2019) is observed. Here Γ is related to the depletion time of the initial state. For intermediate times the trajectories of $\Delta x(t)$ strongly depend on the interaction strength; a power-law decay presumably governs the large-λ simulations while in

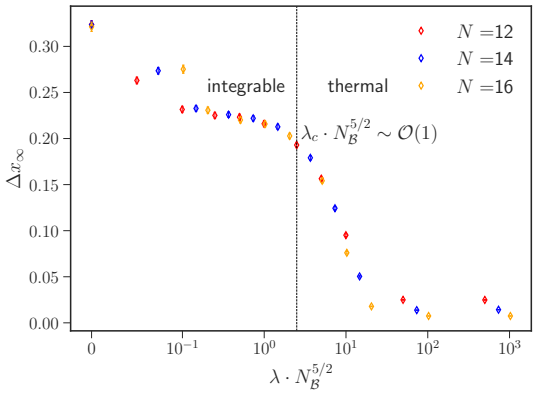

Figure 33: Long time limit $\Delta x(t \to \infty)$ as a function of the rescaled interaction strength $\lambda \times N_{\mathcal{B}}^{5/2}$. The curves intersect approximately at the vertical line, separating the integrable (localized) from the ergodic (delocalized) regime. Adapted from Dieplinger and Bera, 2023, ©2023 American Physical Society.

the vicinity of the transition at λ_c again plateaus of a similar shape as in the density correlations emerges. The thermalization time at which we observed the eventual decay of the density correlations to the thermal limit are marked in colored arrows, depending on the interaction strength λ. The overall qualitative shape of $\Delta x(t)$ is very similar to Fig. 30, suggesting that the Fock space structure, quantified by the distance d_H, has a very direct impact on the correlation functions of the model. A similar observation was made by Creed *et al.*, 2023. They showed that the combination of this metric with the first moment of the probability distribution $\mathcal{P}_d$ can be related rigorously to two-point correlations, such as density-density correlators, in disordered spin chains.

Finally, to validate this measure we calculate the long time limit of $\Delta x(t)$ as a function of the interaction strength λ and find the critical λ_c for given $N_{\mathcal{B}}$ at which the transition from ergodic to localized behavior occurs. Fig. 33 shows $\Delta x_\infty = \Delta x(t \to \infty)$, calculated using exact time evolution to $t \gg t_H$, as a function of the interaction strength λ, which has been rescaled to account for the finite-size scaling of the critical λ_c, cf. (57). Clearly, the average of the distribution Δx changes from zero, indicating uniform distribution, in the ergodic regime at large λ to a finite imbalance of the distribution towards the initial state – reminiscent of the Fock space localization with respect to the metric d_H – at small λ. Curves for different system sizes cross at $\lambda \cdot N^{5/2} \sim \mathcal{O}(1)$, as expected by Monteiro *et al.*, 2021a; Tikhonov and Mirlin, 2021b.

Coming back to the very introduction of the second part of this thesis the observed scaling of λ_c with the number of basis sites matches the prediction obtained from random regular graphs (RRG). Herre *et al.*, 2023 recently observed a critical disorder strength in RRG calculations scaling as $W_c^{RRG} \sim N_{\mathcal{B}}^4 \ln N_{\mathcal{B}}$. It is possible to connect the RRG critical point to the critical interaction strength of our model, i.e. the modified SYK Hamiltonian, such that $W_c \propto \lambda_c^{-1} N_B^{3/2}$, where the different normalization of the Hamiltonian conventions account for the factor

$N_{\mathcal{B}}^{3/2}$. Also quantitatively the numerical values of the transition points for given $N_{\mathcal{B}}$ are consistent (Herre *et al.*, 2023; Dieplinger and Bera, 2023).

8.3 Conclusion: emergence of a cross-over time scale close to the finite-size ergodic-integrable transition

Summarizing the results of this chapter, an interesting dynamical phase diagram of the modified SYK model Eq. (70) has been found, most prominently featuring a finite-size transition between an integrable, Fock space localized and an ergodic regime. In the latter a cross-over time scale was found, which separates finite time pre-thermal behavior from the thermodynamic ergodic limit, cf. Fig. 29. The long time limit of our observables, the density-density correlations as well as Fock space wave function propagation, is consistent with previous studies which found an analytical expression for the finite-size transition between the two infinite-time regimes.

Interestingly, we have been able to associate actual localization of the wave function propagation in time with the integrable regime, bridging the SYK literature further towards many-body localization problems in the more conventional sense. This localization, however, must not be understood in real space, but in Fock space, using the metric defined by d_H, inspired by the Hamming distance between occupation numbers in real space orbitals. Actual real space localization presumably requires a spatially local disorder potential ("mass disorder") instead of non-local random all-to-all hoppings as studied here.[5] The analytical form of the Fock space localization observed here is dominated by a stretched exponential.

The big question to begin with in the present chapter was how to understand the dynamics of observables in strongly disordered many-body models; potentially close to a MBL transition. Here we have studied a toy model of such a system and focused on the dynamics of the ergodic side of such a (finite-size) transition. How does the specific fingerprint of the pre-thermal behavior of our minimal model compare to the slow-thermalization behavior found in more common models of many-body localization, for instance in Weiner *et al.*, 2019; Evers *et al.*, 2023; Bera *et al.*, 2015; Luitz and Lev, 2017; Doggen *et al.*, 2021? In fact the slow thermalization behavior of short range spin models does not show signs of pre-thermalization; the decay of observables such as the imbalance of charge densities proceeds with power-laws with decreasing exponents. No cross-over time scale can be observed (Schiulaz *et al.*, 2019; Creed *et al.*, 2023; Torres-Herrera and Santos, 2015).

However, a possible and very interesting candidate for showing such pre-thermal plateaus also in more realistic models of many-body localization are long-range models with a decaying interaction of the form $\sim 1/r^{\alpha}$; r representing

5 It is an open question how the lack of energy level correlations in a mass-disordered SYK Hamiltonian compared to the single-particle spectrum of $\mathcal{H}_{SYK_2}$ influences the many-body properties. It is believed that the effect is not qualitative (Monteiro *et al.*, 2021a).

a real space distance between interacting electrons. These types of models do exhibit some aspects of the (infinite range) modified SYK model; a finite-size localization transition occurs, scaling similarly, namely as $W_c \sim N_{\mathcal{B}}^{2d-\alpha} \ln N_{\mathcal{B}}$ for dimension $d < \alpha < 2d$ (Burin, 2015b; Gutman *et al.*, 2016; Tikhonov and Mirlin, 2018; Nag and Garg, 2019; De Tomasi, 2019; Roy and Logan, 2019; Thomson and Schiró, 2020; Deng *et al.*, 2020). The scaling very much resembles the modified SYK model studied here and e.g. by Monteiro *et al.*, 2021a; Tikhonov and Mirlin, 2021b. It is therefore conceivable that a pre-thermal behavior could be observed in long-range spin chains, warranting future studies.

9

CONCLUSION

This thesis is devoted to localization phenomena in ensembles of disordered Hamiltonians. In the absence of electron-electron interactions, namely in a single-particle picture, wave functions of disordered systems generically Anderson localize in two dimensions. A systematic way to protect systems against becoming pure Anderson insulators is offered by topology and the bulk-boundary principle. The most famous incarnation of this concept is the integer quantum Hall effect, where edge states form at the boundaries of an insulating sample and carry quantized current. The critical theory of transitions between quantum Hall plateaus of different conductivity is still unknown. In the first part of this thesis some properties of the quantum Hall plateau transitions have been explored, in different microscopic realizations.

UNIVERSALITY OF QUANTUM HALL CRITICALITY. Recent studies, such as Gruzberg *et al.*, 2017; Zirnbauer, 2019; Sbierski *et al.*, 2021 or Dresselhaus *et al.*, 2021 suggested that the critical exponents of the quantum Hall plateau transition either diverge, rendering the critical theory marginal, or that they are non-universal suggesting a second fixed point or even a critical line in renormalization group flow (cf. e.g Sbierski *et al.*, 2021). In particular geometric disorder, by distorting a regular lattice, or Dirac fermions have been suggested as candidate systems where the quantum Hall critical exponents show non-universality with respect to more conventional models, such as the Chalker-Coddington network, where most high-performance simulations have been carried out.

Two high-precision studies – the first examining finite energy critical properties as a function of energy in a disordered Chern insulator; the second an amorphous realization of the anomalous quantum Hall effect – have been presented in this thesis. Both establish that the critical exponents, in particular those connected with the divergence of the localization length, are fully consistent with universality within class A. The numerical values of the exponents ν agree well with previous results on more conventional models of the quantum Hall effect. In the case of the disordered Chern insulator on a square lattice, the functional dependence of the localization length markers investigated even collapse for different energies together with a fully different microscopic realization built on Landau levels, cf. chapter 4. Additionally, multifractal properties of the critical point in the amorphous realization of the quantum Hall effect have been studied.

The anomalous dimension has been found to be consistent with previous studies on the Chalker-Coddington network models, showing small but finite quartic corrections. This result offers evidence against the parabolic scaling paradigm proposed by Zirnbauer, 2019. Furthermore, numerical values of the (quartic) corrections agree across different microscopic models, once again suggesting consistency with universality within class A. As in all numerical finite-size studies in the quantum Hall realm, a caveat in the presented investigations are the sizable and slowly decaying finite-size corrections. It is very difficult to exclude transient observations which may still differ in the true asymptotic limit. In general, the studies presented in chapter 4 will hopefully help in establishing narrow conditions for possible candidate theories of the quantum Hall plateau transition.

UBIQUITOUS APPEARANCE OF QUANTUM HALL STATES BEYOND CLASS A. Usually, quantum Hall criticality is observed only upon fine-tuning a physical system to the quantum Hall plateau transition, for instance the energy, the electronic density or the magnetic field. The quantum Hall critical fixed point is unstable, which is why the interest in the critical properties derives mainly from academic curiosity and a theoretical perspective.

Recently however, Sbierski *et al.*, 2020 have discovered a relatively stable regime of quantum Hall critical states, extended over the entire surface spectrum of a class AIII topological insulator in three dimensions. This is striking for two reasons: First, states at finite energy which break the AIII underlying (chiral) symmetry explicitly are usually expected to generically fall into the quantum Hall insulating phase, but they apparently do not. Second, this offers an escape from the notorious difficulty of accessing (unstable) quantum Hall critical states: No fine-tuning to specific system parameters seems to be needed – all states in a broad range of energies are critical.

In collaboration with analytical theory by A. Altland, P. Brouwer, M. Moreno-Gonzalez, M. Foster and L. Trifunovic a systematic approach to the emergence of spectrum-wide criticality on surfaces of topological insulators has been attempted, cf. chapter 5 and Altland *et al.*, 2024.

We have succeeded in finding simple criteria, which depend on the underlying fundamental symmetries in the ten-fold way, when finite energy (i.e. low-symmetry) wave functions are protected against localization and spectrum-wide criticality can emerge; or – on the contrary – when only the high-symmetry point in the spectrum (i.e. zero energy) is delocalized. In particular, for the class AIII topological insulator a symmetry conserving surface potential term is found which can open a gap between bulk and surface spectra of the full three-dimensional system and thereby localize the surface spectrum. The underlying argument is connected to the principle of spectral flow between surface and bulk states, which can be interrupted by this fragmenting surface potential. This bridges back to Laughlin's gauge argument for the quantization of the Hall conductivity, again closing the circle to the ubiquitous quantum Hall

effect. Additionally, we have been able to generalize the underlying argument to all non-Wigner-Dyson symmetry classes in the ten-fold classification, adding information about the "localizability" of surface and bulk spectra depending on the symmetry and the spatial dimension, cf. table 3.

An important consequence of this work is that the popular minimal Dirac Hamiltonians, employed to model the two-dimensional surface states of a three-dimensional topological insulators suffer serious shortcomings: They do not contain information about the surface band structure in the vicinity of the bulk spectrum, which is – as seen in chapter 5 – important for assessing the validity of the spectral flow principle. Therefore minimal Dirac models cannot capture the possibly finite Berry curvature of surface states, which leads to non-zero surface Chern numbers in the case of a detached surface spectrum. Thus the localization physics emerging, when a corresponding fragmenting surface potential is present, is fully missed. Consequently, these types of models cannot even reliably reproduce the most basic of all properties of disordered wave functions – namely whether they are extended and conducting or localized and insulating (Altland *et al.*, 2024).

THERMALIZATION VS. "QUANTUM MEMORY". Generically, low-dimensional non-interacting quantum systems localize in the presence of disorder. In the first part of this thesis as well as in literature one overarching question is how to escape this omnipresent emergence of Anderson insulators.

In the second part of the thesis – in the presence of strong interactions – the relationship of localized and extended systems is reversed to some extent: electronic interactions induce decoherence among quantum mechanical paths of scattering electrons. Consequently, the mechanism found by Anderson looses its rigour, localization breaks down and wave functions may extend over the entire Hilbert space. For experiments, many-body wave functions time-evolving to a fully extended state typically look thermal, since usually only local observables are probed, while the information about the initial state remains hidden in global properties. The following questions hence have been posed: How can an interacting quantum system escape thermalization? How can it stabilize localized wave functions even in the presence of decoherence?

Apart from theoretical and experimental interest, localized many-body wave functions could be relevant for quantum computing, since they potentially "remember" their initial state forever, instead of hiding it in global degrees of freedom, rendering them inaccessible for (local) read-out procedures. As such many-body localized phases may serve as candidate systems to realize a quantum memory (Nandkishore and Huse, 2015). Some other candidate systems which do evade thermalization, such as integrable Hamiltonians, suffer the shortcoming that they require fine-tuning of its parameters, and even small perturbations may render them thermalizing again. In contrast, many-body localization would offer a more generic path to a "quantum memory".

MINIMALLY MODELING MANY-BODY LOCALIZATION. Unfortunately, the huge Hilbert space of many-body interacting quantum systems and their highly correlated matrix elements make it very hard to reliably assess the localization properties of wave functions for realistic systems both analytically and numerically. Therefore, in the second part of this thesis we have chosen to follow a different path inspired by Monteiro *et al.*, 2021a: As a starting point we use a (microscopically non-realistic) toy model, based on the Sachdev-Ye-Kitaev Hamiltonian, where a finite-size localization transition and interesting accompanying ergodic regimes have been found even analytically. Compared to more conventional models, e.g. disordered spin chains, simplifications such as the structureless interaction Hamiltonian have made this possible (Monteiro *et al.*, 2021a).

The numerical study presented in chapter 7 extends this work by reintroducing some structure present in microscopically realistic electronic Hamiltonians, in particular, the density-density form of electron interaction, reminiscent of real-space Coulomb repulsion. Interestingly, the different delocalized regimes, where wave functions have spread ergodically only on a subset of the Fock space, compare quantitatively to the original SYK-based model. Additionally, dual regimes close to a second finite-size localization transition in the strongly interacting limit have been revealed, which can be described on the same footing. After all, two important messages can be derived from this investigation: First, it is possible to come closer to microscopic realism by giving up on some of the analytical tractability. Still much of the physical properties remains present even on a quantitative level. In fact, also newly emerging regimes can be described using the original, simple SYK-based toy model. Related to that, secondly, the observation that as complex properties as the wave function scaling close to the finite-size transition survive as drastic alterations of the SYK model as reducing the interaction structure to a density-density form (Dieplinger *et al.*, 2021) is highly interesting. It can be hoped that this extends also to different properties of the SYK model for instance its low temperature characteristics where the holographic duality to gravity theory emerges. At the moment it remains an open question whether this stability of SYK characteristics survives even stronger alterations of its microscopic definition, for instance introducing a spatial structure and a finite (but possibly long) range of the interaction kernel.

EMERGENCE OF PRE-THERMAL BEHAVIOR BEFORE EVENTUAL THERMALIZATION. In the previous study of the minimal ergodic-integrable transition only statistical properties of the spectrum and eigenstates have been analyzed so far, corresponding to a long-time limit of time evolution. However, in experiments physicists often have access to finite-time properties of a given Hamiltonian, for instance in cold atom experiments, which realize disordered spin or fermion chains in the context of many-body localization[1].

1 There, often an imbalance of charges between two spatial regions in a sample system is monitored when time-evolving a localized initial state, cf. Schreiber *et al.*, 2015; Lüschen *et al.*, 2017.

Chapter 8 has studied dynamical properties of such a minimal model, a close relative of the deformed SYK Hamiltonian of Monteiro *et al.*, 2021a. In previous numerical studies on short-range interacting systems, for instance disordered spin-chains, a slowing-down of thermalization over a long time window has been observed when disorder is increased to values potentially close to the many-body localization transition[2], e.g. the real space charge imbalance following a slow power-law decay. In our study, however, we observe a qualitatively different behavior: Even in the thermal phase, where eventually information about initial states, like charge imbalance, is lost, the system looks non-thermal for a long time. Specifically, (local) information about the initial state is present while time evolving, while at a certain thermalization time scale, its temporal behavior crosses over to its actual long-time lime, i.e. equilibrates, leading to a complete loss of memory of the system's initial state.

In chapter 8 we have been able to quantitatively associate a time scale with this cross-over during time evolution, cf. Fig. 29 for a dynamical phase diagram. This means that even on the ergodic side of the finite-size ergodic-integrable transition remnants of localization can be observed, for a long (but finite) time window. Circling back to the concept of "quantum memory" this could be interesting for quantum computing as well; since the time scale at which the system thermalizes is potentially exponentially large, there is a huge time window where information about its initial state is stored, before it is eventually lost. Even if it turns out that the localization transition does not exist at all for large disorder strengths, or like in the model studied here, it is only present for finite sizes and the localized phase vanishes in the thermodynamic limit, this could be useful.

It is known that a relatively sharp cross-over from pre-thermal to thermal behavior as observed here does not exist for short-range spin chain models. Instead, a uniform decrease of key localization signatures has been reported. However, it would be highly interesting if we were able to observe a pre-thermal plateau in long-range spin or fermion chains, which could be related more closely to the deformed SYK model studied in this thesis.

OUTLOOK AND CLOSING REMARKS. Many future paths of research extending the understanding both of topological materials as well as thermalization and its break-down, its appearance in better-controlled toy models and potential applications have already been discussed. This thesis started out with an attempt to interconnect several subfields of condensed matter physics with each other on a theory level. The concept of an effective theory was elaborated upon in the introduction. Here it originated from a topological interpretation of single-particle models of disordered materials, or by the categorization of generic many-body interacting systems in thermalizing – where qualitatively different and interesting regimes emerged – and non-thermalizing, e.g. many-body localizing.

2 Still, at this point there is no consensus on the existence of such a transition in the strict sense for large disorder due to analytical and numerical difficulties, cf. Evers *et al.*, 2023.

While some bridges to even further subfields of theoretical physics have been hinted at – thermalizing quantum systems can be naturally related to the field of quantum chaos, for instance in recent literature on the Sachdev-Ye-Kitaev model (Maldacena *et al.*, 2016a; Maldacena and Stanford, 2016) – some obvious questions remain open: To date, for instance, it is very challenging to find a way to classify disordered Hamiltonian ensembles analogously to the ten-fold way for single-particle models whenever interactions are present. If possible such an extension could offer a more natural connection between the research areas *topology/localization* and *many-body ergodicity/localization*, corresponding to part I and II of this thesis, respectively.

A promising potential intermediary step between the two topics could be disordered Hamiltonian ensembles emerging from self-consistent mean-field theories: They include electronic interactions but keep a form which is beneficial for classification along the lines established in single-particle Anderson localization. This route has already been hinted at by Stosiek, 2020.

"More is different."
– P. W. Anderson

The perspective adopted by this thesis emphasizes the need for a theory capable to break down many degrees of freedom into an effective theory with only a handful of important tuning parameters. Anderson's paper *More is different* expresses a similar idea from a slightly different angle. While the fundamental laws which govern physics and other sciences, namely the standard model of elementary particles, remain the same, this does not mean that all higher-level phenomena become their direct corollaries. On the contrary, Anderson highlights that dealing with several, many or even infinitely many of the same degrees of freedom, which are individually understood in the most fundamental theories of physics, opens the door to an entirely new world of phenomena hosting qualitatively different physical effects (Anderson, 1972).

While Anderson's statement probably applies to all natural and even social sciences, in this thesis we have seen some interesting examples within condensed matter theory. For instance, in the first part we observed topological protection against Anderson localization emerging from the multitude of fermionic degrees of freedom in a topological insulator; in the second part we studied many-body localization phenomena coming from microscopic degrees of freedom of the studied toy models. Both phenomena have emerged in systems whose fundamental laws are the same: Particles moving and interacting according to the Schrödinger equation of quantum mechanics – the same idea as in any other (quantum) condensed matter problem we can imagine.

The huge difference between these problems cannot be explained by different microscopic origins. On the contrary, because of subtle variations in relevant energy, length or time scales, the multitude of the same microscopic constituents

leads to a large variety of emergent phenomena. Therefore, while this thesis focused on localization, criticality and ergodicity, other observable effects could span from viscous electron flow to emergent relativistic effects to unconventional superconductivity.

Part III

APPENDIX

A

SUPPORTING NUMERICAL DATA

A.1 DISORDERED CHERN INSULATOR ON A SQUARE LATTICE

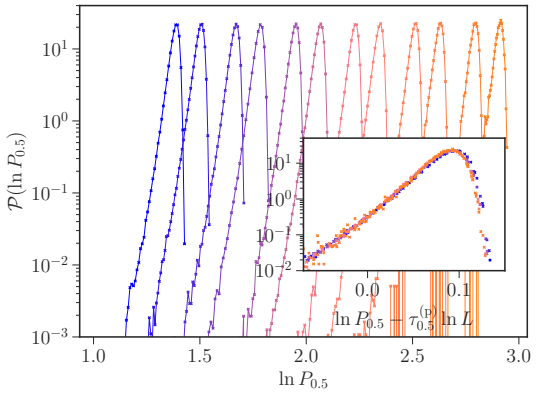

Figure 34: Full distribution functions of wave function moments $\mathcal{P}(\ln P_q)$ at $q = 0.5$ at the critical point of the Chern insulator $(E_c, W_c, R_c) = (0.59, 1.45, 1.2)$, corresponding to the critical point in Fig. 6 **a**. The colors encode increasing system sizes from blue to orange, $L = 16, 24, 32, 48, 64, 96, 128, 192, 256, 384, 512, 768, 1024$. Inset: logarithmic plot rescaled by the parabolic prediction for the multifractal dimension by Zirnbauer. Adapted from Moreno-Gonzalez *et al.*, 2023, ©2023 Elsevier.

In Fig. 34 the distribution functions of the wave function moments $P_{q=0.5}$ are shown for increasing system sizes. The parameter set shown belongs to the green arrow, pointing at the maximum of the multifractal dimension shown in the main text chapter in Fig. 6 **a**. The shape of the distribution functions becomes almost invariant for large system sizes, indicating criticality. In the inset the horizontal axis is rescaled by the theoretical scaling exponent predicted by Zirnbauer, $\tau_q^{(p)}$. The shape as well as the mean of the distributions collapse approximately. The residual differences can be explained by possible corrections to Zirnbauer's parabolic prediction for τ_q and by additional non-zero finite-size scaling corrections. Both are analyzed for the disordered Chern insulator on a square lattice in the main text in chapter 4.

Distribution functions of wave function moments with and without fragmenting surface potential

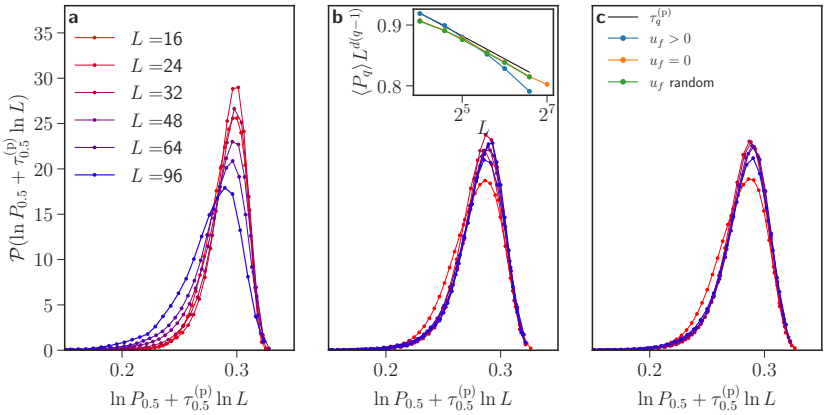

Figure 35: Distribution function of wave function moments for the cases shown in Fig. 22, at $E = 0.2, M = 2$ with fragmenting potential $u_f = 0.3$, $W_\phi = 0.1$ (**a**) $u_f = 0$, $W_\phi = 0.15$ (**b**) and zero mean and standard deviation 0.3, $W_\phi = 0.15$ (**c**). The moments have been rescaled with the parabolic prediction for the multifractal dimension $\tau_q^{(p)}$. (inset) Scaling of the mean wave function moment $\langle P_q \rangle$ with the system size, compared to the parabolic prediction (black). Adapted from Altland *et al.*, 2024, ©2024 American Physical Society.

A more direct diagnostic of quantum Hall criticality compared to the effective multifractal dimension, Eq. (22), are the distributions of the wave function moments P_q directly; they are shown in Fig. 35, the panels **a,b,c** corresponding to the data in Fig. 22 with constant, zero and random fragmenting potential u_f. The energy is chosen to be $E = 0.2$. The horizontal axes are rescaled with the parabolic prediction for $\tau_q \approx \tau_q^{(p)}$, such that for quantum Hall critical states an approximate collapse should be observed (up to finite-size and quartic corrections to $\tau_q^{(p)}$).

In panel **b** the scenario of spectrum-wide criticality as in the first section of chapter 5 can be identified; when no fragmenting potential is present spectral flow survives and surface states are quantum Hall critical even at finite energies. When $u_f \neq 0$, as in panel **a**, quantum Hall criticality breaks down; the data does not collapse to a master curve and the distribution functions are not scale-invariant for increasing system sizes. The effective "flow" with system size becomes gradually slower hinting at eventual localization with $\tau_q|_{q>0} = 0$.

When a fragmenting potential is present but distributed randomly around zero, the picture resembles the $u_f = 0$ case again, cf. panel **c**: Chiral domain wall states percolate through the entire surface and generate critically delocalized states, as explained in the main text.

The inset of Fig. 35 shows the mean $\langle P_q \rangle$ with subtracted metallic scaling, to enhance visibility: The trend observed in the shape of the distribution functions is corroborated; the green and yellow data corresponding to zero fragmenting potential and zero mean fragmenting potential eventually closely follow the theoretical curve for quantum Hall criticality (black) while the blue data shows a clear curvature away from the quantum Hall critical fingerprint, corresponding to a non-zero mean of the fragmenting potential.

Uncorrelated phase disorder model

In the main text the simulations on the AIII topological insulator with disorder and fragmenting potential, chapter 5, in particular for Fig. 22 and 35, have assumed correlated disorder of strength W_ϕ and a small short-range correlation length $\xi_\phi = 1$. Both localization – in case of non-zero mean fragmenting potential – and criticality of finite energy surface states have been resolved well. Alternatively, it is possible to choose zero correlation length, i.e. uncorrelated Gaussian disorder for the phases, Eq. (46). The data corresponding to such a setting is published in Altland *et al.*, 2024 and shows the same qualitative trends, depending on the nature of the fragmenting potential u_f as presented in the main text and the previous section. Details in the convergence are however slightly different: The localization length presumably is shorter, the effective exponent $\tilde{\tau}_q$ approaches zero faster (for $q > 0$); and the distributions, analogously to Fig. 35 differ more strongly for the shown system sizes. At the same time, however, in particular the case with random fragmenting potential u_f shown in green in Fig. 22 and in panel **c** of Fig. 35 converges more slowly than in the correlated case shown in this thesis; it seems the additional finite-size scaling corrections are more pronounced in this case. Qualitatively, the two data sets do agree; however some details, for instance prefactors of scaling corrections, may differ. This is not important at all for this thesis; the origin of these details may lie in the microscopics of the two disorder models and has no influence on the coarse-grained theory in the regime of large system sizes. For the complementary data, showing uncorrelated disorder models, the interested reader is referred to the original publication Altland *et al.*, 2024.

Convergence of slab thickness of three dimensional samples

To calculate wave function properties of the surface of the investigated topological insulator, full three-dimensional lattice simulations of the Hamiltonian Eq. (42) are necessary. To optimize the linear surface length, which we want to scale to maximally large sizes, an optimal geometry has to be found.

We here present evidence that calculations of surface properties converge very fast in the transverse direction of the three-dimensional slab, orthogonal to the surfaces. This is because the surface localization in the bulk gap is exponentially

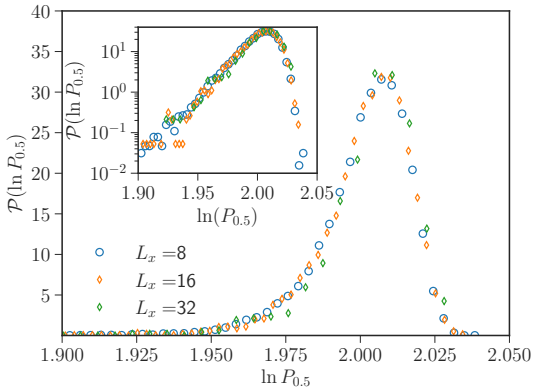

Figure 36: Convergence of the distribution function of the surface wave function moments P_q with the slab width L_x. The parameters are $E = 0.1$, $u_f = 0$, $W_A = 2.66$, $\xi_A = 1.1$, corresponding to the data shown in Fig. 20. Adapted from Altland *et al.*, 2024, ©2024 American Physical Society.

strong – even in the disordered case only very few layers of lattice points below the actual surface host significant wave function weight in the bulk gap.

An example parameter set with distribution functions when spectrum-wide criticality is present, corresponding to the simulations shown in Fig. 20 in the main text, is shown in Fig. 36 for different slab widths L_x (transverse to the surface). The distribution functions are shape-invariant and do not move when L_x is increased, indicating convergence of the surface wave function moments already at transverse slab thickness $L_x \geqslant 8$. Here and in all simulations presented in chapter 5 only surface states with $> 75\%$ surface weight are taken into account to avoid spurious effects due to low-lying in-gap bulk states (which exist due to disorder).

Due to the strong surface localization and fast convergence of the moments P_q with L_x all simulations are carried out at $L_x = 8$ to maximize the possible system sizes in the in-surface directions.

B

DETAILED INFORMATION ABOUT ENSEMBLE AVERAGES

part I, L	16	24	32	48	64	96	128	192	256	384	512	768
dis. Chern ins. $E = 0$	–	–	5700	2500	930	1050	490	200	56	56	30	16
dis. Chern ins. $E = 0.6$	–	–	1200	530	750	290	140	108	62	52	46	15
amorph. QH MFA	28000	11200	6050	2220	1030	318	146	187	259	159	109	14
amorph. QH transport	–	–	1500	1500	1250	750	500	500	315	225	190	45
AIII top. ins. vector pot.	21	12	4.5	9.4	3.6	1.8	1.1	–	–	–	–	–
AIII top. ins. phase dis.	100	81	39	16	6	1.2	0.3	–	–	–	–	–
part II, $N_{\mathcal{B}}$	10	12	14	16	18	20						
density int.	–	5	–	0.2	–	0.005						
dynamics deformed SYK	0.2	0.9	1.1	0.37	0.19	–						

Table 5: Ensembles information for different projects covered in this thesis in part I (top) and part II (bottom) for all shown system sizes $L, N_{\mathcal{B}}$, respectively. The numbers denotes the number of ensemble configurations calculated for each system sizes $\times 10^3$. Since in many problems more than a single disorder average have to be performed, the numbers only represent a reference value for a single parameter set (typically at a critical point).

Table 5 summarizes the numbers of configurations calculated for the sub-projects studied in this thesis. The columns correspond to system sizes $L, N_{\mathcal{B}}$, while the rows denote the different projects. The numbers correspond to a disorder average of a single parameter set, for example at a critical point of the disordered Chern insulator (E_c, W_c, R_c). Therefore, the numbers cited serve only as a guideline: In most calculations much more configurations have to be calculated in total to extract relevant information. In the disordered Chern insulator for instance it is necessary to collect data for parameter sets away from the critical point to gain access to the localization length exponent. The full information about all ensemble averages necessary for all data figures shown in the main text is not shown here; however, it is encoded in the errorbars of the data points which are propagated through every fitting or post-processing

procedure performed. The errorbars always represent one standard error of the mean for uncorrelated data sets.

C

DETAILS OF SUPPORTIVE NUMERICAL ALGORITHMS

RECURSIVE GREENS FUNCTION ALGORITHM (RGFA)

The full details of the RFGA method used for Fig. 8 and developed and applied by M. Puschmann are explained in the publication by Puschmann and Vojta, 2021. This section merely introduces the most important objects entering the method.

The recursive Green's function algorithm is a technique to calculate the Lyapunov exponent of a quasi-1d lattice of width L and length N with $N \gg L$, and by that investigate its localization properties. The time-independent Green's function is $\mathcal{G}(L; R, W) = \lim_{\eta\to 0} [(E + i\eta)\mathbb{1} - \mathcal{H}(R, W)]^{-1}$ with E, R, W being the system parameters of the disordered Chern insulator on a square lattice, Eq. (16). The lattice is constructed as a stack of layers. The Lyapunov exponent γ can then be represented by a single block of $\mathcal{G}$,

$$\gamma(L; E, R, W) = \lim_{N\to\infty} \frac{1}{2N} \ln | \mathcal{G}^N_{1N} |^2 . \tag{87}$$

Hence, it effectively measures the exponential decay of the wave function between the first and the last layer of the lattice of width L. $\mathcal{G}^N_{1N}, \gamma$ can be constructed recursively; for details the interested reader is referred to publications by Puschmann and Vojta, 2021; Huckestein, 1995; Huckestein and Kramer, 1990.

In the analysis of the localization length exponent, the dimensional Lyapunov exponent $\Gamma = L\langle\gamma\rangle_{ens}$ is considered, where $\langle\cdot\rangle_{ens}$ represents the ensemble average over disorder realizations. The data presented in the main text, cf. Fig. 8, was calculated for $N = 10^6$ taking into account 72 disorder realizations for system sizes between $L = 8 \to 256$. The RGFA calculations shown in Fig. 8 in the main text have been performed by and are presented with permission from M. Puschmann; they are based on the code developed by Puschmann and Vojta, 2021.

2-TERMINAL CONDUCTANCE CALCULATION

This section is a very short introduction to the calculation of the conductance shown in Fig. 13 and applied by S. Bera and N. P. Nayak. Its main goal is to define the objects appearing in the main text. For more details about the concrete calculation of the

conductance in chapter 4.4 the reader is referred to the original publication Bera et al., 2024; for a comprehensive review over transport coefficients in the context of scattering and transmission to Imry and Landauer, 1999.

LANDAUER CONDUCTANCE. In a two-terminal transport set-up two leads are connected to the sample, which is modeled by the tight binding Hamiltonian in the main text, cf. Eq. (35).

Plane-wave electronic states in the lead channels scatter with the sample region, represented by a scattering matrix S. The latter transforms incoming waves ψ^{in} to outgoing modes ψ^{out}, by

$$\psi^{out} = S\psi^{in}, \tag{88}$$

with

$$S = \begin{pmatrix} r & t' \\ t & r' \end{pmatrix}. \tag{89}$$

r, r' represent the reflection and t, t' the transmission matrices (from left to right, and right to left).

The differential conductance g can consequently be expressed as

$$g = \frac{e^2}{h} \mathrm{Tr}[t^\dagger t]. \tag{90}$$

The conductance g characterizes quantum Hall plateaus and hence can be adopted as an order parameter of the zero temperature quantum Hall plateau transitions appearing in the main text in chapter 4.4. The conductance g is calculated for a given set of parameters and system sizes using the python package `KWANT`, Groth *et al.*, 2014. The conductance calculations in the main text have been performed by S. Bera and N. P. Nayak; the data is presented with their permission.

FITTING MODEL OF CONDUCTANCE. The conductance g as a function of the system parameters and the linear sample size is modeled by a one-parameter scaling approach, similar to Eq. (28). Specifically, g is expanded as

$$g = \mathcal{F}_0(x) + b_0 L^{-y} \mathcal{F}_1(x) + c_0 L^{-2y} \mathcal{F}_2(x), \tag{91}$$

with $\mathcal{F}_j = \sum_{n=0}^{r} a_{jn} x^n$, and $x = (M - M_c)/M_c \cdot L^{1/\nu}$, where M_c is the position of the critical point, ν, y are the relevant and irrelevant scaling exponents and b_0, c_0, a_{jn} expansion coefficients. Note that in comparison to the scaling ansatz used in the analysis of the quantum Hall transition of the disordered Chern insulator on a square lattice, the subleading irrelevant contribution is assumed to scale with $2y$ instead of a second independent scaling exponent y'.

To corroborate numerical values of ν, y originating from this model, the fitting orders of the irrelevant expansion and the series expansion r are varied. A detailed analysis is presented in the original publication, Bera *et al.*, 2024.

In the main text we present a scaling collapse of the conductance across the transition, Fig. 13. To this end the conductance has to be corrected, because of its irrelevant scaling contributions, therefore,

$$g_{\text{corr.}} = g - b_0 L^{-y} \mathcal{F}_1(x) - c_0 L^{-2y} \mathcal{F}_2(x), \tag{92}$$

is defined.

KERNEL POLYNOMIAL METHOD (KPM)

A comprehensive overview of the kernel polynomial method and Chebyshev expansion is provided by Weiße et al., *2006 and Stosiek, 2020.*

The kernel polynomial method relies on the expansion of quantum mechanical operators, which are functions of the Hamiltonian, in polynomials of the latter. By that the matrix dimension of the computational problem can be reduced significantly, while only sparse matrix operations remain to be performed. Mostly Chebyshev polynomials are chosen as a polynomial basis, because of advantageous convergence properties and the existence of a simple recursion relation, cf. Stosiek, 2020; Weiße *et al.*, 2006; Bera *et al.*, 2017;

$$T_{k+1}(x) = 2xT_k(x) - T_{k-1}(x), \tag{93}$$

where the argument needs to be $-1 < x < 1$ and $T_0(x) = 1, T_1(x) = x$.

In particular relevant for this thesis, chapter 8, is the time evolution operator,

$$U(t) = e^{-it\mathcal{H}}, \tag{94}$$

for instance for a many-body Hamiltonian as in Eq. (70); it appears both in the density-density correlator and in the Fock space wave function propagation.

Expanded in terms of Chebyshev polynomials T_k, it reads

$$U(t) \approx e^{-ibt} \sum_{k=0}^{N_{\text{KPM}}} \mu_k T_k(\tilde{\mathcal{H}}), \tag{95}$$

with

$$\mu_k = (-i)^k J_k(at). \tag{96}$$

Here $\mathcal{H} = (\mathcal{H} - a)/b$ is the rescaled Hamiltonian where the parameters a, b derive from the maximum and minimal eigenvalues of $\mathcal{H}$; $a = (E_{\text{max}} - E_{\text{min}})/2, b =$

$(E_{max} + E_{min})/2$ and $J_k(x)$ are the kth Bessel functions. In simulations shown above, the number of Chebyshev moments $N_{KPM} > 2at$ to ensure convergence (Weiße *et al.*, 2006).

The original time evolution code which the calculations in the main text are based upon has been developed by S. Bera and has previously been employed in Bera *et al.*, 2017; Weiner *et al.*, 2019, where further details about the numerical implementations as well as convergence benchmarks can be obtained. It has been adjusted and further developed to be applicable to the problem studied in chapter 8 by the author of the thesis.

BIBLIOGRAPHY

Abanin, D. A., E. Altman, I. Bloch, and M. Serbyn, *Colloquium: Many-body localization, thermalization, and entanglement*, Reviews of Modern Physics **91**, 021001 (2019).

Abrahams, E., P. W. Anderson, D. C. Licciardello, and T. V. Ramakrishnan, *Scaling theory of localization: Absence of quantum diffusion in two dimensions*, Physical Review Letters **42**, 673 (1979).

Agarwal, K., E. Altman, E. Demler, S. Gopalakrishnan, D. A. Huse, and M. Knap, *Rare-region effects and dynamics near the many-body localization transition*, Annalen der Physik **529**, 1600326 (2017).

Agarwala, A. and V. B. Shenoy, *Topological Insulators in Amorphous Systems*, Physical Review Letters **118**, 236402 (2017).

Akhmerov, A., J. Sau, B. van Heck, S. Rubbert, R. Skolasiński, B. Nijholt, I. Muhammad, and T. Rosdahl, *Online course on topology in condensed matter*, topocondmat.org , (2021).

Altland, A., D. Bagrets, and A. Kamenev, *Quantum criticality of granular Sachdev-Ye-Kitaev matter*, Physical Review Letters **123**, 106601 (2019).

Altland, A., P. W. Brouwer, J. Dieplinger, M. S. Foster, M. Moreno-Gonzalez, and L. Trifunovic, *Fragility of Surface States in Non-Wigner-Dyson Topological Insulators*, Physical Review X **14**, 011057 (2024).

Altland, A. and B. D. Simons, *Condensed matter field theory*, Cambridge University Press, 2010.

Altland, A. and M. R. Zirnbauer, *Nonstandard symmetry classes in mesoscopic normal-superconducting hybrid structures*, Physical Review B **55**, 1142 (1997).

Altshuler, B. L., Y. Gefen, A. Kamenev, and L. S. Levitov, *Quasiparticle lifetime in a finite system: A nonperturbative approach*, Physical Review Letters **78**, 2803 (1997).

Amado, M, A. V. Malyshev, A Sedrakyan, and F Dominguez-Adame, *Numerical Study of the Localization Length Critical Index in a Network Model of Plateau-Plateau Transitions in the Quantum Hall Effect*, Physical Review Letters **107**, 66402 (2011).

Anderson, P. W., *Absence of Diffusion in Certain Random Lattices*, Physical Review **109**, 1492–1505 (1958).

Anderson, P. W., *More is different*, Science **177**, 393–396 (1972).

Ando, Y. and L. Fu, *Topological Crystalline Insulators and Topological Superconductors: From Concepts to Materials*, Annual Reviews of Condensed Matter Physics **6**, 361–381 (2015).

Atas, Y. Y., E. Bogomolny, O. Giraud, and G. Roux, *Distribution of the ratio of consecutive level spacings in random matrix ensembles*, Physical Review Letters **110**, 084101 (2013).

Babkin, S. S., J. F. Karcher, I. S. Burmistrov, and A. D. Mirlin, *Generalized surface multifractality in two-dimensional disordered systems*, Physical Review B **108**, 104205 (2023).

Bäcker, A., F. Steiner, and P. Stifter, *Spectral statistics in the quantized cardioid billiard*, Physical Review E **52**, 2463 (1995).

Bagrets, D., A. Altland, and A. Kamenev, *Power-law out of time order correlation functions in the SYK model*, Nuclear Physics B **921**, 727–752 (2017).

Bardeen, J., L. N. Cooper, and J. R. Schrieffer, *Theory of superconductivity*, Physical Review **108**, 1175 (1957).

Basko, D. M., I. L. Aleiner, and B. L. Altshuler, *Metal-insulator transition in a weakly interacting many-electron system with localized single-particle states*, Annals of Physics **321**, 1126–1205 (2006).

Behrends, J. and B. Béri, *Supersymmetry in the Standard Sachdev-Ye-Kitaev Model*, Physical Review Letters **124**, 236804 (2020).

Bera, S., G. De Tomasi, I. M. Khaymovich, and A. Scardicchio, *Return probability for the Anderson model on the random regular graph*, Physical Review B **98**, 134205 (2018).

Bera, S., G. De Tomasi, F. Weiner, and F. Evers, *Density Propagator for Many-Body Localization: Finite-Size Effects, Transient Subdiffusion, and Exponential Decay*, Physical Review Letters **118**, 196801 (2017).

Bera, S., J. Dieplinger, and N. P. Nayak, *Quantum Hall criticality in an amorphous Chern insulator*, Physical Review B **109**, 174213 (2024).

Bera, S., H. Schomerus, F. Heidrich-Meisner, and J. H. Bardarson, *Many-Body Localization Characterized from a One-Particle Perspective*, Physical Review Letters **115**, 046603 (2015).

Bernevig, B. A. and T. L. Hughes, *Topological Insulators and Topological Superconductors*, Princeton University Press, 2013.

Berry, M. V., *Quantal phase factors accompanying adiabatic changes*, Proceedings of the Royal Society of London. A. Mathematical and Physical Sciences **392**, 45–57 (1984).

Biroli, G. and M. Tarzia, *Delocalized glassy dynamics and many-body localization*, Physical Review B **96**, 201114(R) (2017).

Bloch, F., *Über die Quantenmechanik der Elektronen in Kristallgittern*, Zeitschrift für Physik **52**, 555–600 (1929).

Bohigas, O., M. J. Giannoni, and C. Schmit, *Characterization of chaotic quantum spectra and universality of level fluctuation Laws*, Physical Review Letters **52**, 1 (1984).

Bollini, C. G. and J. J. Giambiagi, *Dimensional renormalization: The number of dimensions as a regularizing parameter*, Il Nuovo Cimento B (1971-1996) **12**, 20–26 (1972).

Bondesan, R, D Wieczorek, and M. R. Zirnbauer, *Gaussian free fields at the integer quantum Hall plateau transition*, Nuclear Physics B **918**, 52–90 (2017).

Brézin, E. and S. Hikami, *Spectral form factor in a random matrix theory*, Physical Review E **55**, 4067 (1997).

Bruus, H. and K. Flensberg, *Many-Body Quantum Theory in Condensed Matter Physics*, Oxford University Press, 2004.

Burin, A. L., *Localization in a random XY model with long-range interactions: Intermediate case between single-particle and many-body problems*, Physical Review B **92**, 104428 (2015).

Burin, A. L., *Many-body delocalization in a strongly disordered system with long-range interactions: Finite-size scaling*, Physical Review B **91**, 094202 (2015).

Castellanits, C and L Peliti, *Multifractal wavefunction at the localisation threshold*, Journal of Physics A **19**, 429–432 (1986).

Chalker, J. T. and P. D. Coddington, *Percolation, quantum tunneling and the integer Hall effect*, Journal of Physics: Condensed Matter **21**, 2665–2679 (1988).

Chang, C.-Z., C.-X. Liu, and A. H. MacDonald, *Colloquium: Quantum anomalous Hall effect*, Reviews of Modern Physics **95**, 11002 (2023).

Choi, J. Y., S. Hild, J. Zeiher, P. Schauß, A. Rubio-Abadal, T. Yefsah, V. Khemani, D. A. Huse, I. Bloch, and C. Gross, *Exploring the many-body localization transition in two dimensions*, Science **352**, 1547–1552 (2016).

Chowdhury, D., A. Georges, O. Parcollet, and S. Sachdev, *Sachdev-Ye-Kitaev models and beyond: Window into non-Fermi liquids*, Reviews of Modern Physics **94**, 035004 (2022).

Chowdhury, D., Y. Werman, E. Berg, and T. Senthil, *Translationally Invariant Non-Fermi-Liquid Metals with Critical Fermi Surfaces: Solvable Models*, Physical Review X **8**, 031024 (2018).

Cotler, J. S., G. Gur-Ari, M. Hanada, J. Polchinski, P. Saad, S. H. Shenker, D. Stanford, A. Streicher, and M. Tezuka, *Black holes and random matrices*, Journal of High Energy Physics **2017**, 118 (2017).

Creed, I., D. E. Logan, and S. Roy, *Probability transport on the Fock space of a disordered quantum spin chain*, Physical Review B **107**, 094206 (2023).

Cuevas, E., M. Feigel'Man, L. Ioffe, and M. Mezard, *Level statistics of disordered spin-1/2 systems and materials with localized Cooper pairs*, Nature Communications **3**, 1128 (2012).

De Luca, A., B. L. Altshuler, V. E. Kravtsov, and A. Scardicchio, *Anderson localization on the Bethe lattice: Nonergodicity of extended states*, Physical Review Letters **113**, 046806 (2014).

De Tomasi, G., *Algebraic many-body localization and its implications on information propagation*, Physical Review B **99**, 054204 (2019).

Deng, X., G. Masella, G. Pupillo, and L. Santos, *Universal Algebraic Growth of Entanglement Entropy in Many-Body Localized Systems with Power-Law Interactions*, Physical Review Letters **125**, 010401 (2020).

Deutsch, J. M., *Quantum statistical mechanics in a closed system*, Physical Review A **43**, 2046 (1991).

Dieplinger, J. and S. Bera, *Finite-size prethermalization at the chaos-to-integrable crossover*, Physical Review B **107**, 224207 (2023).

Dieplinger, J., S. Bera, and F. Evers, *An SYK-inspired model with density–density interactions: Spectral & wave function statistics, Green's function and phase diagram*, Annals of Physics **435**, 168503 (2021).

Doggen, E. V., I. V. Gornyi, A. D. Mirlin, and D. G. Polyakov, *Many-body localization in large systems: Matrix-product-state approach*, Annals of Physics **435**, 168437 (2021).

Doggen, E. V., F. Schindler, K. S. Tikhonov, A. D. Mirlin, T. Neupert, D. G. Polyakov, and I. V. Gornyi, *Many-body localization and delocalization in large quantum chains*, Physical Review B **98**, (2018).

Dresselhaus, E. J., A. Avdoshkin, Z. Jia, M. Secli, B. Kante, and J. E. Moore, *A tale of two localizations: coexistence of flat bands and Anderson localization in a photonics-inspired amorphous system*, arxiv:2404.17578 , (2024).

Dresselhaus, E. J., B. Sbierski, and I. A. Gruzberg, *Numerical evidence for marginal scaling at the integer quantum Hall transition*, Annals of Physics **435**, 168676 (2021).

Dresselhaus, E. J., B. Sbierski, and I. A. Gruzberg, *Scaling Collapse of Longitudinal Conductance near the Integer Quantum Hall Transition*, Physical Review Letters **129**, 26801 (2022).

Dumitrescu, P. T., A. Goremykina, S. A. Parameswaran, M. Serbyn, and R. Vasseur, *Kosterlitz-Thouless scaling at many-body localization phase transitions*, Physical Review B **99**, 094205 (2019).

Essin, A. M. and V Gurarie, *Delocalization of boundary states in disordered topological insulators*, Journal of Physics A **48**, 11FT01 (2015).

Evers, F and A. D. Mirlin, *Fluctuations of the Inverse Participation Ratio at the Anderson Transition*, Physical Review Letters **84**, 3690 (2000).

Evers, F., A Mildenberger, and A. D. Mirlin, *Multifractality of wave functions at the quantum Hall transition revisited*, Physical Review B **64**, 241303 (2001).

Evers, F., A Mildenberger, and A. D. Mirlin, *Multifractality at the quantum Hall transition: Beyond the parabolic paradigm*, Physical review letters **101**, 116803 (2008).

Evers, F. and A. D. Mirlin, *Anderson transitions*, Reviews of Modern Physics **80**, 1355 (2008).

Evers, F., I. Modak, and S. Bera, *Internal clock of many-body delocalization*, Physical Review B **108**, 134204 (2023).

Fu, W., D. Gaiotto, J. Maldacena, and S. Sachdev, *Supersymmetric Sachdev-Ye-Kitaev models*, Physical Review D **95**, 026009 (2017).

Fu, W. and S. Sachdev, *Numerical study of fermion and boson models with infinite-range random interactions*, Physical Review B **94**, 035135 (2016).

Fulga, I. C., F Hassler, A. R. Akhmerov, and C. W. J. Beenakker, *Topological quantum number and critical exponent from conductance fluctuations at the quantum Hall plateau transition*, Physical Review B **84**, 245447 (2011).

García-Álvarez, L., I. L. Egusquiza, L. Lamata, A. Del Campo, J. Sonner, and E. Solano, *Digital Quantum Simulation of Minimal AdS/CFT*, Physical Review Letters **119**, 040501 (2017).

García-García, A. M., B. Loureiro, A. Romero-Bermúdez, and M. Tezuka, *Chaotic-Integrable Transition in the Sachdev-Ye-Kitaev Model*, Physical Review Letters **120**, 241603 (2018).

García-García, A. M. and J. J. Verbaarschot, *Spectral and thermodynamic properties of the Sachdev-Ye-Kitaev model*, Physical Review D **94**, 126010 (2016).

García-García, A. M. and J. J. Verbaarschot, *Analytical spectral density of the Sachdev-Ye-Kitaev model at finite N*, Physical Review D **96**, 066012 (2017).

García-Mata, I., O. Giraud, B. Georgeot, J. Martin, R. Dubertrand, and G. Lemarié, *Scaling Theory of the Anderson Transition in Random Graphs: Ergodicity and Universality*, Physical Review Letters **118**, 012020(R) (2017).

García-Mata, I., J. Martin, R. Dubertrand, O. Giraud, B. Georgeot, and G. Lemarié, *Two critical localization lengths in the Anderson transition on random graphs*, Physical Review Research **2**, (2020).

Geim, A. K., *Graphene: Status and Prospects*, Science **324**, 1530–1534 (2009).

Georges, A., O. Parcollet, and S. Sachdev, *Quantum fluctuations of a nearly critical Heisenberg spin glass*, Physical Review B **63**, 134406 (2001).

Ghorashi, S. A. A., J. F. Karcher, S. M. Davis, and M. S. Foster, *Criticality across the energy spectrum from random artificial gravitational lensing in two-dimensional Dirac superconductors*, Physical Review B **101**, 214521 (2020).

Ghorashi, S. A. A., Y. Liao, and M. S. Foster, *Critical Percolation without Fine-Tuning on the Surface of a Topological Superconductor*, Physical Review Letters **121**, 16802 (2018).

Giuliani, G. and G. Vignale, *Qauntum theory of the electron liquid*, Cambridge University Press, 2008.

Gornyi, I. V., A. D. Mirlin, M. Müller, and D. G. Polyakov, *Absence of many-body localization in a continuum*, Annalen der Physik **529**, 1600365 (2017).

Gornyi, I. V., A. D. Mirlin, and D. G. Polyakov, *Interacting electrons in disordered wires: Anderson localization and low-T transport*, Physical Review Letters **95**, 206603 (2005).

Gornyi, I. V., A. D. Mirlin, and D. G. Polyakov, *Many-body delocalization transition and relaxation in a quantum dot*, Physical Review B **93**, 125419 (2016).

Gornyi, I. V., A. D. Mirlin, D. G. Polyakov, and A. L. Burin, *Spectral diffusion and scaling of many-body delocalization transitions*, Annalen der Physik **529**, 1600360 (2017).

Grissonnanche, G., Y. Fang, A. Legros, S. Verret, F. Laliberté, C. Collignon, J. Zhou, D. Graf, P. A. Goddard, L. Taillefer, and B. J. Ramshaw, *Linear-in temperature resistivity from an isotropic Planckian scattering rate*, Nature **595**, pages 667–672 (2021).

Groth, C. W., M. Wimmer, A. R. Akhmerov, and X. Waintal, *Kwant: a software package for quantum transport*, New Journal of Physics **16**, 63065 (2014).

Gruzberg, I. A., A Klümper, W Nuding, and A Sedrakyan, *Geometrically disordered network models, quenched quantum gravity, and critical behavior at quantum Hall plateau transitions*, Physical Review B **95**, 125414 (2017).

Gruzberg, I. A., A. D. Mirlin, and M. R. Zirnbauer, *Classification and symmetry properties of scaling dimensions at Anderson transitions*, Physical Review B **87**, 125144 (2013).

Gu, Y., A. Kitaev, S. Sachdev, and G. Tarnopolsky, *Notes on the complex Sachdev-Ye-Kitaev model*, Journal of High Energy Physics **2020**, 157 (2020).

Guhr, T., A. Müller-Groeling, and H. A. Weidenmüller, *Random-matrix theories in quantum physics: Common concepts*, Physics Report **299**, 189–425 (1998).

Guo, H., Y. Gu, and S. Sachdev, *Transport and chaos in lattice Sachdev-Ye-Kitaev models*, Physical Review B **100**, 045140 (2019).

Gutman, D. B., I. V. Protopopov, A. L. Burin, I. V. Gornyi, R. A. Santos, and A. D. Mirlin, *Energy transport in the Anderson insulator*, Physical Review B **93**, 245427 (2016).

Haldane, F. D. M., *Model for a Quantum Hall Effect without Landau Levels: Condensed-Matter Realization of the "Parity Anomaly"*, Physical Review Letters **61**, 2015–2018 (1988).

Haldar, A., S. Banerjee, and V. B. Shenoy, *Higher-dimensional Sachdev-Ye-Kitaev non-Fermi liquids at Lifshitz transitions*, Physical Review B **97**, 241106(R) (2018).

Haldar, A., P. Haldar, S. Bera, I. Mandal, and S. Banerjee, *Quench, thermalization, and residual entropy across a non-Fermi liquid to Fermi liquid transition*, Physical Review Research **2**, 013307 (2020).

Halperin, B. I., *Quantized Hall conductance, current-carrying edge states, and the existence of extended states in a two-dimensional disordered potential*, Physical Review B **25**, 2185 (1982).

Haque, M. and P. A. McClarty, *Eigenstate thermalization scaling in Majorana clusters: From chaotic to integrable Sachdev-Ye-Kitaev models*, Physical Review B **100**, 115122 (2019).

Hartnoll, S. A. and A. P. MacKenzie, *Colloquium: Planckian dissipation in metals*, Reviews of Modern Physics **94**, 041002 (2022).

Hasan, M. Z. and C. L. Kane, *Colloquium: Topological insulators*, Reviews of Modern Physics **82**, 3045 (2010).

Herre, J. N., J. F. Karcher, K. S. Tikhonov, and A. D. Mirlin, *Ergodicity-to-localization transition on random regular graphs with large connectivity and in many-body quantum dots*, Physical Review B **108**, 014203 (2023).

Heydeman, M., L. V. Iliesiu, G. J. Turiaci, and W. Zhao, *The statistical mechanics of near-BPS black holes*, Journal of Physics A: Mathematical and Theoretical **55**, 014004 (2022).

Huckestein, B, *Scaling Theory of the Integer Quantum Hall Effect*, Reviews of Modern Physics **67**, 357 (1995).

Huckestein, B. and B. Kramer, *One-parameter scaling in the lowest Landau band: Precise determination of the critical behavior of the localization length*, Physical Review Letters **64**, 1437–1440 (1990).

Iliesiu, L. V. and G. J. Turiaci, *The statistical mechanics of near-extremal black holes*, Journal of High Energy Physics **2021**, 145 (2021).

Imry, Y. and R. Landauer, *Conductance viewed as transmission*, Reviews of Modern Physics **71**, S306 (1999).

Ivaki, M. N., I. Sahlberg, and T. Ojanen, *Criticality in amorphous topological matter: Beyond the universal scaling paradigm*, Physical Review Research **2**, 43301 (2020).

Janssen, M., *Multifractal Analysis of Broadly Distributed Observables at Criticality*, International Journal of Modern Physics B **8**, 943–984 (1994).

Jordan, P. and E. Wigner, *Über das Paulische Äquivalenzverbot*, Zeitschrift für Physik **47**, 631–651 (1928).

Kane, C. L. and E. J. Mele, *Quantum spin Hall effect in graphene*, Physical review letters **95**, 226801 (2005).

Karcher, J. F., N. Charles, I. A. Gruzberg, and A. D. Mirlin, *Generalized multifractality at spin quantum Hall transition*, Annals of Physics **435**, 168584 (2021).

Karcher, J. F. and M. S. Foster, *How spectrum-wide quantum criticality protects surface states of topological superconductors from Anderson localization: Quantum Hall plateau transitions (almost) all the way down*, Annals of Physics **435**, 168439 (2021).

Karcher, J. F., I. A. Gruzberg, and A. D. Mirlin, *Generalized multifractality at metal-insulator transitions and in metallic phases of two-dimensional disordered systems*, Physical Review B **106**, 104202 (2022).

Karcher, J. F., I. A. Gruzberg, and A. D. Mirlin, *Generalized multifractality in two-dimensional disordered systems of chiral symmetry classes*, Physical Review B **107**, 104202 (2023).

Khmelnitskii, D. E., *Quantization of Hall conductivity*, ZhETF Pisma Redaktsiiu **38**, 454–458 (1983).

Kitaev, A., *A simple model of quantum holography*, talks given at KITP , (2015).

Kitaev, A. and S. J. Suh, *The soft mode in the Sachdev-Ye-Kitaev model and its gravity dual*, Journal of High Energy Physics **2018**, 183 (2018).

Klitzing, K. v., G Dorda, and M Pepper, *New Method for High-Accuracy Determination of the Fine-Structure Constant Based on Quantized Hall Resistance*, Physical Review Letters **45**, 494–497 (1980).

Kloss, B. and Y. Bar Lev, *Spin transport in disordered long-range interacting spin chain*, Physical Review B **102**, 060201(R) (2020).

Klümper, A, W Nuding, and A Sedrakyan, *Random network models with variable disorder of geometry*, Physical Review B **100**, 140201 (2019).

Kobrin, B., Z. Yang, G. D. Kahanamoku-Meyer, C. T. Olund, J. E. Moore, D. Stanford, and N. Y. Yao, *Many-Body Chaos in the Sachdev-Ye-Kitaev Model*, Physical Review Letters **126**, 030602 (2021).

Koch, S, R. J. Haug, K. v. Klitzing, and K Ploog, *Size-dependent analysis of the metal-insulator transition in the integral quantum Hall effect*, Physical Review Letters **67**, 883–886 (1991).

Kondo, J., *Resistance Minimum in Dilute Magnetic Alloys*, Progress of Theoretical Physics **32**, (1964).

Kravtsov, V. E., B. L. Altshuler, and L. B. Ioffe, *Non-ergodic delocalized phase in Anderson model on Bethe lattice and regular graph*, Annals of Physics **389**, 148–191 (2018).

Landau, L. D. and E. M. Lifshitz, *Statistical Physics*, Pergamon Press, 1976.

Landauer, R., *Spatial variation of currents and fields due to localized scatterers in metallic conduction*, IBM Journal of research and development **1**, 223–231 (1957).

Lapierre, B., T. Neupert, and L. Trifunovic, *Topologically Localized Insulators*, Physical Review Letters **129**, 256401 (2022).

Larzul, A. and M. Schiró, *Quenches and (pre)thermalization in a mixed Sachdev-Ye-Kitaev model*, Physical Review B **105**, 045105 (2022).

Laughlin, R. B., *Quantized Hall conductivity in two dimensions*, Physical Review B **23**, 5632–5633 (1981).

Laughlin, R. B., *Anomalous Quantum Hall Effect: An Incompressible Quantum Fluid with Fractionally Charged Excitations*, Physical Review Letters **50**, 1395–1398 (1983).

Lee, P. A. and T. V. Ramakrishnan, *Disordered electronic systems*, Reviews of Modern Physics **57**, 287–337 (1985).

Lehoucq, R. B., D. C. Sorensen, and C. Yang (1998). *ARPACK users guide: Solution of large scale eigenvalue problems with implicitly restarted Arnoldi methods*. URL: `https://github.com/opencollab/arpack-ng`.

Levine, H., S. B. Libby, and A. M. M. Pruisken, *Theory of the quantized Hall effect (I)*, Nuclear Physics B **240**, 30–48 (1984).

Lezama, T. L., S. Bera, and J. H. Bardarson, *Apparent slow dynamics in the ergodic phase of a driven many-body localized system without extensive conserved quantities*, Physical Review B **99**, 161106(R) (2019).

Li, W., C. L. Vicente, J. S. Xia, W Pan, D. C. Tsui, L. N. Pfeiffer, and K. W. West, *Scaling in Plateau-to-Plateau Transition: A Direct Connection of Quantum Hall Systems with the Anderson Localization Model*, Physical Review Letters **102**, 216801 (2009).

Liao, Y., A. Vikram, and V. Galitski, *Many-Body Level Statistics of Single-Particle Quantum Chaos*, Physical Review Letters **125**, 250601 (2020).

Luitz, D. J., N. Laflorencie, and F. Alet, *Many-body localization edge in the random-field Heisenberg chain*, Physical Review B **91**, 081103(R) (2015).

Luitz, D. J. and Y. B. Lev, *The ergodic side of the many-body localization transition*, **529**, 1600350 (2017).

Lunkin, A. V., K. S. Tikhonov, and M. V. Feigel'Man, *Sachdev-Ye-Kitaev Model with Quadratic Perturbations: The Route to a Non-Fermi Liquid*, Physical Review Letters **121**, 236601 (2018).

Lüschen, H. P., P. Bordia, S. Scherg, F. Alet, E. Altman, U. Schneider, and I. Bloch, *Observation of Slow Dynamics near the Many-Body Localization Transition in One-Dimensional Quasiperiodic Systems*, Physical Review Letters **119**, 260401 (2017).

Macé, N., F. Alet, and N. Laflorencie, *Multifractal Scalings Across the Many-Body Localization Transition*, Physical Review Letters **123**, 180601 (2019).

Maldacena, J., S. H. Shenker, and D. Stanford, *A bound on chaos*, Journal of High Energy Physics **2016**, 106 (2016).
Maldacena, J. and D. Stanford, *Remarks on the Sachdev-Ye-Kitaev model*, Physical Review D **94**, 106002 (2016).
Maldacena, J., D. Stanford, and Z. Yang, *Conformal symmetry and its breaking in two-dimensional nearly anti-de Sitter space*, Progress of Theoretical and Experimental Physics **2016**, (2016).
Mandelbrot, B. B., *The fractal geometry of nature*, WH Freeman New York, 1982.
Mehta, M, *Random Matrices*, Elsevier, 2014.
Metz, F. L. and I. P. Castillo, *Level compressibility for the Anderson model on regular random graphs and the eigenvalue statistics in the extended phase*, Physical Review B **96**, 064202 (2017).
Micklitz, T., F. Monteiro, and A. Altland, *Nonergodic Extended States in the Sachdev-Ye-Kitaev Model*, Physical Review Letters **123**, 125701 (2019).
Mirlin, A. D. and F. Evers, *Multifractality and critical fluctuations at the Anderson transition*, Physical Review B **62**, 7920 (2000).
Mirlin, A. D., Y. V. Fyodorov, A Mildenberger, and F Evers, *Exact Relations between Multifractal Exponents at the Anderson Transition*, Physical Review Letters **97**, 46803 (2006).
Modak, R. and T. Nag, *Many-body localization in a long-range model: Real-space renormalization-group study*, Physical Review E **101**, 052108 (2020).
Moitra, U., S. P. Trivedi, and V. Vishal, *Extremal and near-extremal black holes and near-CFT1*, Journal of High Energy Physics **2019**, 55 (2019).
Monteiro, F., T. Micklitz, M. Tezuka, and A. Altland, *Minimal model of many-body localization*, Physical Review Research **3**, 013023 (2021).
Monteiro, F., M. Tezuka, A. Altland, D. A. Huse, and T. Micklitz, *Quantum Ergodicity in the Many-Body Localization Problem*, Physical Review Letters **127**, (2021).
Moreno-Gonzalez, M., J. Dieplinger, and A. Altland, *Topological quantum criticality of the disordered Chern insulator*, Annals of Physics **456**, 169258 (2023).
Morningstar, A., L. Colmenarez, V. Khemani, D. J. Luitz, and D. A. Huse, *Avalanches and many-body resonances in many-body localized systems*, Physical Review B **105**, 174205 (2022).
Morningstar, A., D. A. Huse, and J. Z. Imbrie, *Many-body localization near the critical point*, Physical Review B **102**, (2020).
Mudry, C., C. Chamon, and X.-G. Wen, *Two-dimensional conformal field theory for disordered systems at criticality*, Nuclear Physics B **466**, 383–443 (1996).
Müller, S., S. Heusler, P. Braun, F. Haake, and A. Altland, *Semiclassical foundation of universality in quantum chaos*, Physical Review Letters **93**, 014103 (2004).
Müller, S., S. Heusler, P. Braun, F. Haake, and A. Altland, *P*eriodic-orbit theory of universality in quantum chaos, Physical Review E **72**, 046207 (2005).
Nag, S. and A. Garg, *Many-body localization in the presence of long-range interactions and long-range hopping*, Physical Review B **99**, 224203 (2019).

Nandkishore, R. and D. A. Huse, *Many-body localization and thermalization in quantum statistical mechanics*, Annual Review of Condensed Matter Physics **6**, 15–38 (2015).

Nandy, D. K., T. Čadež, B. Dietz, A. Andreanov, and D. Rosa, *Delayed thermalization in the mass-deformed Sachdev-Ye-Kitaev model*, Physical Review B **106**, 245147 (2022).

Nuding, W, A Klümper, and A Sedrakyan, *Localization length index and subleading corrections in a Chalker-Coddington model: A numerical study*, Physical Review B **91**, 115107 (2015).

Obuse, H, A. R. Subramaniam, A Furusaki, I. A. Gruzberg, and A. W. W. Ludwig, *Boundary Multifractality at the Integer Quantum Hall Plateau Transition: Implications for the Critical Theory*, Physical Review Letters **101**, 116802 (2008).

Obuse, H., A. R. Subramaniam, A. Furusaki, I. A. Gruzberg, and A. W. Ludwig, *Conformal invariance, multifractality, and finite-size scaling at Anderson localization transitions in two dimensions*, Physical Review B **82**, 035309 (2010).

Obuse, H., I. A. Gruzberg, and F. Evers, *Finite-Size Effects and Irrelevant Corrections to Scaling Near the Integer Quantum Hall Transition*, Physical Review Letters **109**, 206804 (2012).

Oganesyan, V. and D. A. Huse, *Localization of interacting fermions at high temperature*, Physical Review B **75**, 155111 (2007).

Ohtsuki, T., K. Slevin, and T. Kawarabayashi, *Review of recent progress on numerical studies of the Anderson transition*, Annalen der Physik **511**, 655–664 (1999).

Parcollet, O. and A. Georges, *Non-fermi-liquid regime of a doped mott insulator*, Physical Review B **59**, 5341 (1999).

Patel, A. A. and S. Sachdev, *Theory of a Planckian Metal*, Physical Review Letters **123**, 066601 (2019).

Pauli, W and F Villars, *On the Invariant Regularization in Relativistic Quantum Theory*, Reviews of Modern Physics **21**, 434–444 (1949).

Polini, M. and A. K. Geim, *Viscous electron fluids*, Physics Today **73**, (2020).

Prakash, A., J. H. Pixley, and M. Kulkarni, *Universal spectral form factor for many-body localization*, Physical Review Research **3**, L012019 (2021).

Pruisken, A. M. M., *On localization in the theory of the quantized hall effect: A two-dimensional realization of the θ-vacuum*, Nuclear Physics B **235**, 277–298 (1984).

Puschmann, M. (2017). "Anderson transitions on random Voronoi-Delaunay lattices." PhD thesis. Technische Universität Chemnitz. URL: http://nbn-resolving.de/urn:nbn:de:bsz:ch1-qucosa-231900.

Puschmann, M., P. Cain, M. Schreiber, and T. Vojta, *Multifractal analysis of electronic states on random Voronoi-Delaunay lattices*, The European Physical Journal B **88**, 314 (2015).

Puschmann, M., P. Cain, M. Schreiber, and T. Vojta, *Integer quantum Hall transition on a tight-binding lattice*, Physical Review B **99**, 121301 (2019).

Puschmann, M., D. Hernangómez-Pérez, B. Lang, S. Bera, and F. Evers, *Quartic multifractality and finite-size corrections at the spin quantum Hall transition*, Physical Review B **103**, 235167 (2021).

Puschmann, M. and T. Vojta, *Green's functions on a renormalized lattice: An improved method for the integer quantum Hall transition*, Annals of Physics **435**, 168485 (2021).

Qi, X.-L., Y.-S. Wu, and S.-C. Zhang, *Topological quantization of the spin Hall effect in two-dimensional paramagnetic semiconductors*, Physical Review B **74**, 85308 (2006).

Qi, X.-L. and S.-C. Zhang, *Topological insulators and superconductors*, Reviews of Modern Physics **83**, 1057 (2011).

Rigol, M., V. Dunjko, and M. Olshanii, *Thermalization and its mechanism for generic isolated quantum systems*, Nature **452**, 854–858 (2008).

Robnik, M., *Classical dynamics of a family of billiards with analytic boundaries*, Journal of Physics A **16**, 3971 (1983).

Rodriguez, A., L. J. Vasquez, and R. A. Römer, *Multifractal analysis of the metal-insulator transition in the three-dimensional Anderson model. II. Symmetry relation under ensemble averaging*, Physical Review B **78**, 195107 (2008).

Rodriguez, A., L. J. Vasquez, K. Slevin, and R. A. Römer, *Critical parameters from a generalized multifractal analysis at the Anderson transition*, Physical Review Letters **105**, 046403 (2010).

Rodriguez, A., L. J. Vasquez, K. Slevin, and R. A. Römer, *Multifractal finite-size scaling and universality at the Anderson transition*, Physical Review B **84**, 134209 (2011).

Rotunno, R., *The fluid dynamics of tornadoes*, **45**, 59–84 (2013).

Roushan, P., C. Neill, J. Tangpanitanon, V. M. Bastidas, A. Megrant, R. Barends, Y. Chen, Z. Chen, B. Chiaro, A. Dunsworth, A. Fowler, B. Foxen, M. Giustina, E. Jeffrey, J. Kelly, E. Lucero, J. Mutus, M. Neeley, C. Quintana, D. Sank, A. Vainsencher, J. Wenner, T. White, H. Neven, D. G. Angelakis, and J. Martinis, *Spectroscopic signatures of localization with interacting photons in superconducting qubits*, Science **358**, 1175–1179 (2017).

Roy, S. and D. E. Logan, *Self-consistent theory of many-body localisation in a quantum spin chain with long-range interactions*, SciPost Physics **7**, 042 (2019).

Rubio-Abadal, A., J. Y. Choi, J. Zeiher, S. Hollerith, J. Rui, I. Bloch, and C. Gross, *Many-Body Delocalization in the Presence of a Quantum Bath*, Physical Review X **9**, 041014 (2019).

Ryu, S., A. P. Schnyder, A. Furusaki, and A. W. W. Ludwig, *Topological insulators and superconductors: tenfold way and dimensional hierarchy*, New Journal of Physics **12**, 65010 (2010).

Saad, P., S. H. Shenker, and D. Stanford, *A semiclassical ramp in SYK and in gravity*, arXiv:1806.06840 , (2018).

Sachdev, S., *Quantum Phase Transitions*, Cambridge University Press, 2011.

Sachdev, S., *Bekenstein-hawking entropy and strange metals*, Physical Review X **5**, 041025 (2015).

Sachdev, S., *Universal low temperature theory of charged black holes with AdS 2 horizons*, Journal of Mathematical Physics **60**, 052303 (2019).

Sachdev, S. and J. Ye, *Gapless spin-fluid ground state in a random quantum Heisenberg magnet*, Physical Review Letters **70**, 3339 (1993).

Safavi-Naini, A., M. L. Wall, O. L. Acevedo, A. M. Rey, and R. M. Nandkishore, *Quantum dynamics of disordered spin chains with power-law interactions*, Physical Review A **99**, 033610 (2019).

Sakurai, J. J. and J. Napolitano, *Modern Quantum Mechanics*, Cambridge University Press, 2020.

Sbierski, B., E. J. Dresselhaus, J. E. Moore, and I. A. Gruzberg, *Criticality of Two-Dimensional Disordered Dirac Fermions in the Unitary Class and Universality of the Integer Quantum Hall Transition*, Physical Review Letters **126**, 76801 (2021).

Sbierski, B., J. F. Karcher, and M. S. Foster, *Spectrum-Wide Quantum Criticality at the Surface of Class AIII Topological Phases: An "Energy Stack" of Integer Quantum Hall Plateau Transitions*, Physical Review X **10**, 21025 (2020).

Schiulaz, M., E. J. Torres-Herrera, and L. F. Santos, *Thouless and relaxation time scales in many-body quantum systems*, Physical Review B **99**, 174313 (2019).

Schreiber, M., S. S. Hodgman, P. Bordia, H. P. Lüschen, M. H. Fischer, R. Vosk, E. Altman, U. Schneider, and I. Bloch, *Observation of many-body localization of interacting fermions in a quasirandom optical lattice*, Science **349**, 842–845 (2015).

Sels, D., *Bath-induced delocalization in interacting disordered spin chains*, Physical Review B **106**, L020202 (2022).

Serbyn, M., D. A. Abanin, and Z. Papić, *Quantum many-body scars and weak breaking of ergodicity*, , 2021.

Sieber, M. and K. Richter, *Correlations between periodic orbits and their role in spectral statistics*, **2001**, 128 (2001).

Sierant, P., M. Lewenstein, A. Scardicchio, L. Vidmar, and J. Zakrzewski, *Many-Body Localization in the Age of Classical Computing*, arxiv:2403.07111 , (2024).

Sierant, P., M. Lewenstein, and J. Zakrzewski, *Polynomially Filtered Exact Diagonalization Approach to Many-Body Localization*, Physical Review Letters **125**, 156601 (2020).

Sierant, P. and J. Zakrzewski, *Challenges to observation of many-body localization*, Physical Review B **105**, 224203 (2022).

Silvestrov, P. G., *Decay of a quasiparticle in a quantum dot: The role of energy resolution*, Physical Review Letters **79**, 3994 (1997).

Silvestrov, P. G., *Chaos thresholds in finite Fermi systems*, Physical Review E **58**, 5629 (1998).

Simon, B., *Holonomy, the quantum adiabatic theorem, and Berry's phase*, Physical Review Letters **51**, 2167 (1983).

Slevin, K. and T. Ohtsuki, *Corrections to Scaling at the Anderson Transition*, Physical Review Letters **82**, 382–385 (1999).

Slevin, K. and T. Ohtsuki, *Critical exponent for the quantum Hall transition*, Physical Review B **80**, 41304 (2009).

Slevin, K. and T. Ohtsuki, *Finite size scaling of the Chalker-Coddington model*, International Journal of Modern Physics Conference Series **11**, 60–69 (2012).

Smrcka, L and P Streda, *Transport coefficients in strong magnetic fields*, Journal of Physics C **10**, 2153–2161 (1977).
Song, X. Y., C. M. Jian, and L. Balents, *Strongly Correlated Metal Built from Sachdev-Ye-Kitaev Models*, Physical Review Letters **119**, 216601 (2017).
Srednicki, M., *Chaos and quantum thermalization*, Physical Review E **50**, 888 (1994).
Stanford, D. and E. Witten, *Fermionic localization of the schwarzian theory*, Journal of High Energy Physics **2017**, 8 (2017).
Stosiek, M. (2020). "Self-consistent-field ensembles of disordered Hamiltonians: Efficient solver and application to superconducting films." PhD thesis. Universität Regensburg. URL: https://epub.uni-regensburg.de/43593/.
Su, W., J. R. Schrieffer, and A. J. Heeger, *Solitons in polyacetylene*, Physical Review Letters **42**, 1698 (1979).
Succi, S., *The lattice boltzmann equation: For complex states of flowing matter*, Oxford University Press, 2018.
't Hooft, G. and M Veltman, *Regularization and renormalization of gauge fields*, Nuclear Physics B **44**, 189–213 (1972).
Tasaki, H., *From quantum dynamics to the canonical distribution: General picture and a rigorous example*, Physical Review Letters **80**, 1373 (1998).
Teo, J. C. and C. L. Kane, *Topological defects and gapless modes in insulators and superconductors*, Physical Review B **82**, 115120 (2010).
Thiery, T., F. Huveneers, M. Müller, and W. De Roeck, *Many-Body Delocalization as a Quantum Avalanche*, Physical Review Letters **121**, 140601 (2018).
Thomson, S. J. and M. Schiró, *Quasi-many-body localization of interacting fermions with long-range couplings*, Physical Review Research **2**, 043368 (2020).
Thouless, D. J., *Electrons in disordered systems and the theory of localization*, Physics Reports **13**, 93–142 (1974).
Thouless, D. J., M Kohmoto, M. P. Nightingale, and M den Nijs, *Quantized Hall Conductance in a Two-Dimensional Periodic Potential*, Physical Review Letters **49**, 405–408 (1982).
Tikhonov, K. S. and A. D. Mirlin, *Many-body localization transition with power-law interactions: Statistics of eigenstates*, Physical Review B **97**, 214205 (2018).
Tikhonov, K. S. and A. D. Mirlin, *Critical behavior at the localization transition on random regular graphs*, Physical Review B **99**, 214202 (2019).
Tikhonov, K. S. and A. D. Mirlin, *Statistics of eigenstates near the localization transition on random regular graphs*, Physical Review B **99**, 024202 (2019).
Tikhonov, K. S. and A. D. Mirlin, *Eigenstate correlations around the many-body localization transition*, Physical Review B **103**, 064204 (2021).
Tikhonov, K. S. and A. D. Mirlin, *From Anderson localization on random regular graphs to many-body localization*, Annals of Physics **435**, 168525 (2021).
Tikhonov, K. S., A. D. Mirlin, and M. A. Skvortsov, *Anderson localization and ergodicity on random regular graphs*, Physical Review B **94**, 220203(R) (2016).
Torres-Herrera, E. J. and L. F. Santos, *Dynamics at the many-body localization transition*, Physical Review B **92**, 014208 (2015).

Vallis, G. K., *Atmospheric and Oceanic Fluid Dynamics*, Cambridge University Press, 2006.

Wegner, F. J., *Electrons in Disordered Systems. Scaling Near the Mobility Edge*, Zeitschrift für Physik **25**, 327–337 (1976).

Weidenmüller, H. A. and G. E. Mitchell, *Random matrices and chaos in nuclear physics: Nuclear structure*, Reviews of Modern Physics **81**, 539 (2009).

Weiner, F., F. Evers, and S. Bera, *Slow dynamics and strong finite-size effects in many-body localization with random and quasiperiodic potentials*, Physical Review B **100**, 104204 (2019).

Weiße, A., G. Wellein, A. Alvermann, and H. Fehske, *The kernel polynomial method*, Reviews of Modern Physics **78**, 275 (2006).

Winer, M., S. K. Jian, and B. Swingle, *Exponential Ramp in the Quadratic Sachdev-Ye-Kitaev Model*, Physical Review Letters **125**, 250602 (2020).

Xu, K., J. J. Chen, Y. Zeng, Y. R. Zhang, C. Song, W. Liu, Q. Guo, P. Zhang, D. Xu, H. Deng, K. Huang, H. Wang, X. Zhu, D. Zheng, and H. Fan, *Emulating Many-Body Localization with a Superconducting Quantum Processor*, Physical Review Letters **120**, 050507 (2018).

Zhang, P., *Dispersive Sachdev-Ye-Kitaev model: Band structure and quantum chaos*, Physical Review B **96**, 205138 (2017).

Zhu, Q., P. Wu, R. N. Bhatt, and X. Wan, *Localization-length exponent in two models of quantum Hall plateau transitions*, Physical Review B **99**, 24205 (2019).

Zirnbauer, M. R., *Conformal field theory of the integer quantum Hall plateau transition*, arXiv:hep-th/9905054 , (1999).

Zirnbauer, M. R., *The integer quantum Hall plateau transition is a current algebra after all*, Nuclear Physics B **941**, 458 –506 (2019).

ACKNOWLEDGEMENTS

This thesis would not have been possible without the many people who supported me and my scientific work throughout. Therefore, I would particularly like to thank

- Prof. Dr. Ferdinand Evers, for advising me during the last couple of years. I am grateful for him teaching me a new perspective on the field and physics in general and the opportunities to work in fruitful collaborations with physicists from different backgrounds, which gave me the chance to touch upon very different subjects in theoretical physics;

- Prof. Dr. Klaus Richter, for agreeing to examine this dissertation, and Prof. Dr. Jascha Repp and Prof. Dr. Sara Collins for assessing this work as members of the examination committee;

- Prof. Dr. Soumya Bera and Dr. Martin Puschmann for their excellent support in all scientific questions, for countless discussions and for working with me on several topics;

- Prof. Dr. Alexander Altland, Mateo Moreno-Gonzalez, Prof. Dr. Piet Brouwer, Dr. Luka Trifunovic, Prof. Dr. Matthew Foster and Prof. Dr. Soumya Bera for a very fruitful and exciting collaboration over the last three years on disordered topological insulators and for broadening my scientific horizon. Special thanks to Prof. Dr. Alexander Altland for hosting me in Cologne;

- Prof. Dr. Ravin Bhatt and Dr. Rhine Samajdar for hosting me at Princeton University for a collaboration on Nagaoka magnetism in strongly correlated materials, giving me the opportunity to learn about another fascinating field of condensed matter physics;

- Dr. Matthias Stosiek for working with me on the interesting topic of disordered superconductors and for broadening my horizon by giving me another perspective on disordered systems;

- Torsten Weber and Prof. Dr. Klaus Richter for co-supervising several Bachelor theses about the localization landscape method, and Christoph Forster, Lucas Resch and Christoph Müller for being great Bachelor students;

- Harald Schmid, Andrea Solfanelli, Prof. Dr. Sauro Succi and Prof. Dr. Stefano Ruffo for collaborating with me on a fun project concerning many-body spin models;

- Alexandra Prem, Katja Herrmann-Nadolski, Sabine Lang and Doris Meier for invaluable support with all the bureaucratic and administrative matters which have occurred during the last years;
- Dr. Martin Puschmann, Torsten Weber, Christina Jäger, Adrian Seith, Max Graml, Julian Siegl and Hannah Eder for proof-reading parts of this thesis;
- the *Studienstiftung des Deutschen Volkes* for financially supporting my research;
- my awesome fellow students and friends Max Graml, Adrian Seith, Nithin Thomas, Patrick Größing, Christina Jäger, Dr. Martin Puschmann, Josef Pichlmeier, Torsten Weber, Dr. Moritz Frankerl, Dr. Christoph Brückner, Dr. Vanessa Junk, Julian Siegl, Dr. Jordi Picó-Cortés and Dr. Luca Magazzù, Dr. Bashab Dey, Isabella Knott and Daniel Reitinger for many discussions and coffee breaks. Without you the last couple of years would have been a lot less fun!
- my parents Veronika and Martin and my brother Andreas for supporting me in all my endeavors;
- and Hannah for being such an important part of my life and for her emotional support during all phases of my time as a doctoral student.